JOURNAL OF APPLIED PHYSICS

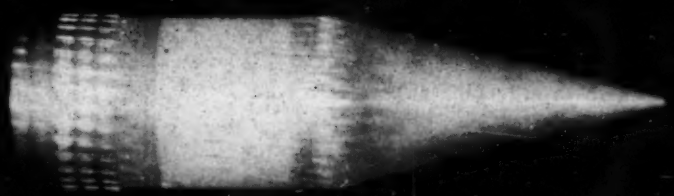

JOURNAL
OF
APPLIED PHYSICS

Vol. 19, No. 3 MARCH, 1948

In This Issue

Page

Microflash Unit for Ballistic Photography W. W. McCormick, L. Madansky, and A. F. Fairbanks 221

Erratum: Remarks on Some Recently Developed Devices for Summing Fourier Series for Crystal Structure Analysis C. L. Christ 225

On the Investigation of Specimen Contamination in the Electron Microscope James Hillier 226

Possible Fluctuations in Electron Streams Due to Ions J. R. Pierce 231

Application of the Laplace Transform in the Solution of Linear Integral Equations Lawrence Baylor Robinson 237

Response of Linear Resonant Systems to Excitation of a Frequency Varying Linearly with Time Gunnar Hok 242

Simple Relations for Calculating Certain Transient Responses W. J. Cunningham 251

On Creep and Relaxation. II B. Gross 257

Determination of the Elastic Constants for Beta-Quartz E. W. Kammer, T. E. Pardue, and H. F. Frissel 265

Dark-Field Electron Microscopy C. E. Hall 271

Mass Emissivity of Powder Gases in Solid Fuel Rockets S. S. Penner 278

Viscous Slip Along Grain Boundaries and Diffusion of Zinc in Alpha-Brass T'ing-Sui Kê 285

Plastic Flow of Thick-Walled Tubes with Large Strains C. W. MacGregor, L. F. Coffin, Jr., and J. C. Fisher 291

Gyrograms for Simple Harmonic Systems Subjected to External Forces V. Rojansky 297

Large Plastic Flow and the Collapse of Hollow Cylinders P. W. Bridgman 302

Letters to the Editor:

"Physical Basis of Bird Navigation" Joseph Slepian 306

Remarks on: "A Preliminary Study of a Physical Basis of Bird Navigation" Russell H. Varian 306

Remarks on: "The Physical Basis of Bird Navigation" Leverett Davis, Jr. 307

New Method of Measuring Diffusion Coefficient in Solids with Radioactive Tracers G. C. Kuczynski 308

In Every Issue

Calendar of Meetings 256

New Booklets 309

Here and There 309

Index to Advertisers xxxviii

BOARD OF EDITORS

Elmer Hutchisson, *Editor*

Associate Editors

R. Bowling Barnes
Otto Beeck
W. F. Busse
W. James Lyons
Philip Morrison
Paul E. Sabine
Frederick Seitz
J. R. Townsend
John Von Neumann

Publication of the American Institute of Physics

ADMINISTRATIVE STAFF

Henry A. Barton, *Director*

Cleveland Norcross, *Assistant Director*

Ruth F. Bryans, *Publication Manager*

Theodore Vorburger, *Business Manager*

John T. Tate, *Adviser on Publications*

GOVERNING BOARD

George R. Harrison, *Chairman*

Wallace Waterfall, *Secretary*

George B. Pegram, *Treasurer*

E. U. Condon
A. J. Dempster
W. F. Fair, Jr.
Floyd A. Firestone
Harvey Fletcher
R. C. Gibbs
K. S. Gibson
Paul E. Klopsteg
A. H. Pfund
John T. Tate
M. W. White
A. G. Worthing

The Journal of Applied Physics, published monthly at Prince and Lemon Sts., Lancaster, Pa., is devoted to physics in its role as the science basic to other natural sciences and to the arts and industries. Previous to 1937 this publication was known as Physics. The Journal of Applied Physics publishes editorials, news of physicists, and reviews, as well as technical papers of applied physics.

Manuscripts should be submitted to Elmer Hutchisson, Editor, Case Institute of Technology, Cleveland 6, Ohio.

Subscriptions and orders for back numbers should be addressed to Prince and Lemon Streets, Lancaster, Pa. or to the American Institute of Physics, 57 East 55 Street, New York 22, N. Y.

Subscription Price

	U.S. and Canada	Elsewhere
To members and associate members of the American Institute of Physics	$6.00	$7.00
To all others	8.00	9.00

Back Number Prices

Complete set: Vol. 1, July, 1931–Vol. 18, 1947—$132.00
Yearly back number rate: $10.00
Single copies: $1.00 each.

Changes of address should be sent to the Business Manager, American Institute of Physics; **corrected proofs** should be sent to the Publication Manager, American Institute of Physics.

Advertising rates supplied on request. Orders, advertising copy, and cuts should be sent to the American Institute of Physics.

Entered as second class matter January 22, 1937, at the Post Office at Lancaster, Pennsylvania, under the Act of March 3, 1879.
Accepted for mailing at the special rate of postage provided for in the Act of February 28, 1925, authorized May 2, 1932.

Copyright 1948, by the American Institute of Physics.

Journal
of
Applied Physics

Volume 19, Number 3 March, 1948

A Microflash Unit for Ballistic Photography*

W. W. McCormick, L. Madansky,** and A. F. Fairbanks***
Randall Laboratory of Physics, University of Michigan, Ann Arbor, Michigan
(Received August 19, 1947)

A flash unit has been developed for photographing large projectiles in flight. The light source combines high intensity with short duration. Details of the geometry and processing of the lamp are given, together with a discussion of the methods of measuring intensity and duration. Several of the units described have been in use at the Aberdeen Proving Ground and some photographs taken there are reproduced.

THE condensed spark has long been used as a source in ballistic photography to obtain shadow photographs of small projectiles in flight. For projectiles larger than, say, three inches in diameter, however, the area of film required becomes excessive since no lenses are used, and the field of illumination is insufficient. These limitations may be overcome by substituting for the spark, which is essentially a point source of light, an extended source such as a flash lamp. The projectile is then photographed by light reflected from the surface into one or more cameras advantageously placed about the trajectory. In addition to furnishing information regarding the orientation in space of the projectile, this technique permits examination of the surface for flaws which sometimes develop during firing. It does not, however, yield any information regarding shock wave patterns as does the condensed spark source.

At the time that the work reported in this paper was begun, some reflection photographs using a commercial flash unit had been taken at the Aberdeen Proving Ground. As a result of these tests it was decided that further investigation of the flash lamp source, with particular emphasis on reduction of the duration of the flash, was desirable. This was undertaken at the Randall Laboratory of Physics, University of Michigan, in cooperation with the Ballistic Research Laboratory at Aberdeen.

THE LIGHT SOURCE

Basically, a flash lamp consists of two electrodes sealed into a glass envelope in a rare gas atmosphere at a pressure of from 10 to 60 cm of mercury. The flash occurs when a condenser, charged to a potential difference of several thousand volts, is discharged through the lamp, the flash being initiated by a suitable triggering arrangement.

For satisfactory ballistic photography the duration of the flash, that is, the time during which the illumination of the projectile surface is sufficient to produce noticeable blackening on

* This paper is based on work completed in 1944 under Contract NDCrc-185 between the University of Michigan and the Office of Scientific Research and Development and submitted for clearance in 1946.
** National Research Fellow.
*** Now at the North American Aviation Company.

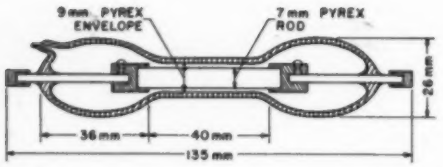

FIG. 1. The light source, approximately to scale.

the photographic film, must be very short in order to prevent blurring of the image. The permissible time is of the order of one or two microseconds for projectile velocities of 3000 ft./sec. and faster.

The light pulse produced by a flash lamp rises rapidly to a peak of very high intensity, often in a fraction of a microsecond, and then decays more slowly. The duration of the flash therefore depends principally on the decay time. Some of the lamp designs tested, using a photo-cell receiver coupled to an oscilloscope, showed a plateau in the decay curve which prolonged the duration beyond the limits of tolerance. Others exhibited oscillations, the output consisting of four or more distinct flashes. By arranging the geometry of the lamp so that the discharge is confined to a relatively narrow space between two glass surfaces, it is found that these objectionable phenomena may be satisfactorily reduced. The duration is then fixed by the capacitance of the condenser used to fire the lamp[1] and by the time constant of the discharge circuit. By using a small enough capacitance the quenching becomes sufficiently rapid to yield a duration time of the desired magnitude. The addition of some hydrogen to the gas content has been found to aid in quenching the discharge.

The energy input to the lamp, upon which the peak intensity depends, is also decreased as the capacitance is reduced, but, if the voltage to which the condenser is charged is increased, the intensity may be maintained at the desired level. This voltage, of course, must not be high enough to cause the lamp to fire without being triggered. The allowable voltage depends on the kind of gas used in the lamp and upon the pressure. The addition of some hydrogen, mentioned previously as an aid in quenching the discharge, also raises the breakdown voltage.

The lamp design finally adopted† may be seen

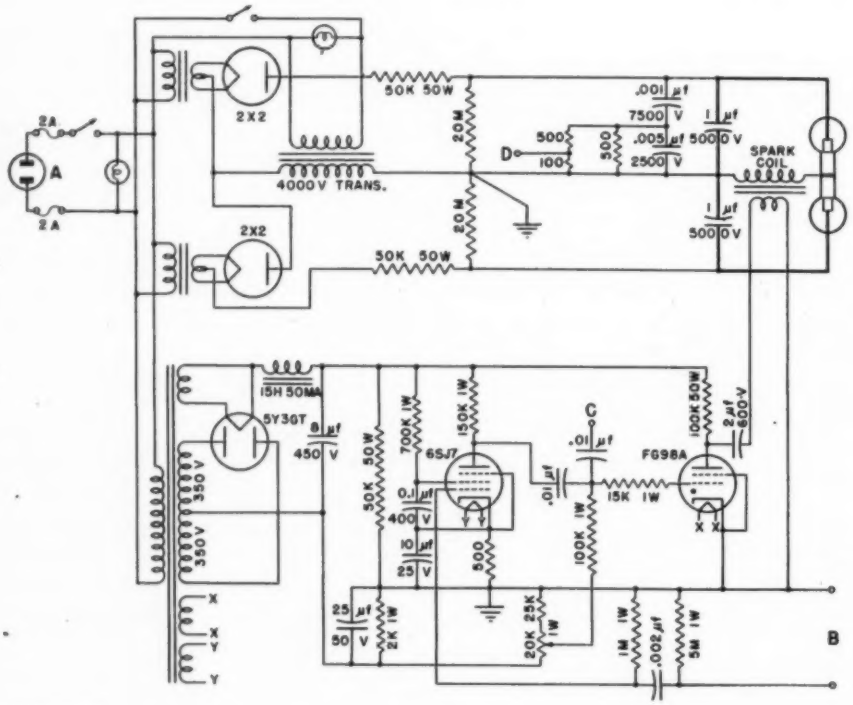

FIG. 2. The electric circuit (firing circuit in upper part of diagram; triggering circuit, arranged for microphone pick-up, below).

[1] P. M. Murphy and H. E. Edgerton, J. App. Phys. 12, 848 (1941).

† The lamp is now being manufactured by Sylvania Electric Products, Inc., Salem, Massachusetts (manufacturer's numbers R-4210 and R-4211).

in Fig. 1. The Pyrex rod is supported by the electrodes, each of which is $\frac{3}{8}$ inch in diameter and $\frac{1}{2}$ inch long. Made of steel, they are drilled at one end to permit easy insertion of the Pyrex rod and at the other end to receive a 100-mil tungsten support rod. The Pyrex envelope is blown out at each end to form a bulb. It should be noted in the figure that the "flare out" for each bulb begins before the electrode is reached so that the 1-mm spacing is preserved between the edge of the electrode and adjacent glass wall. This construction permits the gas, heated by the discharge, to expand into the bulbs. The tungsten support rods are beaded with Nonex and sealed into the envelope with uranium glass. The dimensions of the various parts of the lamp are shown in the figure. Pyrex tubing with a 2-mm wall has been used for the envelope, but a somewhat thicker wall is permissible and would probably extend the life of the lamp.

The lamps are evacuated, baked at 360° C for one-half hour in a furnace, and filled to a pressure of 45 to 60 cm of mercury with a mixture of hydrogen and commercial krypton (90 percent Kr and 10 percent Xe). The amount of hydrogen (approximately 25 percent of the total pressure) and the total pressure are adjusted by trial so that, unless triggered, the lamp will not break down when a potential difference of about 10,000 volts is applied. The life of the lamps when operated at such high energy inputs varies considerably from one specimen to another and is generally terminated by mechanical failure.

An external electrode for triggering (not shown) is finally added. It consists of one turn of annealed brass wire around the middle of the lamp.

THE ELECTRIC CIRCUIT

The electric circuit, shown in Fig. 2, was developed from that of Edgerton, Germeshausen, and Grier.[2] The triggering circuit was designed for a microphone pick-up, to be connected at *B*, with one stage of amplification. The amplified signal from the pick-up device causes an FG-98A thyratron to become conducting. The condenser in the plate circuit then discharges through the thyratron and the primary of an automobile-type spark coil and the high voltage pulse from the coil secondary triggers the lamp. The thyratron bias voltage may be adjusted as indicated for the desired triggering sensitivity. Provision is made for by-passing the amplifier (terminal *C*) when a high level signal from some other type of pick-up is available.

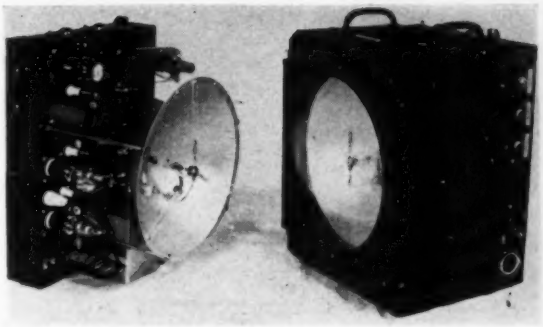

FIG. 3. Photograph of the complete unit.

The lamp is fired by a capacitance of 0.5 mf charged to somewhat more than 10,000 volts. The power supply utilizes two 1-mf condensers in series in a voltage doubler circuit, these condensers also being used to fire the lamp. The leads from the condensers to the lamp must be very short for satisfactory performance. The weight of the power supply has been reduced by the use of a small 4000-volt neon sign transformer. A potential divider across one of the firing condensers furnishes a pulse for operating a chronograph (terminal *D*) when the lamp is fired.

The addition of a small Variac (not shown) to the lamp power supply circuit is advisable in order to permit operation of the lamp at somewhat reduced voltage when maximum intensity is not required.

The circuit components are mounted on a metal chassis. Brass rods, fastened to the chassis, serve to hold a 14-inch metal reflector in which the lamp is mounted with shock resistant supports. The electrical connections to the lamp are passed through holes in the reflector in polystyrene tubes. A sheet metal case with a plate glass window completes the assembly (see Fig. 3). The total weight of the unit is about 40 lbs.

MEASUREMENT OF DURATION

The duration of the flash must, of course, be defined in terms of the type of light sensitive

[2] H. E. Edgerton, K. J. Germeshausen, and H. E. Grier, J. App. Phys. **8**, 2 (1937).

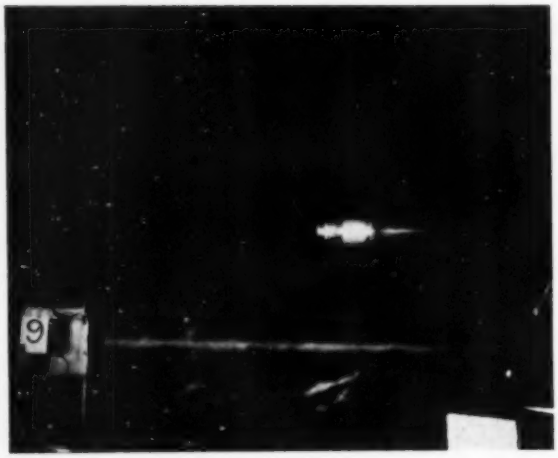

FIG. 4. Photograph of a 90-mm shell in flight. Velocity 3000 ft./sec.

receiver employed. Since in ballistic photography an image of the projectile is formed on a photographic film, the following method of measuring duration time was devised.

A narrow slit, illuminated by radiation from the flash lamp, was imaged on a distant screen by a lens. A rotating mirror, driven at 3600 r.p.m., was inserted into the light path near the lens in order to sweep the image of the slit across the screen. The lamp was triggered at the proper instant to cause the image to pass over a strip of Verichrome film tacked to the screen. The length of the blackened area on the film in the direction of motion of the light beam was then measured, and the duration of the flash determined. Values obtained in this way from several lamps ranged from one to two microseconds.

FIG. 5. Photograph of an 8-inch, armor piercing shell in flight. Velocity 2800 ft./sec.

Another type of receiver, consisting of a caesium-surface, vacuum photo-cell coupled to the vertical deflection plates of a cathode-ray tube through a wide-band amplifier, was also available. Traces taken with this equipment indicate a duration of about four microseconds measured from the beginning of the rise to a point where the intensity has fallen to about one-tenth of the peak value.

The difference between these values of the duration time may be due to failure of the film to respond to the lower levels of intensity at the beginning and at the end of the flash.

MEASUREMENT OF PEAK INTENSITY

The peak intensity of the flash has been measured with the photo-cell receiver mentioned in the preceding section. A 55-candlepower tungsten lamp operated at a color temperature of 2848 K was used for calibrating the receiver. The peak intensities of various lamps fired from a $\frac{1}{2}$-mf condenser at 10,000 volts were found to lie between 4×10^6 and 6×10^6 equivalent candlepower with respect to a caesium detector. For these measurements the lamps were not mounted in a reflector. If a photo-tube possessing the approximate spectral response for some common photographic emulsion together with other essential characteristics had been available it might have yielded an intensity rating more appropriate for photographic purposes.

PERFORMANCE

As an indication of the performance to be expected, two photographs, taken at the Aberdeen Proving Ground, are reproduced. Figure 4 shows a 90-mm shell at a velocity of 3000 ft./sec. Electrostatic triggering was employed. An 8-inch shell at 2800 ft./sec. is shown in Fig. 5. The shell was painted white in order to improve the reflectivity, but only the "windshield" retained the paint during firing. Magnetic triggering was

employed, part of the solenoid in which the pulse is induced appearing in the photograph.

Both photographs were taken with a 4×5 Eastman Graphic View Camera using a 127-mm, f:4.7, lens and Ansco Triple S Ortho film.

The use of several of the flash units suitably placed along the trajectory has yielded quantitative information on spin velocity and deceleration.

ACKNOWLEDGMENTS

The authors wish to express their appreciation of the cooperation of the Ballistic Research Laboratory at Aberdeen. Particular thanks are due Dr. A. C. Charters, Head, Free Flight, Aerodynamics Branch, and Mr. Walter Braun.

The lamps were made by Mr. Gunther Kessler, Physics Department Glass Blower, University of Michigan.

Erratum: Remarks on Some Recently Developed Devices for Summing Fourier Series for Crystal Structure Analysis

[J. App. Phys. **18**, 1133 (1947)]

C. L. CHRIST

Stamford Research Laboratories, American Cyanamid Company, Stamford, Connecticut

A DOUBLE summation sign was inadvertently omitted in Eq. (1); this should read

$$\rho(x, y)' = \sum_{h=-\infty}^{\infty} \sum_{k=-\infty}^{\infty} |F_{hk0}| + \sum_{h=-\infty}^{\infty} \sum_{k=-\infty}^{\infty} |F_{hk0}| \cos[2\pi(hx+ky) - \alpha_{hk0}].$$

On the Investigation of Specimen Contamination in the Electron Microscope*

JAMES HILLIER
RCA Laboratories, Princeton, New Jersey
(Received March 11, 1947)

A number of experiments directed toward determining the nature and cause of deposits which occur on electron microscope specimens under electron bombardment are described. From these the conclusion is drawn that the material is a result of chemical reaction, occurring at any surface simultaneously bombarded by electrons and organic molecules. The organic vapors are shown to arise in two ways: (1) by diffusion out of the metal walls, gaskets, and greases exposed to the vacuum, (2) by the outgassing of metal parts of the instrument exposed to electron bombardment. To eliminate the effect both sources must be removed.

I. INTRODUCTION

ELECTRON microscopists have been aware that specimens examined in the electron microscope undergo changes in character upon bombardment by electrons. A few of these changes in character are due to effects which are characteristic of the specimen or some part of it. One phenomenon, however, appears for all specimens and seems to be more or less independent of them. It consists of a deposition upon the specimen under bombardment of a light amorphous material. This particular effect has become known among electron microscopists as specimen "contamination." The observed effects of this contamination are somewhat different, depending on the nature of the specimen and the method by which it has been mounted. In the case of filmless mounting or of particles mounted on a membrane, the effect appears as a continual increase in particle size. In the case of very small particles, either on or imbedded in a plastic membrane, the effect appears simply as an increase of thickness of the whole membrane accompanied by a loss of contrast. The effect has become increasingly important as the techniques of application and the resolving power of the electron microscope have been increased until, at present, in this laboratory, it has become one of the major technical difficulties. In the presence of this effect it is extremely difficult to obtain accurate measurements of particle size of low density materials in the size range below 100A. In the case of film specimens which contain only small density differences, it quickly reduces the contrast to the vanishing point. This effect has also precluded any possibility of preserving interesting fields of view for subsequent examination.

In a recent paper, Watson[1] has described some observations made on the changes resulting from this effect in the particle size of various carbon black preparations. He offers the hypothesis that the deposit is the result of a polymerization and condensation of organic vapors and gases under electron bombardment.

In this laboratory, contamination phenomena have also been observed, and intensive studies have been made over a long period for a great variety of specimens and operating conditions. While the results obtained cannot be considered to be completely conclusive, they do throw considerably more light on the mechanism of this phenomena and give an indication as to a method by which it can be minimized.

II. EXPERIMENTAL RESULTS

The experimental results and conclusions presented below have been collected over several years time and are the results of the efforts of a number of workers and from work on a number of different instruments in addition to the electron microscope.

(1) The first appearing deposits observed by ordinary light are brownish and translucent. Heavy deposits obtained after long electron bombardment are black and opaque.

(2) The deposits are insoluble in any of the common solvents and are not affected by strong

* The main part of this paper was presented at the Pittsburgh 1946 meeting of the Electron Microscope Society of America as discussion to a paper by J. H. L. Watson, "An effect of electron bombardment on carbon black." (J. H. L. Watson, J. App. Phys. **18**, 153 (1947).)

FIG. 1. High magnification electron micrograph of carbon black particles on which a layer of contamination has been deposited. The image was taken on the long focal length side of focus to enhance contrast. The original carbon black particles can be just distinguished as slightly denser regions inside the mass of contamination.

acids or alkalies. Deposits on metal surfaces disappear if heated to red heat in air. Qualitatively, their properties appear to be independent of the substrate upon which they are deposited.

(3) They have an electron scattering power slightly less than that of carbon (Fig. 1). They are structureless to the electron microscope and amorphous to electron diffraction.

(4) The deposits formed in the beam of the electron microanalyzer[1] on a silica substrate[2] have been analyzed by that instrument. Carbon only was found, but, because of the inability of the instrument to detect hydrogen, the observation does not exclude the possibility that the material contains hydrogen. Similarly, there may be other elements present in low concentration.

(5) The material is not stable in thick layers in air. When a membrane and screen is bombarded for several hours so that an excessively thick deposit is produced (Fig. 2a) it is often found that on standing overnight in a partial vacuum of the instrument the deposit loses its homogeneity and also shows signs of having migrated over considerable distances (Fig. 2b).

(6) The rate of formation is roughly proportional to the intensity of bombardment.

(7) It has occurred on all materials examined, and, while it has not been proven that the rate of formation is the same for all substrates, quali-

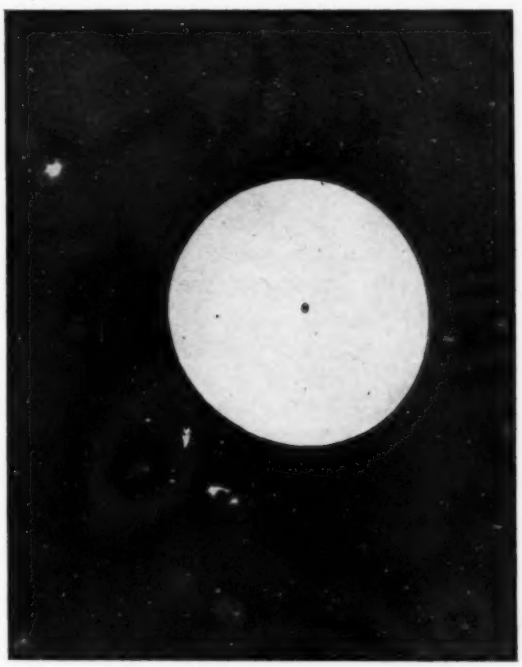

(a)

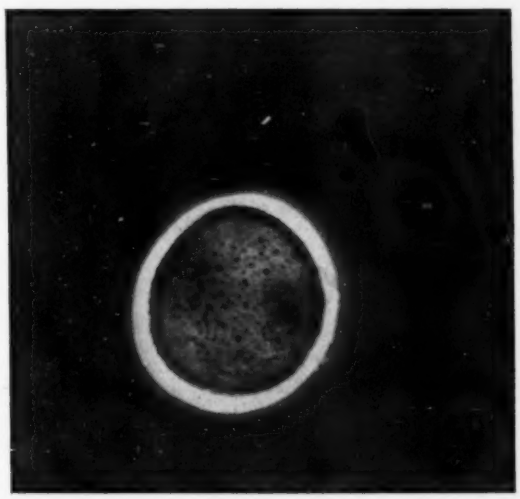

(b)

FIG. 2. (a) Electron micrograph of a hole in a collodion membrane. The membrane has been greatly thickened by contamination. (b) A similar hole in the same membrane after it had stood overnight in a partial vacuum of the electron microscope. The migrating contamination has bridged the hole with a thin film and has collected into a granulated layer in the central region.

[1] J. Hillier and R. F. Baker, "Microanalysis by means of electrons," J. App. Phys. **15**, 663 (1944).
[2] J. Hillier and R. F. Baker, "Further developments on the microanalyzer," J. App. Phys. **16**, 266 (1945).

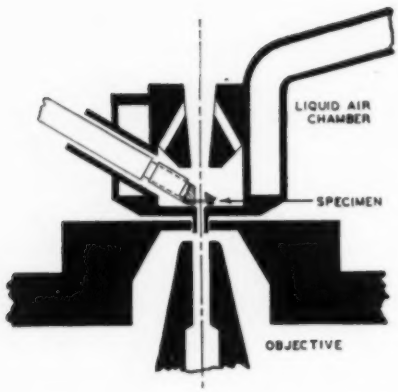

FIG. 3. Cross section of the arrangement of a liquid air chamber enclosing the specimen in the microanalyzer. In this arrangement the electron beam travels upwards on the axis of the system.

tative observations indicate this to be the case if all other experimental conditions are carefully controlled. Actually, it would be expected that the initiation of the deposit might vary for different substrates, but, obviously, once the deposit is initiated the substrate is the material formed. Thus, once the deposition has been started, it would be expected that the addition of further material would proceed at a rate determined only by the experimental conditions in the instrument.

(8) Surrounding the specimen (microanalyzer) and the beam near the specimen in a liquid air trap (Fig. 3) produced the following results:

a. Introduction of the copper chamber (it had been freshly cleaned) around the specimen at room temperature quickly reduced the rate of the deposit to approximately one-fifth of its original value.

b. Cooling the chamber to liquid air temperature made no further change.

These observations are consistent with those made on instruments including liquid air traps in the pumping line, in which case no observable change in the rate of contamination of the specimen has been observed. This was even true in a particular case where the system was never allowed to be opened to the oil diffusion pump without the liquid air trap in operation. It is believed in this laboratory that oil vapors from the diffusion pumps are not responsible for contamination. At first sight, it appears that the experiment eliminated the possibility of the phenomena being due to the polymerization of hydrocarbons, since all of these would be condensed out at liquid air temperatures. However, the arrangement of the experiment was such that the rod bearing the specimen was not cooled more than a few degrees below room temperature, and hence the rate of diffusion of gases or vapors from the metal parts would not be affected greatly.

9. When three membranes separated by 50μ were introduced in the microanalyzer, it was found that the rate of deposition on the central membrane when the probe was focused on it would decrease rapidly with time but would return to its original value when the beam was turned off for a few minutes. The results of this experiment, as well as those described in 8a, can be explained on the assumption that the material from which the contamination comes is in the vapor phase and that its partial pressure is very low. The action of the electron beam appears to reduce this partial pressure rapidly within the restricted volume near the specimen. In both experiments the arrangement is such that it takes considerable time for equilibrium to be reestablished after the electron beam is turned off.

10. Changing the potential of the specimen relative to its surroundings by as much as a thousand volts positively or negatively made no change in the rate of deposition. This observation eliminates the possibility that the deposition is the result of electrostatic attraction of gas or vapor molecules which have been ionized by the electron beam. It is known that in the electron microscope, where the bombardment usually includes part of a wire screen connected to ground, the area of the thin membrane under bombardment is not charged.[3] This is not true if that area includes extremely large particles (greater than 10 microns) or if the electron beam is so concentrated that none of it strikes the supporting wire screen. The latter is invariably true in the case of the probe diffraction camera[3] or microanalyzer. Assuming the most favorable case, i.e., when equal numbers of negative and positive ions are involved, at least a 50 percent reduction in the rate of deposition should be observed upon application of the potential. Since no such change was observed, it can only be assumed that the

[3] J. Hiller and R. F. Baker, "On the improvement of resolution in electron diffraction cameras," J. App. Phys. 17, 12 (1946).

electrostatic attraction of the ions to the bombarded area is not responsible for the observed deposits. It should be noted that 1000 volts is sufficient to repel ions which have been given maximum possible kinetic energy by the electron beam.

11. The introduction of magnetic or electrostatic fields for the deflection of beams (the microanalyzer probe was used), immediately before it strikes the specimen, have shown that the material is deposited only in the area where the deflected beam irradiates the specimen. This experiment was carried out in order to prove that the deposit was not due to an ion beam arising in the gun of the instrument. It also strengthens the suggestion that the surface bombarded by the electron beam takes part in the chemical reaction resulting in the deposit.

12. It is observed that the rate of deposition decreases with time when the total current of the beam is sufficient and if the beam *does not* strike the metal supporting screen. In the electron microscope an illuminating current of 3 to 5 microamperes, focused to a 10-micron diameter spot and allowed to run for 20 minutes, reduces the rate of deposition to the vanishing point. Once the rate of deposition has been reduced to a negligible value under the above conditions, it does not return to its original value for many hours, even if the instrument is opened to the air several times in that period.

13. If the conditions described in (12) are achieved and if part of the beam is allowed to impinge on the copper specimen screen, the rate of deposition of the material on the irradiated part of the membrane returns to the higher value for as long as the copper screen receives some bombardment. In this connection, another phenomena was often observed, namely, that in the case of a film mount a narrow clear strip on which there appeared to be no deposits and which followed the contour of the wire could be seen (Fig. 4).

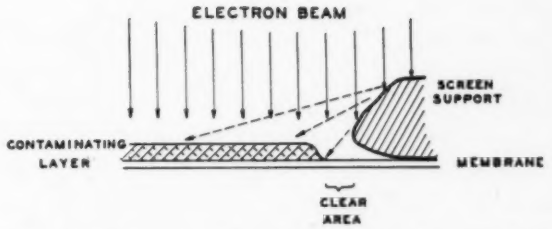

FIG. 4. A schematic representation of the factors giving rise to the clear uncontaminated border that is often observed near the edge of a grid wire. It is presumed that contaminating vapors are released from the grid wire (screen support) by the electron bombardment but that the released molecules travel in straight lines and are deposited only when they strike another area. The region of the membrane very close to the grid wire is sheltered from the bombardment of gas molecules, and hence no contamination appears even though that region is under electron bombardment.

III. CONCLUSIONS

All of the evidence given in the above observations and discussions supports the hypothesis put forward by Watson[4] that the chemical process involved is the polymerization of a hydrocarbon. It indicates further, however, that the deposit requires all three factors—the material in the gas phase, the surface, and the electron bombardment—leading to the suggestion that the surface under bombardment is activated so as to act as a catalyst for the reaction. While the observations do not exclude the possibility that the material is formed in the gas phase, they do show that if this is so the material produced is not responsible for the contamination observed.

The observations indicate that the gas or vapors involved diffuse into the system very slowly and at no time reach a high partial pressure. The probable origins are the metal walls of the instrument, the rubber gaskets, and the sealing or lubricating greases. There is a definite indication that it is released more rapidly by electron bombardment—probably through local heating. This is particularly true in the case of the specimen screen. The observation, 13, provides the strongest evidence that the deposit occurs mainly on the area of the substrate simultaneously bombarded by the gas molecules and the electron beam.

There is good experimental evidence that the gases or vapors do not come from the oil diffusion pump. The same contamination problem has been encountered in instruments which have never used anything except mercury diffusion pumps with liquid air cold traps. Furthermore, it was found that when Octoil vapor was bombarded in an experimental arrangement, the solid deposit obtained was *white* and consisted of phthalic anhydride.

[4] J. H. L. Watson, J. App. Phys. **18**, 153 (1947).

While the evidence is not conclusive it does *not* support the suggestion put forward by Watson that there is a dependence on the conductivity of the specimen.

In a recent note Cosslett[5] suggests that the contamination is due to the ejection of absorbed matter and perhaps of metal itself from the grid wires under electron bombardment. He excludes organic impurities from the "absorbed matter" since cleaning and heating in vacuum prior to use brought about little improvement. The presented observations, namely, that the contamination is largely carbon, has lower electron scattering than carbon, and is structure free to the limit of resolution of the microscope in this laboratory (10A), are almost in direct contradiction to his statements. The explanation for the discrepancy probably lies in the fact that the contamination has two sources (the object chamber space and the grid wires), a possibility which Cosslett does not seem to have considered. Since these can vary greatly in their relative strengths, observations in which the results are not separated have little meaning. The use of the fine probe in the microanalyzer system has made this separation possible in many of the above experiments.

IV. ELIMINATION OF THE EFFECT IN THE ELECTRON MICROSCOPE

These observations and conclusions point to a possible method of eliminating this very troublesome phenomenon.

In the probe type of instrument where the extremely fine beam seldom strikes the wires of the specimen screen, the rate of deposit can be reduced by several orders of magnitude[6] by the simple introduction of an electron source in the specimen chamber. Spraying the chamber with an electron current of 50 ma at an accelerating potential of 1000 v for 1 minute cleans the system for several hours operation. Apparently it cleans the chamber space and also releases and redeposits the gas near the surface of the walls of the chamber. In the microscope a similar scheme can be used. In this case, however, the deposit occurring as a result of the bombardment of the specimen screen still remains and must be avoided if the difficulty is to be completely eliminated. While this has not been investigated in this laboratory, it appears evident that the use of screen material from which hydrocarbons can be removed, probably by heating *in a furnace*, should provide an answer. The author has received reports that the deposit is appreciably less in the case of stainless steel screens that have been cleaned by heating. It would appear logical to investigate the use of specimen screen materials such as platinum or tantalum for critical electron microscope work where extensive study of a single specimen is desirable. These could be cleaned and outgassed by heating in a furnace; a vacuum furnace might be preferable in extreme cases.

[5] V. E. Cosslett, J. App. Phys. **18**, 844 (1947).

[6] N. Davidson and J. Hillier, "Single crystal electron diffraction by micro-crystalline materials," J. App. Phys. 18, 499 (1947).

IV. ACKNOWLEDGMENTS

The work described above is a summary of observations made in this laboratory by a number of individuals pursuing other investigations. R. F. Baker made the analysis of the deposit in the microanalyzer and first observed the changes which occur in the deposit on standing. N. R. Davidson collaborated with the author in making the multiple membrane, deflection, and electron spray tests. T. F. Anderson made an early study showing the dependence of the contamination on the bombardment of the screen.

Possible Fluctuations in Electron Streams Due to Ions

J. R. PIERCE

(Received August 11, 1947)

The equations for low amplitude space-charge waves in an electron stream containing heavy positive ions are considered. At frequencies a little below the ion plasma frequency there should be a wave which increases in amplitude as it travels (negative attenuation). Ion motion tends to limit the rate of increase. In a beam filling a conducting cylinder and confined by a uniform magnetic field there should be an increasing wave at frequencies near the ion cyclotron frequency. Such waves *might explain observed fluctuations in long electron beams.*

1. INTRODUCTION

IN the course of work at the Bell Telephone Laboratories on traveling wave tubes, Dr. L. M. Field and the writer observed fluctuations in electron streams in high vacua. Subsequently, Mr. J. A. Morton and the writer have found similar fluctuations in electron streams under a variety of conditions. The fluctuations can be observed as a fluctuating division of current between electrodes due to fluctuations in the position of electron flow.

In electron flow in a high vacuum, the electronic space charge tends to form a potential minimum and this provides a mechanism by which positive ions can be trapped in the electron stream. The presence and motions of ions in the electron stream might afford one source of fluctuations. The purpose of this memorandum is not to present experimental data, but to give an analysis of the situation which shows that fluctuations should build up along an electron stream if ions are present. The analysis is carried out for a case in which the positive space charge of ions is just equal to the negative space charge of electrons, so there is no average charge density in the electron stream. The analysis is a small-signal or perturbation theory.

First an essentially one-dimensional case is treated, in which neither d. c. nor a. c. quantities vary normal to the direction of electron motion. If the ions have no d. c. velocity, this leads to a wave which builds up infinitely rapidly with distance at a frequency which may be called the ion plasma frequency. Such a wave might result in the amplification of small initial disturbances, such as those due to shot noise, to give the large fluctuations observed in some traveling wave tubes. Small ion velocities are shown to give a finite rate of build-up. Collisions might result in some sort of "damping."

The case of a beam filling a conducting tube and an axial magnetic field is also considered. It is found that there is an increasing wave in this case for typical conditions.

1.1 One-Dimensional Case, Ions at Rest

We will consider first an essentially one-dimensional case, in which there are no electric fields in the x or y directions and a. c. quantities are functions of z only. We will use m.K.S units throughout. We will consider the case of a current of electrons of magnitude I_0/cm^2, traveling in the $+z$ direction with a mean velocity

$$u_0 = \left(2\frac{e}{m}V_0\right)^{\frac{1}{2}}. \tag{1}$$

Here e/m is a positive quantity, the charge to mass ratio of the electron. The mean charge density of electrons will be

$$\rho_{e0} = -I_0/u_0 = -\rho_0. \tag{2}$$

We will assume a mean ion charge density

$$\rho_{i0} = -\rho_{e0} = \rho_0, \tag{3}$$

composed of ions of charge to mass ratio

$$q/M = (e/m)/N. \tag{4}$$

We will assume that the frequency is low enough so that a. c. magnetic fields can be neglected and the electric fields can be given well enough in terms of a scalar electric potential. We will consider small a. c. disturbances only, omitting all but first-order a. c. terms. This will linearize the equations and result in solutions in

which the a. c. quantities vary as

$$\exp(-\Gamma z+j\omega t).$$

The a. c. quantities will then be represented by the constant factors identified below multiplied by $\exp(-\Gamma z+j\omega t)$.

V = potential,
ρ_e = electron charge density,
ρ_i = ion charge density,
v_e = electron velocity,
v_i = ion velocity,
q_e = electron convection current,
q_i = ion convection current.

In terms of these quantities, we may write (Poisson's equation):

$$\Gamma^2 V=-\frac{1}{\epsilon}(\rho_i+\rho_e). \tag{5}$$

Definition of first-order convection current

$$q_e=\rho_e u_0-\rho_0 v_e, \tag{6}$$

$$q_i=\rho_0 v_i. \tag{7}$$

Conservation of charge

$$j\omega\rho_e=\Gamma q_e, \tag{8}$$

$$j\omega\rho_i=\Gamma q_i. \tag{9}$$

First-order force equation

$$j\omega v_e-u_0\Gamma v_e=-(e/m)\Gamma V, \tag{10}$$

$$j\omega v_i=(e/m)\Gamma V/N. \tag{11}$$

In combining these equations it is convenient to define quantities

$$\omega_e=(\rho_0(e/m)/\epsilon)^{\frac{1}{2}}, \tag{12}$$

$$\omega_i=(\rho_0(q/M)/\epsilon)^{\frac{1}{2}}=\omega_e/N^{\frac{1}{2}}. \tag{13}$$

It is interesting to have some idea of the magnitude of ω_e and ω_i. Suppose I_0 is the current density in amperes/cm^2. Then

$$\omega_e=1.83\times10^{10}I_0^{\frac{1}{2}}/V_0^{\frac{1}{2}}. \tag{12a}$$

For the reasonable conditions of 0.1 ampere/cm^2 and 1500 volts

$$\omega_e=9.3\times10^8=(2\pi)150\times10^6$$

for

$$0^-,\ N=2.9\times10^4,\ N^{\frac{1}{2}}=170$$
$$\omega_i=5.5\times10^6=(2\pi).87\times10^6.$$

Combining (5)–(13), we obtain

$$\Gamma^2 V=\left(\frac{\omega_e^2}{(\omega+j\Gamma u_0)^2}+\frac{\omega_i^2}{\omega^2}\right)\Gamma^2 V. \tag{14}$$

We might expect three types of solution, $\Gamma=0$, $V=0$, and

$$1=\frac{\omega_e^2}{(\omega+j\Gamma u_0)^2}+\frac{\omega_i^2}{\omega^2}. \tag{15}$$

Those represented by (15) are the ones of interest. We can solve (15) for Γ

$$-\Gamma=-j\frac{\omega}{u_0}\pm\frac{\omega_e}{u_0}\left[\left(\frac{\omega_i}{\omega}\right)^2-1\right]^{-\frac{1}{2}}. \tag{16}$$

If $\omega<\omega_i$ this represents two waves traveling to the right with a phase velocity equal to that of the electron stream. One wave has a positive attenuation and the other a negative attenuation.

We may imagine, for instance, that small irregularities in the electron stream at a point (say, a starting point) can be represented as having a component of the increasing wave. Then such irregularities can be the basis of large irregularities further to the right, as the wave increases according to (16). The wave increases at an infinite rate for $\omega=\omega_i$, and hence we would expect very large disturbances near this frequency.

1.2 Effect of Small Ion Velocities

The ions are presumably generated by electron collision, and we would expect a small ion drift in the direction of electron motion and a distribution of ion velocities.

Suppose we say that there is an ion charge density $d\rho_0$ associated with ions having z components of d. c. velocity lying in the range du at u. We will now have instead of (7), (9), and (11)

$$dq_i=d\rho_i u+d\rho_0 v_i, \tag{7a}$$

$$j\omega d\rho_i=\Gamma dq_i, \tag{9a}$$

$$j\omega v_i=u\Gamma v_i=\frac{1}{N}\frac{e}{m}\Gamma V. \tag{11a}$$

From these we obtain

$$d\rho_i=-\frac{(e/m)}{N}d\rho_0\frac{\Gamma^2 V}{(\omega+j\Gamma u)^2}. \tag{17}$$

And, corresponding to (15) we have

$$1=\frac{\omega_e^2}{(\omega+j\Gamma u_0)^2}+\omega_i^2\frac{1}{\rho_0}\int_{u=-\infty}^{u=\infty}\frac{d\rho_0}{(\omega+j\Gamma u)^2}. \quad (18)$$

We can progress a step further by assuming that none of the ions has a very large velocity, so that always

$$\Gamma u\ll\omega. \quad (19)$$

In this case we can rewrite (18), expanding the denominator of the integral

$$\frac{1}{\rho_0}\int_{u=-\infty}^{u=\infty}\frac{d\rho_0}{(\omega+j\Gamma u)^2}$$
$$=\frac{1}{\omega^2}\frac{1}{\rho_0}\int_{u=-\infty}^{u=\infty}\left(1-2\frac{j\Gamma}{\omega}u-3\frac{\Gamma^2}{\omega^2}u^2\cdots\right)d\rho_0$$
$$=\frac{1}{\omega^2}\left(1-2\frac{j\Gamma}{\omega}\bar{u}-3\frac{\Gamma^2}{\omega^2}\langle u^2\rangle-\cdots\right). \quad (20)$$

Here we are describing the ion velocity distribution in terms of the moments $\bar{u}$, $\langle u^2\rangle$, etc. If we use this expression, in connection with (18) we obtain

$$1=\frac{\omega_e^2}{\omega^2\left(1+j\frac{\Gamma u_0}{\omega}\right)^2}+\frac{\omega_i^2}{\omega^2}\left(1-j2\frac{\Gamma\bar{u}}{\omega}-3\frac{\Gamma^2\langle u^2\rangle}{\omega^2}-\cdots\right). \quad (21)$$

For each additional moment included in describing the ions, the equation becomes one degree higher in Γ. This is natural, as inclusion of $\bar{u}$, $\langle u^2\rangle$, etc., requires some means for adjusting the ion motions at boundaries where the ions enter.

The reasonable step is to include only the term in $\bar{u}$. Let us do this, rewriting (21) in terms of the parameters W and γ

$$W^2=\left(\frac{\omega}{\omega_i}\right)^2, \quad (22)$$

$$\gamma=\frac{\Gamma u_0}{\omega_i}. \quad (23)$$

We obtain

$$\left(\frac{\omega_e}{\omega_i}\right)^2=\left(1+j\frac{\gamma}{W}\right)^2\left[W^2-1+j2\frac{\bar{u}}{u_0}\frac{\gamma}{W}\right]. \quad (24)$$

We are interested in frequencies such that W is very nearly equal to unity.

$$\frac{\omega_e}{\omega_i}\gg 1, \quad (25)$$

$$\frac{\bar{u}}{u_0}\ll 1. \quad (26)$$

Hence

$$|\gamma|\gg 1. \quad (27)$$

We may thus write approximately

$$\left(\frac{\omega_e}{\omega_i}\right)^2=\frac{-\gamma^2}{W^2}\left[W^2-1+j2\frac{\bar{u}}{u_0}\frac{\gamma}{W}\right]. \quad (28)$$

For a special case, $W=1$, this yields

$$\gamma=(j)^{\frac{1}{3}}\left(\frac{\omega_e}{\omega_i}\right)^{\frac{2}{3}}\left(\frac{2\bar{u}}{u_0}\right)^{-\frac{1}{3}}, \quad (29)$$

$$\frac{2\bar{u}}{u_0}\gamma=(j)^{\frac{1}{3}}\left(\frac{\omega_e}{\omega_i}\right)^{\frac{2}{3}}\left(\frac{2\bar{u}}{u_0}\right)^{\frac{2}{3}}. \quad (30)$$

For singly charged ions we have from (4)

$$M/m=N.$$

If $\bar{u}$, $\bar{u}^2$, etc., are produced by collisions with electrons, we might expect $\bar{u}/u_0$ to be of the order of $1/N$, $\langle u^2\rangle/u_0^2$ to be of the order of $1/N^2$, etc. We have from (13) that $(\omega_e/\omega_i)^2=N$. Assuming

$$\frac{\bar{u}}{u_0}=1/N, \quad (31)$$

we obtain

$$\gamma=(j)^{\frac{1}{3}}(2)^{-\frac{1}{3}}N^{\frac{2}{3}}, \quad (32)$$

$$\frac{2\bar{u}}{u_0}\gamma=(j)^{\frac{1}{3}}(2)^{+\frac{2}{3}}N^{-\frac{1}{3}}. \quad (33)$$

For 0^-, $N=2.9\times10^4$ we have

$$\left|\frac{2\bar{u}}{u_0}\gamma\right|=5\times10^{-2}.$$

Thus, (20) and (24) appear to be reasonably well justified. We have, then, using (31),

$$-\gamma_1=7.50\times10^4(-.866-j.5),$$
$$-\gamma_2=7.50\times10^4(+.866-j.5),$$
$$-\gamma_3=7.50\times10^4(j).$$

γ_1 represents a decreasing wave traveling to the

right, γ_2 an increasing wave traveling to the right, and γ_3 an unattenuated wave traveling to the left.

1.3 Damping, as by Collisions

The kinetic energy of an electron is for a given velocity, proportional to its mass. If we assumed some sort of frictional force (as, due to collisions) the effect could be taken into account in our analysis by assuming the mass or the charge-to-mass ratio to have a small complex component. It would seem offhand that the electrons would be more affected by collisions than the ions. However, we see that a complex value of e/m, meaning a complex value of ω_e, would not prevent Γ from going to infinity. It requires damping of the ions to do this. Suppose, then, that there is a damping term, so that

$$\omega_i = \omega_1(1+j\delta),$$
$$j\omega_i = j\omega_1 - \delta\omega_1. \tag{34}$$

If $\delta \ll 1$, this gives approximately

$$-\Gamma = -j\frac{\omega}{u_0} \pm \frac{\omega_e}{u_0}\left[\left(\frac{\omega_1}{\omega}\right)^2 - 1 + 2j\delta\left(\frac{\omega_1}{\omega}\right)^2\right]^{-\frac{1}{2}}. \tag{35}$$

For instance, at $\omega = \omega_1$, this gives

$$-\Gamma = -j\left(\frac{\omega}{u_0} \pm \frac{1}{2\delta^{\frac{1}{2}}}\frac{\omega_e}{u_0}\right) \pm \frac{1}{2\delta^{\frac{1}{2}}}\frac{\omega_e}{u_0}, \tag{36}$$

and obviously Γ does not go to ∞ for any real value of ω.

1.4 Cylindrical Beam with Magnetic Field

The question now arises, what is the effect of confining the beam in a conducting tube and of having a uniform axial magnetic field. Suppose we assume an axial field of strength B in the z direction. Let us deal initially merely with the motions of electrons, dropping the subscript e. Let v_x, v_y, v_z be the Cartesian components of velocity. If we assume a variation in the z direction, $\exp -\Gamma z$, as before, we obtain, saving first-order terms,

$$(j\omega - \Gamma u_0)v_x = \frac{e}{m}\left(\frac{\partial V}{\partial x} + Bv_y\right), \tag{37}$$

$$(j\omega - \Gamma u_0)v_y = \frac{e}{m}\left(\frac{\partial V}{\partial y} - Bv_x\right), \tag{38}$$

$$(j\omega - \Gamma u_0)v_z = -\frac{e}{m}\Gamma V. \tag{39}$$

We further have from the conservation of charge

$$-\rho_0\left(\frac{\partial v_x}{\partial x} + \frac{\partial v_y}{\partial y} + \frac{\partial v_z}{\partial z}\right) + u_0\frac{\partial \rho}{\partial z} = -j\omega\rho,$$

$$(j\omega - \Gamma u_0)\rho = \rho_0\left(\frac{\partial v_x}{\partial x} + \frac{\partial v_y}{\partial y} - \Gamma v_z\right). \tag{40}$$

If we solve (37) and (38) we obtain

$$v_x = \frac{\frac{e}{m}(j\omega - \Gamma u_0)\frac{\partial V}{\partial x} + \frac{e}{m}\omega_0\frac{\partial V}{\partial y}}{(j\omega - \Gamma u_0)^2 + \omega_0^2}, \tag{41}$$

$$v_y = \frac{\frac{e}{m}(j\omega - \Gamma u_0)\frac{\partial V}{\partial y} - \frac{e}{m}\omega_0\frac{\partial V}{\partial x}}{(j\omega - \Gamma u_0)^2 + \omega_0^2}, \tag{42}$$

where

$$\omega_0 = \frac{e}{m}B. \tag{43}$$

Combining (39), (41), and (42) with (40) we obtain

$$\rho = -\frac{e}{m}\rho_0\left(\frac{\frac{\partial^2 V}{\partial x^2} + \frac{\partial^2 V}{\partial y^2}}{(\omega + j\Gamma u_0)^2 - \omega_0^2} + \frac{\Gamma^2 V}{(\omega + j\Gamma u_0)^2}\right). \tag{44}$$

It has been convenient to work the problem out in rectangular coordinates. However, we wish to apply the result to an axially symmetrical system with a conducting wall. Suppose we choose a solution in which V varies as

$$J_0(kr)e^{-\Gamma z},$$

where

$$ka = 2.4. \tag{45}$$

The radius of the conducting tube being a, then

$$\frac{\partial^2 V}{\partial x^2} + \frac{\partial^2 V}{\partial y^2} = -k^2 V. \tag{46}$$

Poisson's equation will be

$$\frac{\partial^2 V}{\partial x^2} + \frac{\partial^2 V}{\partial y^2} + \frac{\partial^2 V}{\partial z^2} = -\frac{\rho_e + \rho_i}{\epsilon},$$
$$(-k^2 + \Gamma^2)V = -\frac{\rho_e + \rho_i}{\epsilon}. \tag{47}$$

It is easy to see that using (12) and (13) and letting

$$\frac{e}{m}B=\omega_{0e}, \tag{48}$$

$$\frac{q}{M}B=\omega_{0i}=\omega_{0i}/N, \tag{49}$$

we obtain, disregarding the solution $V=0$ (for which v_x and v_y need not be zero),

$$-k^2+\Gamma^2=\omega_e{}^2\left[\frac{-k^2}{(\omega+j\Gamma u_0)^2-\omega_{0e}{}^2}+\frac{\Gamma^2}{(\omega+j\Gamma u_0)^2}\right]+\omega_i{}^2\left[\frac{-k^2}{\omega^2-\omega_{0i}{}^2}+\frac{\Gamma^2}{\omega^2}\right]. \tag{50}$$

If there is no magnetic field ($\omega_{0e}=\omega_{0i}=0$), this reduces to (15) and

$$-k^2+\Gamma^2=0. \tag{51}$$

Thus, we have the waves given by (16) and also

$$\Gamma=\pm k. \tag{52}$$

The waves given by (52), however, have a potential identical with that in the tube in the absence of charge and are essentially "field waves" as opposed to "space charge" waves.

It is important to know the values of ω_{0e} and ω_{0i}. If H is the magnetic field in gauss,

$$\omega_{0e}=17.8\times10^6H. \tag{53}$$

A focusing field of 100 gauss is common in a traveling wave tube. In this case

$$\omega_{0e}=1780\times10^6=(2\pi)280\times10^6. \tag{54}$$

For 0^-, $N=2.9\times10^4$ and for this case

$$\omega_{0i}=61{,}000=(2\pi)10{,}000.$$

As (50) is rather complicated, it is helpful to use dimensionless units.

We have earlier found important effects in the frequency range around ω_i. Let

$$\frac{\omega}{\omega_i}=W, \tag{55}$$

$$\frac{\Gamma u_0}{\omega_i}=\gamma, \tag{56}$$

$$\frac{ku_0}{\omega_i}=m. \tag{57}$$

We then obtain

$$1-\frac{1}{W^2}=\frac{m^2}{\gamma^2}\left[1-\frac{1}{W^2-\left(\frac{\omega_{0i}}{\omega_i}\right)^2}\right]+\left(\frac{\omega_e}{\omega_i}\right)^2\left[\frac{1}{(W+j\gamma)^2}-\frac{m^2/\gamma^2}{(W+j\gamma)^2-\left(\frac{\omega_{0e}}{\omega_i}\right)^2}\right]. \tag{58}$$

It is important to know the magnitude of the factors m^2 and $(\omega_e/\omega_i)^2$. For 0^- as compared with electrons

$$\left(\frac{\omega_e}{\omega_i}\right)^2=N=2.9\times10^4. \tag{59}$$

Let us assume that $r=0.24$ cm. Then

$$kr=.24k=2.4,$$
$$k=10.$$

Also, let us assume, $u_0=c/10=3\times10^9$ cm/sec. If we take the value of ω_i we assumed previously, $\omega_i=5.5\times10^6$, we find from (57) that

$$m^2=3.0\times10^7.$$

The left-hand member of (58) is very small, while γ appears in the denominator of all the terms on the right. Thus, one solution is one in which γ is very large. If this is so, (58) becomes approximately

$$\gamma=\pm\left[m^2\left[1-\frac{1}{W^2-\left(\frac{\omega_{0i}}{\omega_i}\right)^2}\right]-\left(\frac{\omega_e}{\omega_i}\right)^2\right]^{\frac{1}{2}}\times\left[\frac{1}{1-\frac{1}{W^2}}\right]^2. \tag{60}$$

This can give either imaginary values of γ, or real values representing either increasing or decreasing waves. γ is infinite and changes from

real to imaginary at

$$W=1,$$
$$\omega=\omega_i.$$

Thus, near this value of W our assumption that γ is very large is justified. This is the ion plasma frequency which we previously estimated as 0.88 megacycles. Also, γ is infinite and changes from real to imaginary at

$$W=\frac{\omega}{\omega_i}=\frac{\omega_{0i}}{\omega_i},$$
$$\omega=\omega_{0i}.$$

This is the ion cyclotron frequency, which for 100 gauss is 10 kilocycles.

We see that increasing waves ($-\gamma$ real and positive) are to be expected in a beam surrounded by a conducting tube and confined by a magnetic field, and one of these is of a frequency near the ion plasma frequency while the other is near the ion cyclotron frequency. These are, of course, not the only values of γ, for (58) is of the sixth degree in γ. The other roots of the equation give unattenuated waves.

1.5 Summary of Theory

If we set up the linearized equations for an electron stream containing positive ions, we find that among the solutions there are waves which increase linearly with distance in the direction of electron flow. In both a one-dimensional case, or in the case of a beam surrounded by a conducting tube and confined by a magnetic field of any strength, such increasing waves occur at frequencies of the order of the ion plasma frequency, given by (13) and the ion cyclotron frequency given by (49). For physically reasonable conditions the first may be of the order of one megacycle while the second may be of the order of 10 kilocycles.

When the boundary conditions are imposed at the end of the tube at which electrons enter, it must, in general, be found that the small fluctuations present give rise to an increasing wave which will become much larger further along the stream. Thus, the existence of waves which grow in the direction of electron motion would seem to mean that disturbances at frequencies near the ion plasma frequency and the ion cyclotron frequency should always appear if the beam travels far enough. It is possible also that secondary electrons traveling backward along the beam might provide feedback and result in oscillation as opposed to mere amplification of disturbances.

If there is no damping and the ions have no d. c. velocities, the rate of increase of the waves becomes infinite at a certain frequency. It is shown that if the ions have a d. c. velocity the rate of increase does not become infinite. Presumably, damping of the ion motion, as, by collisions, would make the ion plasma frequency complex, representing a decaying oscillation, and would also preclude an infinite rate of increase of amplitude with distance.

Finally, non-linearities would soon limit the rate of increase along the tube.

2. CONCLUSIONS

Theory predicts that disturbances in an electron stream containing ions will build up in the direction of electron motion. Experiment shows the existence of oscillations of about the right frequency and having roughly the right properties to correspond with theory. Secondary electrons could carry disturbances back to the cathode end of the tube and result in oscillation rather than mere amplification of noise.

Application of the Laplace Transform in the Solution of Linear Integral Equations*

LAWRENCE BAYLOR ROBINSON[1]
Department of Physics, Howard University, Washington 1, D. C.
(Received August 11, 1947)

Integral equations are defined and references are given to the Laplace transform technique. Most of the operations used are illustrated through a solution of Abel's integral equation. It is shown that the Liouville-Neumann series follows logically from an operational solution of Volterra's integral of the second kind. Whittaker obtained solutions to the integral equation with the kernel expressed in the last three forms. His procedure was quite involved and it is shown here that the same solutions are obtained more directly through the operational calculus based on the Laplace transform.

INTRODUCTION

AN integral equation[2] is one in which the unknown function appears under the sign of integration. The integral equations of greatest importance to the physicists are those known as Abel's equations,

$$F(t)=\int_0^t (t-\theta)^{-b}Y'(\theta)d\theta, \quad (0<b<1), \quad (1)$$

and Volterra's equation of the second kind,

$$\Phi(t)=F(t)+\lambda\int_0^t \Phi(\theta)K(t-\theta)d\theta. \quad (2)$$

These equations have been solved by various means.[3] The suitable solutions for computation purposes are those given by Whittaker. The procedures whereby the solutions are obtained are quite involved and a special method of attack is given for each type of problem. A general method of solving equations such as (1) and (2) is given by the operational calculus, based on the Laplace transform.[4] Koizumi used this method to solve some integral equations and H. T. Davis[5] treated integral equations from other operational points of view. It is the purpose of this article to show that the use of the Laplace transform provides a more general method for solving some types of integral equations than is generally utilized, and that the solutions obtained by Whittaker are obtained by a "turn the crank procedure" through the operational calculus. This writer has employed the notations and methods of the operational calculus given by G. Doetsch in his *Theorie und Anwendung der Laplace Transformation*. For the reader unfamiliar with these methods, the clearly written and concise articles of L. A. Pipes[6] will provide a satisfactory background. Pipes defines the transform in a slightly, though not significantly, different manner from Doetsch, however. The operational technique has been used in most cases where the *kern* (also known as kernel and nucleus) of the equation $K(t-\theta)$ is given by a simple expression in closed forms. Herein the method is discussed when the kern is expressed in other ways.

ABEL'S INTEGRAL EQUATION

Equation (1), Abel's integral equation, has been solved by Whittaker and also by Koizumi, Doetsch, and Churchill using the operational calculus. A brief account of the solution is given here largely for purposes of defining the operations contained herein.

$$F(t)=\int_0^t (t-\theta)^{-b}Y'(\theta)d\theta, \quad (0<b<1), \quad (1)$$

* This article is taken from some of the lectures given by the author in a course in Mathematical Methods in Physics at Howard University.

[1] Present address: The Physical Sciences, The College University of Chicago, Chicago, Illinois.

[2] M. Bôcher, *An Introduction to the Study of Integral Equations* (Cambridge University Press, Teddington, England, 1909); W. V. Lovitt, *Linear Integral Equations* (McGraw-Hill Book Company, Inc., New York, 1924).

[3] H. Margenau and G. M. Murphy, *The Mathematics of Physics and Chemistry* (D. Van Nostrand Company, Inc., 1943), pp. 503–525; E. T. Whittaker, Proc. Roy. Soc. London (A)**94**, 367 (1917); S. Koizumi, Phil. Mag. **2**, 432 (1931).

[4] G. Doetsch, *Theorie und Anwendung der Laplace-Transformation* (Dover Publications, New York, 1943), pp. 155–167. R. V. Churchill, *Modern Operational Mathematics in Engineering* (McGraw-Hill Book Company, Inc., New York 1944), pp. 36–44.

[5] H. T. Davis, *The Theory of Linear Operators* (The Principia Press, Bloomington, Indiana, 1936), pp. 468–514.

[6] L. A. Pipes, J. App. Phys. **10**, 172, 260, 301 (1939).

is to be solved for $Y(t)$ where $Y'(t)$ is $dY(t)/dt$. This equation may also be written as

$$F(t)=t^{-b}*Y'(t), \tag{3}$$

where $F_1(t)*F_2(t)$ is defined as

$$F_1(t)*F_2(t)=\int_0^t F_1(t-\theta)F_2(\theta)d\theta. \tag{4}$$

It is also shown that $F_1(t)*F_2(t)\equiv F_2(t)*F_1(t)$. Equation (4) defines the *faltung* of the functions $F_1(t)$ and $F_2(t)$; this is also called the convolution integral. The Laplace transform of a function $F(t)$ is by definition

$$L\{F(t)\}=f(s)=\int_0^\infty e^{-st}F(t)dt, \tag{5}$$

where the real part of s is greater than zero, or $R(s)>0$. $F(t)$ must be sectionally or piece-wise continuous (*stückweise stetig*) and of exponential order so that this integral will converge as $t\to\infty$. The transform of the convolution is the product of the two individual transforms or

$$L\{F_1(t)*F_2(t)\}=f_1(s)f_2(s). \tag{6}$$

The transform of a derivative, as in Eq. (1) is shown to be

$$L\{F'(t)\}=sf(s)-F(+0), \tag{7}$$

where the second term on the right of (7) is read: the value of the function as t approaches zero from the right. When Eq. (4) is transformed, the following equation results:

$$f(s)=\Gamma(1-b)[1/s^b][y(s)-(Y(0)/s)]. \tag{8}$$

Equation (8) is then solved for $y(s)$ and the inverse transform taken, whence the required solution is obtained. The inverse transform is

$$L^{-1}\{x(s)\}=X(t)$$

$$=\frac{1}{2\pi i}\lim_{\beta\to\infty}\int_{\gamma-i\beta}^{\gamma+i\beta}\exp(st)x(s)ds, \tag{9}$$

where s is a complex variable and the integration is performed in the s-plane. From (8) it is apparent that $y(s)$ can be written as

$$y(s)=\frac{Y(0)}{s}+\frac{s^{-b}}{\Gamma(1-b)}f(s). \tag{10}$$

The inverse transform

$$L^{-1}\left\{\frac{s^{-b}}{\Gamma(1-b)}\right\}=\frac{t^b}{\Gamma(b)\Gamma(1-b)}=\frac{\sin b\pi}{\pi}t^b. \tag{11}$$

It is evident that

$$Y(t)=Y(0)+\frac{d}{dt}\frac{\sin b\pi}{\pi}\frac{1}{t^{-b}}*F(t), \tag{12}$$

or

$$Y(t)=Y(0)+\frac{\sin b\pi}{\pi}\frac{d}{dt}\int_0^t F(\theta)\frac{d\theta}{(t-\theta)^b}. \tag{13}$$

As was afore-mentioned, the above solution is well known and is given here only as the means of introducing the definitions of the operations.

VOLTERRA'S INTEGRAL EQUATION OF THE SECOND KIND

1. The Liouville—Neumann Series

Margenau and Murphy solve the Volterra integral equation of the second kind,

$$\Phi(t)=F(t)+\lambda\int_0^t\Phi(\theta)K(t-\theta)d\theta, \tag{2}$$

by the Liouville-Neumann series:

$$\Phi(t)=\sum_{n=0}^{\infty}\lambda^n\Phi_n(t), \tag{14}$$

where

$$\Phi_0(t)=F(t),$$

$$\Phi_1(t)=\int_0^t K(t-\theta)\Phi_0(\theta)d\theta,$$

$$\Phi_2(t)=\int_0^t K(t-\theta)\Phi_1(\theta)d\theta, \tag{15}$$

$$\cdots\cdots\cdots\cdots$$

$$\Phi_n(t)=\int_0^t K(t-\theta)\Phi_{n-1}(\theta)d\theta.$$

It is shown that the series (14) converges uniformly for $|\lambda|<1/Mt$ where M is some positive number. Equations (15) may be also written as

$$\Phi_r(t)=\int_0^t K(t-\theta)\int_0^{t_1}K(t_1-t)\cdots$$

$$\times\int_0^{t_{r-2}}K(t_{r-2}-t_{r-1})F(t_{r-1})dt_{r-1}\cdots dt_1d\theta. \tag{16}$$

Consequently, the solution to Eq. (1) may be written as

$$\Phi(t)=F(t)+\lambda\int_0^t K(t-\theta)\Phi(\theta)d\theta$$
$$+\lambda^2\int_0^t K(t-\theta)\int_0^{t_1} K(t_1-t)F(t)dtd\theta+\cdots+$$
$$+\lambda^n\int_0^t K(t-\theta)\int_0^{t_1} K(t_1-t)\cdots$$
$$\times\int_0^{t_{n-2}} K(t_{n-2}-t_{n-1})$$
$$\times F(t_{n-1})dt_{n-1}\cdots dt_1d\theta+\cdots. \quad (17)$$

Why one would seek the Liouville-Neumann series method as a solution to the equation is not immediately apparent, whereas the operational calculus yields precisely the same solution at once.

Taking the transform of both members of Eq. (2) yields

$$\phi(s)=f(s)+\lambda\phi(s)k(s), \quad (18)$$

whence

$$\phi(s)=\frac{f(s)}{1-\lambda k(s)}. \quad (19)$$

When $|\lambda k(s)|<1$, as is usually the case, Eq. (19) may be written as

$$\phi(s)=f(s)(1+\lambda k(s)+\lambda^2k^2(s)$$
$$+\cdots+\lambda^nk^n(s)+\cdots), \quad (20)$$

or

$$\phi(s)=f(s)\sum_{n=0}^{\infty}\lambda^nk^n(s). \quad (21)$$

The solution $\Phi(t)$ is found by taking the inverse transform of both sides of the equation. The result is

$$\Phi(t)=F(t)+\lambda\int_0^t K(t-\theta)F(\theta)d\theta+\cdots. \quad (17)$$

The solution obtained in this fashion is more apparent than those obtained without the use of the operational calculus.

2. Kernel Expressed as Sum of Exponentials

In physical problems, quite often the kernel can represent tabulated data at regular intervals. It is shown that when such is the case, the data may have an analytical representation as a sum of exponentials, or

$$K(t)=A_1e^{a_1t}+A_2e^{a_2t}+\cdots+A_ne^{a_nt}+\cdots, \quad (22)$$

where the constants are chosen so as to give the best representation of the numerical values.[7] When (22) is substituted in (2), Eq. (19) is obtained where

$$k(s)=\sum_{n=1}^{m}\frac{A_n}{(s-a_n)}. \quad (23)$$

Equation (19) then has the form

$$\phi(s)=\frac{f(s)}{1-\lambda\sum_{n=1}^{m}(A_n/s-a_n)}. \quad (24)$$

The inverse transform of $\phi(s)$ calculated by the inversion integral gives the solution to the problem. Whittaker gives a solution to the problem by a very involved procedure, the method of which is extremely difficult to follow. March and Weaver,[8] also without the use of the operational calculus, arrived at a solution to the problem by assuming that the solution would be given as a sum of exponentials and then evaluated the unknown constants. The inversion integral, applied to (24), gives a more direct solution. The solution is obtained with the aid of Cauchy's residue theorem.

$$\Phi(t)=\frac{1}{2\pi i}\int_{\gamma-i\infty}^{\gamma+i\infty}\frac{f(s)e^{st}ds}{\left(1-\lambda\sum_{n=1}^{m}\frac{A_n}{s-a_n}\right)} \quad (25)$$
$$=\sum_{n=1}^{m}\rho_n\exp(\alpha_nt),$$

where ρ_n is the residue of the denominator at the poles a_n and α_n is a zero of the denominator. The zeros of similar equations have been studied by Raleigh.[9] It is well known that the residues are given by the ratio $f(\alpha_n)/q'(\alpha_n)$, where $q'(\alpha_n)$ means the derivative of the denominator at α_n, and $f(\alpha_n)$ is the value of $f(s)$ at α_n. Equation (25)

[7] E. T. Whittaker and G. Robinson, *The Calculus of Observations*, (Blackie and Son, Limited, London and Glasgow, 1937), pp. 369–371.

[8] H. W. March and W. Weaver, Phys. Rev. **31**, 1072 (1928).

[9] Lord Raleigh, *Theory of Sound* (MacMillan Company, Ltd., London, 1896), Volume 1, p. 334.

is identical with the solution obtained by Whittaker and by March and Weaver.

3. Kernel Expressed as a Polynomial

When the nucleus is expressed as a polynomial,

$$K(t)=a_n t^n+a_{n-1}t^{n-1}+\cdots+a_0, \tag{26}$$

Eq. (19) becomes

$$\phi(s)=\frac{f(s)}{1-a_n\dfrac{n!}{s^{n+1}}-a_{n-1}\dfrac{(n-1)!}{s^n}-\cdots}. \tag{27}$$

The above equation may be rewritten as

$$\phi(s)=\frac{f(s)}{\left(\dfrac{1}{s}-\lambda_1\right)\left(\dfrac{1}{s}-\lambda_2\right)\cdots\left(\dfrac{1}{s}-\lambda_n\right)}, \tag{28}$$

where the λ's are the zeros of

$$1-a_n\frac{n!}{s^{n+1}}-a_{n-1}\frac{(n-1)!}{s^n}-\cdots=0. \tag{29}$$

An alternate form of (28) is

$$\phi(s)=\frac{s^n f(s)}{(-1)^n\lambda_2\lambda_1\cdots\lambda_n\left(s-\dfrac{1}{\lambda_2}\right)\left(s-\dfrac{1}{\lambda_2}\right)\cdots\left(s-\dfrac{1}{\lambda_n}\right)}, \tag{30}$$

or

$$\phi(s)=\frac{L\{F^{(n)}(t)\}+s^{n-1}F(+0)+s^{n-2}F'(+0)+\cdots}{(-1)^n\left[\prod_{i=1}^{n}\lambda_i\right]\left(s-\dfrac{1}{\lambda_1}\right)\left(s-\dfrac{1}{\lambda_2}\right)\cdots\left(s-\dfrac{1}{\lambda_n}\right)}. \tag{31}$$

When the numerator is of lower degree than the denominator (this is the only case discussed here), the nth derivative of $F(t)$, namely, $F^{(n)}(t)$, vanishes and the numerator becomes a polynomial in s whose highest term is not greater than s^{n-1}. The inversion integral of $\phi(s)$ yields

$$\Phi(t)=A_0+A_1e^{b_1t}+A_2e^{b_2t}+\cdots+A_ne^{b_nt}, \tag{32}$$

where $b_i=1/\lambda_i$ (i.e., the zeros of the denominator in (31)). The A's are determined as in (25). Equation (32) was derived assuming that there are no repeated roots. The solution of inversion integral with repeated roots in the denominator is known and, consequently, (32) becomes

$$\Phi(t)=e^{bt}\sum_{n=1}^{r}\frac{F^{(r-n)}(\lambda)t^{n-1}}{(r-n)!(n-1)!}+\sum_{i=1}^{m}A_ie^{b_it}, \tag{33}$$

where the first term on the right corresponds to a factor $(s-b)^r$.

4. Kernel Expressed as Infinite Series

When the kernel is expressed as

$$K(t)=K_0+K_1t+\frac{K_1t^2}{2!}+\cdots+\frac{K_nt^n}{n!}+\cdots, \tag{34}$$

the solution of the Volterra integral equation of the second kind may be written in a form similar to (33) or it may be expressed in a different form as shown below. Equation (19) is

$$\phi(s)=\frac{f(s)}{1-K_0'/s-K_1'/s^2-K_2'/s^3-\cdots-K_{n-1}'/s^n-\cdots}, \tag{35}$$

where $K_i'=\lambda K_i$. Equation (35) may be rewritten in the form below:

$$\phi(s)=\frac{f(s)}{1-K_0'p-K_1'p^2-K_2'p^3-\cdots-K_{n-1}'p^n-\cdots}, \tag{36}$$

where $p_i=1/s_i$. The zeros of the infinite series in the denominator may be found by an extension of Graeffe's root squaring method.[10]

[10] Reference 7, pp. 118–123.

When the factors are found, (36) becomes

$$\phi(s)=\frac{f(s)}{(p-a_1)(p-a_2)\cdots(p-a_n)\cdots}, \tag{37}$$

or

$$\phi(s)=\frac{f(s)}{(-1)^n\left[\prod_{i=1}^{\infty}a_i\right]\left(1-\frac{p}{a_1}\right)(1-p/a_2)\cdots\left(1-\frac{p}{a_n}\right)\cdots}. \tag{38}$$

When conditions are such that each factor in the denominator can be expanded as $(1-x)^{-1}$, then (38) is written as

$$\phi(s)=\frac{f(s)}{(-1)^n\cdots}\frac{1}{\prod_{i=1}^{\infty}a_i}\times\left\{\left(1+\frac{p}{a_1}+\frac{p^2}{a_1{}^2}+\cdots\right)\cdots\times\left(1+\frac{p}{a_n}+\frac{p^2}{a_n{}^2}+\cdots\right)\cdots\right\}, \tag{39}$$

whence

$$\phi(s)=\frac{f(s)}{(-1)^n\cdots}\frac{1}{\prod_{i=1}^{\infty}a_i}\times(1+A_1p+A_2p^2+\cdots+A_np^n+\cdots), \tag{40}$$

where the A's represent the sum of the coefficients of like powers of p. Since p is $1/s$, it is apparent that the inverse transform of $\phi(s)$ in (40) is given by

$$\Phi(t)=B_0F(t)+B_1\int_0^t F(\theta)d\theta+B_2\times\int_0^t\int_0^\theta F(\lambda)d\lambda d\theta+\cdots. \tag{41}$$

An alternate form of the solution is obtained by writing (40) as

$$\phi(s)=M\left(f(s)+\frac{1}{s}f(s)+\frac{1}{s}\frac{f(s)}{s}+\frac{1}{s}\frac{f(s)}{s^2}+\cdots\right). \tag{42}$$

Then

$$\Phi(t)=M\left[F(t)+\int_0^t K(t-\theta)F(\theta)d\theta\right], \tag{43}$$

where

$$K(t)=\left(1+A_1t+A_2\frac{t^2}{2!}+A_3\frac{t^3}{3!}+\cdots+A_n\frac{t^n}{n!}+\cdots\right). \tag{44}$$

Equation (44) is identical with the solution obtained by Whittaker.

REMARKS

Some of the examples have been given which show the utility of the operational calculus, based on the Laplace transform, in solving integral equations. The technique has the advantage over other proceduresin that the operational calculus gives the solution by an automatic method.

Response of Linear Resonant Systems to Excitation of a Frequency Varying Linearly with Time[1]

GUNNAR HOK
Wesleyan University, Middletown, Connecticut
(Received August 13, 1947)

A general solution of this problem is obtained by means of Laplacian transforms. The resulting complex function is evaluated numerically, and universal response curves are presented in order to facilitate the application of the solution to simple or complicated electrical networks as well as to other resonant systems represented by equivalent networks.

MANY modern instruments are designed to plot on a cathode-ray screen the amplitude of a vibration or oscillation as a function of the frequency of excitation. Such instruments incorporate narrow-band resonant systems that in operation are exposed to forces of varying frequency; usually the frequency varies linearly with time, synchronously with the left-to-right motion of the spot on the cathode-ray screen. The author first met this problem in connection with spectrum analyzers for study of the characteristics of microwave oscillators developed during the war. Later, the design of an instrument to portray the admittance spectra of piezoelectric resonators gave the impetus to an attempt to find a formal solution of this problem.

Statements that such a solution has not been known have appeared in the current literature.[2] However, after this work had been essentially completed and presented at the Washington meeting of the Physical Society, the author's attention was directed to an earlier paper on a similar problem in mechanical engineering.[3] Although for this reason complete novelty cannot be claimed, it is believed that a comprehensive study of this problem may be of value because of the frequent applications in present electronic measuring techniques.

The following study is limited to such cases where the resonant system can be represented by a lumped-constant equivalent network (impedance operator Z in Fig. 1a). We consider only systems with relatively low losses, so that the resonance curve of each mode of vibration of the system never extends over more than a few percent of the frequency. This is not a necessary limitation; the mathematical procedure can be easily generalized to include lossy systems and large frequency variations. In a very large class of applications, however, this limitation offers the advantage that universal resonance curves or response curves plotted in dimensionless variables can be applied with very good approximation.[4]

The frequency variation is not necessarily periodic; in fact, photographic recording is very often carried out with one single sweep of the frequency through the admittance band of the resonator. It is therefore logical to attack the subject as a problem in transient circuit analysis.

It is convenient to represent the excitation by a complex vector

$$E\exp[j\varphi(t)]=E\exp[j(\omega_0 t+\epsilon t^2)], \qquad (1)$$

of a constant amplitude E and an instantaneous angular frequency

$$\omega=d\varphi/dt=\omega_0+2\epsilon t. \qquad (2)$$

The differential equation for the simple circuit shown in Fig. 1b is then

$$L\frac{di}{dt}+Ri+\int_{-\infty}^{t}\frac{idt}{C}=E\exp[j(\omega_0 t+\epsilon t^2)]. \qquad (3)$$

Before proceeding with the solution it may be worth while to note an interesting equivalence.

[1] This investigation has been carried out in connection with Contract No. W28-003 sc-1556 with the U. S. Signal Corps. The fundamental solution of the problem was given in the second semi-annual report of July 9, 1946, under that contract. A brief paper on this subject was presented at the meeting of the American Physical Society in Washington, D. C., May 1, 1947.

[2] E. M. Williams, "Radio-frequency spectrum analyzers," Proc. I.R.E., Vol. 34, 18–22 (January 1946).

[3] F. M. Lewis, "Vibration during acceleration through a critical speed," Trans. of the Am. Soc. Mech. Eng. APM 54-24, 253 (1932). The author is indebted to Dr. H. Ekstein of the Armour Research Foundation for this and one later reference (7).

[4] F. E. Terman, *Radio Engineer's Handbook* (McGraw-Hill Book Company, Inc., New York, 1943), p. 136.

Let us change the time variable according to the equation

$$t=\tau-(\epsilon/\omega_0)\tau^2. \tag{4}$$

Remembering that ϵt is always very small compared to ω_0, we can also write

$$\tau\cong t+(\epsilon/\omega_0)t^2, \tag{5}$$

and Eq. (3) is transformed to (6)

$$\frac{L}{1-2(\epsilon/\omega_0)\tau}\cdot\frac{di}{d\tau}+Ri + \int_{-\infty}^{\tau}\frac{i(1-2(\epsilon/\omega_0)\tau)}{C}d\tau\cong E\exp[j\omega_0\tau]. \tag{6}$$

The equivalence of (3) and (6) means that the same solution will be obtained whether the resonance frequency of the system or the frequency of excitation is varied, at least if the relative increments of inductance and capacitance in the former alternative are equal. This point may seem trivial but the author has heard it seriously questioned and believes that it well justifies its place here.

The solution of the general problem presented in Fig. 1a can be obtained conveniently by the method of Laplacian transforms. The differential equations are written down for all meshes of the network Z, and the transform is calculated for each term in all the equations under the assumption that the network is initially at equilibrium. The system is then solved for the transform of the current

$$\bar{\imath}=\frac{\bar{e}}{Z(p)}=\frac{1}{Z(p)} \times\int_{-\infty}^{+\infty}E\exp[j(\omega_0T+\epsilon T^2)]\exp(-pT)dT. \tag{7}$$

If Z is a passive lumped-constant network, $Z(p)$ is the quotient of two polynomials of p, and its reciprocal can be expanded according to the familiar methods of operational and transform calculus

$$\frac{1}{Z(p)}=\frac{g(p)}{h(p)}=\sum_{\nu=1}^{n}\frac{g(p_\nu)}{h'(p_\nu)(p-p_\nu)}, \tag{8}$$

where $p_1\cdots p_n$ are the roots of the equation $h(p)=0$. We consider only circuits for which this equation has no multiple roots.[5]

Equation (7) thus becomes

$$\bar{\imath}=\sum_{\nu=1}^{n}\frac{g(p_\nu)}{h'(p_\nu)(p-p_\nu)} \times\int_{-\infty}^{+\infty}E\exp[j(\omega_0T+\epsilon T^2)]\exp(-pT)dT. \tag{9}$$

The inverse transform is obtained as the sum of the Bromwich-Fourier integrals formed from the terms of the right member of Eq. (9).

$$i(t)=\sum_{\nu=1}^{n}\frac{1}{2\pi j}\frac{g(p_\nu)}{h'(p_\nu)}\int_{Br}\frac{\exp(pt)}{p-p_\nu} \times\int_{-\infty}^{+\infty}E\exp[j(\omega_0T+\epsilon T^2)] \times\exp(-pT)dTdp \tag{10}$$

$$=\sum_{\nu=1}^{n}\frac{g(p_\nu)}{h'(p_\nu)}\int_{-\infty}^{+\infty}E\exp[j(\omega_0T+\epsilon T^2)] \times\left\{\frac{1}{2\pi j}\int_{Br}\frac{\exp[p(t-T)]}{p-p_\nu}dp\right\}dT. \tag{11}$$

The Bromwich-path integrals are equal to their respective residues $\exp[p_\nu(t-T)]$ for $t>T$ and zero for $t<T$. We can therefore write

$$i(t)=\sum_{\nu=1}^{n}\frac{g(p_\nu)}{h'(p_\nu)}\int_{-\infty}^{t}E\exp[j(\omega_0T+\epsilon T^2)] \times\exp[p_\nu(t-T)]dT. \tag{12}$$

At this point the dimensionless variable is introduced that will give the universal response

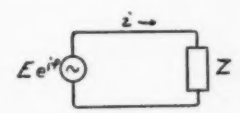

(a)

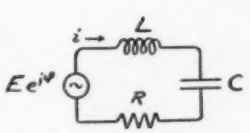

(b)

FIG. 1. Circuit diagrams.

[5] How to cope with multiple roots in transform calculus is well known and does not require special attention here

curves for this type of excitation:

$$\gamma=\alpha+j\beta=\tfrac{1}{2}\epsilon^{-\frac{1}{2}}(j\omega_0-p_\nu)+j\epsilon^{\frac{1}{2}}T. \quad (13)$$

When γ is used outside the integration sign, T is replaced by t.

Equation (12) now assumes the following appearance

$$i(t)=E\exp[j(\omega_0 t+\epsilon t^2)]\sum_{\nu=1}^{n}\frac{g(p_\nu)}{h'(p_\nu)}\cdot\frac{1}{j\epsilon^{\frac{1}{2}}}$$

$$\times\exp(j\gamma^2)\int_{(0-j\infty)}^{\gamma}\exp(-j\gamma^2)d\gamma, \quad (14)$$

$$i(t)=E\exp[j(\omega_0 t+\epsilon t^2)]\sum_{\nu=1}^{n}\frac{g(p_\nu)}{\epsilon^{\frac{1}{2}}h'(p_\nu)}Fr(\gamma). \quad (15)$$

The lower limit of the integral in Eq. (14) is not strictly in accord with the change of variable in Eq. (12), but it is easily seen that any point on the quartcircle between $(\infty-j\cdot 0)$ and $(0-j\infty)$ can be used as a lower limit without changing the value of the function.

The solution is thus obtained in terms of the excitation vector and a function $Fr(\gamma)$. In order to apply Eq. (15) to any specific problem we must have tables or graphs of this function for all practical values of γ. The remaining part of this paper is largely devoted to a study of this function

$$Fr(\gamma)=-j\exp(j\gamma^2)\int_{0-j\infty}^{\gamma}\exp(-j\gamma^2)d_\gamma. \quad (16)$$

The integral is related to the error integral and Fresnel's integrals, which have unfortunately not been tabulated to any appreciable extent for complex values of the variable.[6,7] As this function is likely to find extensive use in the future a convenient name and symbol are desirable. The author suggests the name *Fresnel function* or *fresneloid* and the symbol $Fr(\gamma)$.

In order not to make the discussion of the properties of the Fresnel function too abstract we shall introduce this function in the form of response curves for the simple circuit of Fig. 1b. Here

$$Z(p)=(L/p)(p^2+2\delta-\omega_1^2), \quad (17)$$

$$\left.\begin{matrix}p_1\\p_2\end{matrix}\right\}=-\delta\pm j\omega_1=-\frac{R}{2L}\pm j\left(\frac{1}{LC}-\frac{R^2}{4L^2}\right)^{\frac{1}{2}}. \quad (18)$$

For simplicity, ω_0 can be taken to be $=\omega_1$, the resonance frequency of the circuit. This means that we arbitrarily use negative as well as positive values of time and stipulate that $t=0$ when the excitation frequency coincides with the resonance frequency of the system.

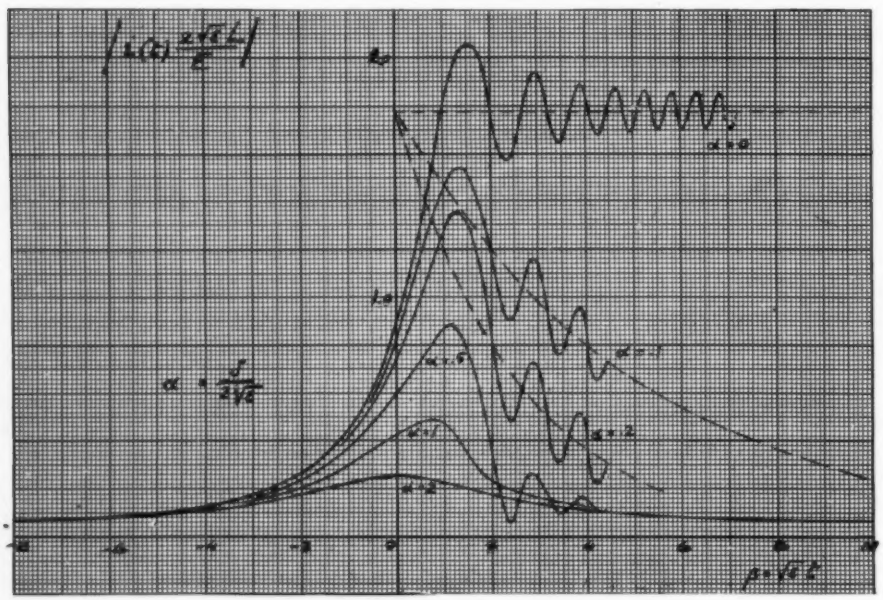

FIG. 2. Universal response curves for a resonant system excited by a linearly varying frequency (amplitude only).

[6] E. Jahnke and F. Emde, *Tables of Functions* (Dover Publications, New York, 1943), pp. 23–40.
[7] J. Barkley Rosser, "Theory and applications of $\int_0^z \exp(-x^2)dx$," OSRD 5861.

Thus

$$\gamma_1 = \tfrac{1}{2}\delta\epsilon^{-\frac{1}{2}} + j\epsilon^{\frac{1}{2}}t, \tag{19}$$

$$\gamma_2 = \tfrac{1}{2}\delta\epsilon^{-\frac{1}{2}} - j(\omega_0\epsilon^{-\frac{1}{2}} + \epsilon^{\frac{1}{2}}t). \tag{20}$$

According to our assumptions, the imaginary component of γ_2 approaches minus infinity and the corresponding integral zero. The solution is, therefore,

$$i(t) = E\exp[j(\omega_0 t + \epsilon t^2)]\frac{1}{2\epsilon^{\frac{1}{2}}L}Fr(\gamma), \tag{21}$$

$$\gamma = \alpha + j\beta = \tfrac{1}{2}\delta\epsilon^{-\frac{1}{2}} + j\epsilon^{\frac{1}{2}}t. \tag{22}$$

The definition of γ in Eq. (13) has purposely been chosen such that α and β are proportional to and have the same sign as the resistance and the steady-state reactance of the circuit at the instantaneous frequency.

If γ is large (α large, ϵ small) the following approximate solution results

$$i(t) \cong E\exp[j(\omega_0 t + \epsilon t^2)]\cdot\frac{1}{2j\epsilon^{\frac{1}{2}}L}\cdot\frac{1}{-2j\gamma}$$

$$\cong \frac{E\exp[j(\omega_0 t + \epsilon t^2)]}{R + 4j\epsilon tL} \cong \frac{E\exp[j(\omega_0 t + \epsilon t^2)]}{R + jX}. \tag{23}$$

The solution is thus consistent with the obvious requirement that for very slow frequency variation the current at any instant shall be equal to the expected steady-state current at that instantaneous frequency.

Figure 2 presents the universal response curves in terms of dimensionless variables.[8] In other words, it is the amplitude of the Fresnel function in terms of $\gamma = \alpha + j\beta$. The real part, α, determines the character of the curve while β gives the time scale of the curve. In any design problem involving the kind of excitation considered here α is the crucial parameter. According to Eq. (22), α is the logarithmic decrement divided by the square root of twice the rate of change of the angular frequency (the rate of change $= 2\epsilon$ according to Eq. (2)). The time scale is the square root of half the rate of change of the angular frequency. The group of curves of the current in the circuit, as shown in Fig. 2, would be observed if the rate of change of the frequency were kept

[8] Some of the expansions used to calculate these curves are quoted in the Appendix to this paper.

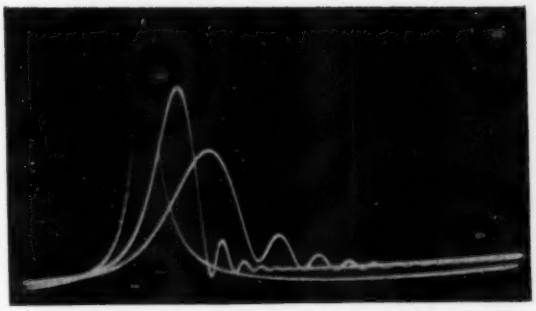

Fig. 3. Observed response of a piezoelectric resonator to excitation of linearly varying frequency.

constant and the resistance varied from one curve to the other. If the resistance were constant and the frequency variation 2ϵ were changed, the actual response would have to be obtained by dividing both coordinates in the diagram by the value of $\epsilon^{\frac{1}{2}}$ for each curve. The order of the curves would then be reversed, the one with the largest α reaching the highest maximum. This is the way the oscillograms in Fig. 3 have been produced. The resonant system for which these curves were recorded is the fundamental mode of vibration of an AT-cut quartz plate excited by a linearly varying frequency of three consecutively different rates of change. The top curve shows a perfectly symmetrical admittance curve obtained at slow sweep, while the other two represent α-values in the neighborhood of 0.5 and 0.2, respectively.

The curves in Fig. 2 give information only about the amplitude of the current. For most calculations it is necessary also to know the phase relations between the current and the exciting voltage. Curves of this phase angle or of the in-phase and quadrature components of the current are very inconvenient to plot and to use because the periodic components are much larger than in Fig. 2, even predominant for small values of α. It is possible, however, to find a function $\Phi(\gamma)$ that has no appreciable periodic components and is continuous for all values of α. Such a function is defined by the equations

$$\Phi(\gamma) = Fr(\gamma) \quad \text{for} \quad \beta < 0, \tag{24}$$

$$\Phi(\gamma) = Fr(\gamma) - (j\pi)^{\frac{1}{2}} \times \exp(j\gamma^2)[1 - \exp(j\beta^2)] \quad \text{for} \quad \beta > 0. \tag{25}$$

It should be pointed out that it is not possible to separate the "forced" and "free" oscillations

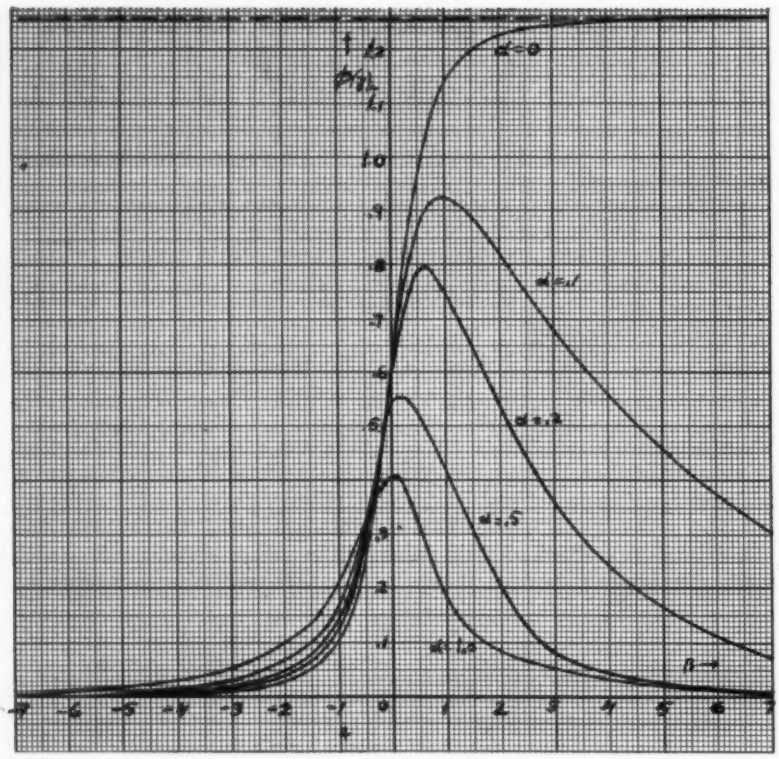

FIG. 4. Graph of the real part of the function $\phi(\gamma)$.

in terms of simple functions. The function $\Phi(\gamma)$ is introduced for practical, not for theoretical reasons. The curves of the real and imaginary components of $\Phi(\gamma)$ in Figs. 4 and 5 make it possible to calculate the in-phase and quadrature components of the current from Eqs. (24) and (25).

The physical interpretation of the response of the resonant circuit is simplest for the ideal case of $R=0$. The reactance of the circuit suddenly changes sign when the frequency of excitation passes through the resonance frequency. This produces a transient oscillation of the latter frequency and of an amplitude equal to twice the current at that moment. Because of the absence of resistance this transient is not attenuated, and it produces beats with the current of the excitation frequency.

In this case, γ is a purely imaginary quantity, and the current of the excitation frequency can easily be calculated from tables of Fresnel's integrals. The curve for $\alpha=0$ in Fig. 2 shows the total amplitude of the current, including the transient as well as the "forced" oscillation. In Figs. 4 and 5 the forced oscillations are represented by the distance from the curves for $\alpha=0$ to the β-axis for negative β, and by the distance from these curves to the dashed line for positive β. The dashed line represents the amplitude of the transient when $\alpha=0$. Both the real and the imaginary components of the forced oscillations are in this case antisymmetrical with respect to the point $\beta=0$, $\Phi=0$, and the transient oscillation is:

$$\exp(p_1 t)\left\{\int_{-\infty}^{0}\exp(j\beta^2)d\beta+\int_{0}^{\infty}\exp(j\beta^2)d\beta\right\}=2\frac{(j\pi)^{\frac{1}{2}}}{2}\exp(p_1 t). \quad (26)$$

When the circuit has resistance ($\alpha>0$) the reactance does not change abruptly; consequently, the transient builds up gradually. The transient is, of course, exponentially attenuated. As is indicated by dashed curves in Fig. 2, the exponentials extrapolated back to $\beta=0$ still have the virtual amplitude $\pi^{\frac{1}{2}}$. As α is increased to 2 and higher, the beats disappear and the curves become symmetrical admittance curves. Figures 4 and 5 show how the current components under the same conditions approach the conductance

and susceptance curves of the simple resonant circuit. A better demonstration of the asymptotic approach of the response curves to the admittance curves for steady state is given by Figs. 6 and 7. In Fig. 6 the real and imaginary components of the current at the steady-state half-power points are plotted in percent of their steady-state values. Similarly, in Fig. 7 the current components at the resonance frequency are plotted in percent of the steady-state resonance current. It is interesting to note that at the lower half-power point the current leads the voltage by 45° regardless of the α-value. A corresponding condition does not prevail at the higher half-power point, where both a free oscillation and a forced oscillation of different frequencies are present.

The current at the lower half-power point is obtained by setting $\beta = -\alpha$ in Eq. (21). The result is

$$I_{-\frac{1}{2}} = \frac{E}{2\epsilon^{\frac{1}{2}}L} j^{\frac{1}{2}} \exp(\delta^2) \int_{\delta}^{\infty} \exp(-\delta^2) d\delta \qquad (\delta = \alpha\sqrt{2}), \quad (27)$$

and at the upper half-power point ($\beta = \alpha$)

$$I_{+\frac{1}{2}} = \frac{E}{2\epsilon^{\frac{1}{2}}L} \cdot j^{\frac{1}{2}} \times \exp(-\delta^2)\left(\tfrac{1}{2}\pi^{\frac{1}{2}} - j\int_0^{\delta} \exp(\delta^2) d\delta\right). \quad (28)$$

Tables of these integrals are available in the literature.[9]

The current at resonance frequency ($\beta = 0$) is

$$I_0 = \frac{E}{2\epsilon^{\frac{1}{2}}L} \cdot j \exp(j\alpha^2) \int_{\alpha}^{\infty} \exp -(j\alpha^2) d\alpha. \quad (29)$$

Since α is real, this expression can be used for numerical computations with the help of tables of Fresnel's integrals.[10]

Figure 6 is of particular interest because it indicates how large α has to be for the response curve to be symmetrical. The half-power points are on the steepest part of the admittance curve and therefore give a very sensitive criterion on

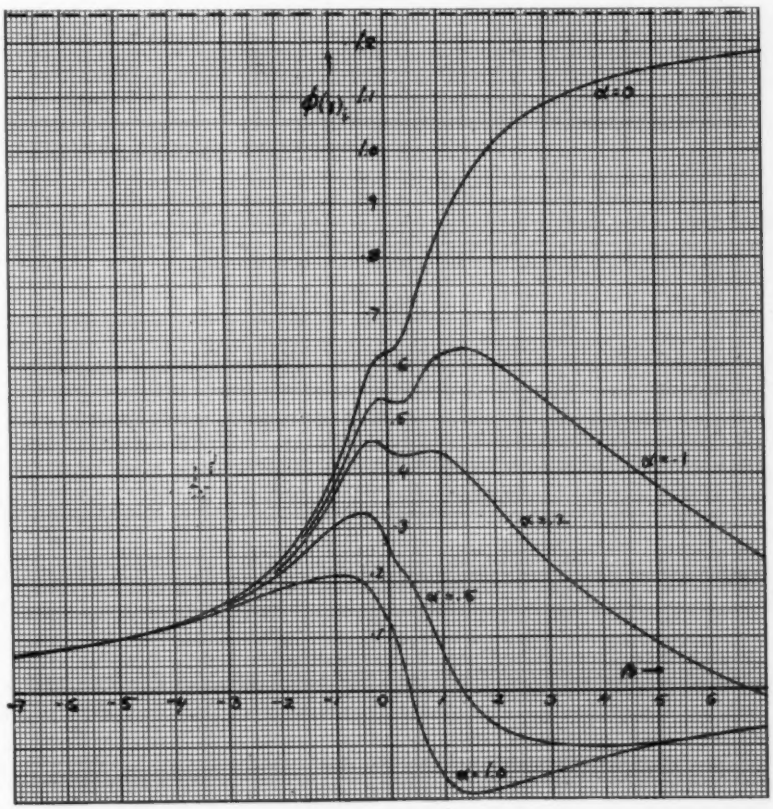

FIG. 5. Graph of the imaginary part of the function $\phi(\gamma)$.

[9] Reference 6, pp. 24 and 32.
[10] Reference 6, pp. 34–35.

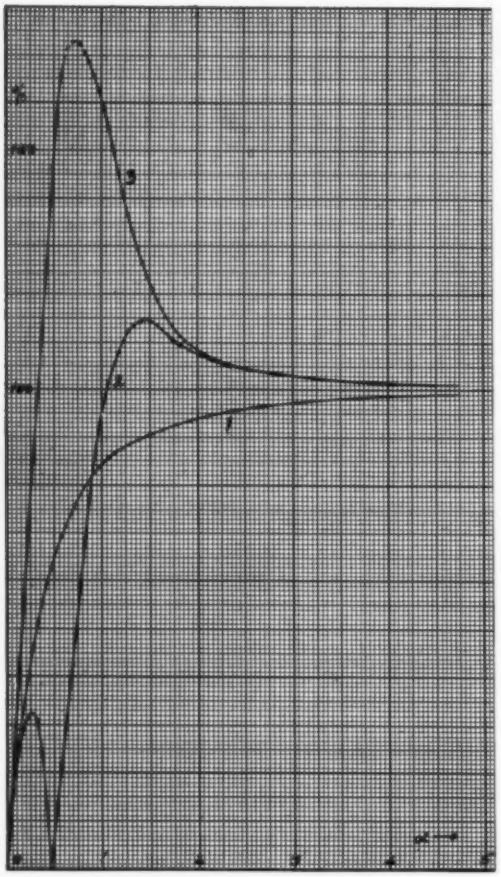

FIG. 6. Curve 1: The current (each component) at the time when $\beta = -\alpha$ in percent of the corresponding steady-state value. Curve 2: The imaginary component of the current at the time $\beta = \alpha$ in percent of the corresponding steady-state value. Curve 3: The real component under the same conditions as curve 2.

symmetry. At $\alpha = 2$ the maximum deviation of the current from the ideal curve is nearly 9 percent. At $\alpha = 3.5$ the deviation is still 2 percent. Figure 7 shows that the quadrature component at the resonance frequency is an even more sensitive criterion. At $\alpha = 3.5$ this component is still 4 percent of the steady-state resonance current.

A graph like Fig. 2, preferably with curves for a larger number of α-values, gives a considerable amount of information about the response of a single circuit. In Fig. 8 the "apparent band width" has been plotted *versus* α as extracted from Fig. 2. By apparent band width we mean the distance in frequency between points of an amplitude of .707 of the maximum. Similar

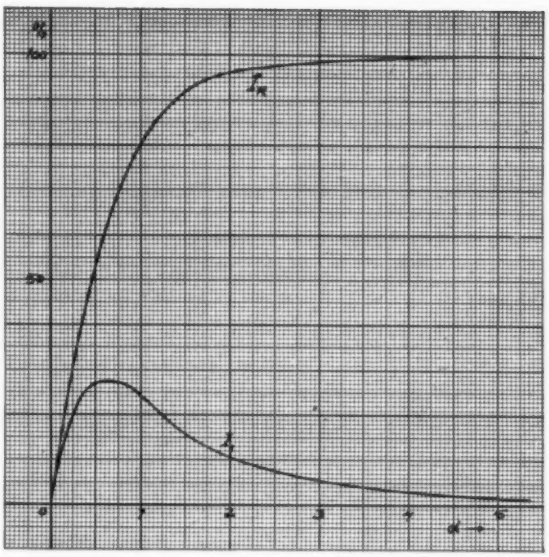

FIG. 7. The real and imaginary components of the current at the instant when the excitation frequency is equal to the resonance frequency.

curves could be shown for the peak current and the displacement of the peak from steady-state resonance as functions of α.

However, a graph like Fig. 2 does not give sufficient information when a network is considered that contains more than one mesh so that not only the amplitude but also the phase of the current must be taken into account when the components are added up. Equation (26) and Figs. 4–5 furnish means to find the in-phase and quadrature components of the current. Because the function $\Phi(\gamma)$ is continuous and non-periodic it is easy to plot with fair accuracy, and reasonably correct interpolations can be made between the curves. With sufficiently large families of curves of this kind, the current components can easily be found for any values of α and β, so that the currents corresponding to various roots p_1, p_2, p_3, etc. can be calculated and combined to form the solution for a multi-mesh network.

The curves given here are few and far between and computed with slide-rule accuracy only. The complete mapping of this function is a task for a large-scale calculating machine. However, the applications usually dictate the small deviations from the steady-state response curves that can be tolerated, and the problem is only to adjust the α-values so that these tolerances are met.

Empirical figures have of course been found and published several years ago.[2]

Some numerical illustrations of the application to a single-mesh circuit may be of interest. At a frequency of 2 Mc per second and a frequency variation of 100 kc per second the maximum displacement of the peak towards higher frequencies, which occurs at zero resistance, is about $1.5\epsilon^{\frac{1}{2}}/2\pi$ or 134 cycles per second. If α shall remain $\geqq 2$, the Q of the circuit must not exceed 5000. A circuit with a Q of 11,000 will appear to have a band width of 207 cycles per second instead of 180; a circuit with a $Q=22{,}000$ will seem to have 147-cycle band width instead of 45. The peak current will in these cases be reduced to about 95 and 88 percent, respectively, of the steady-state value. These figures have been chosen with piezoelectric resonators in mind, which explains the rather high Q's.

Equation (12) can be generalized to apply to all transient frequency modulation that can be represented by an excitation vector of the form

$$\varepsilon = E\exp[j\{\omega_0 t+f(t)\}]. \tag{30}$$

It is helpful to assume, as before, that

$$(df/dt)\ll\omega_0. \tag{31}$$

Now

$$i(t)=\sum_{\nu=1}^{n}\frac{g(p_\nu)}{h'(p_\nu)}\int_{-\infty}^{t}E\exp[j(\omega_0 T+f(T))]\times\exp[p_\nu(t-T)]dT, \tag{32}$$

or

$$i(t)=E\exp[j(\omega_0 t+f(t))]\sum_{\nu=1}^{n}\frac{g(p_\nu)}{h'(p_\nu)}\times\exp[-\varphi(t)]\int_{-\infty}^{t}\exp[\varphi(T)]dT, \tag{33}$$

where

$$\varphi(T)=(j\omega_0-p_\nu)T+jf(T). \tag{34}$$

In this way one can quickly reach the core of the problem which is the evaluation of a complex function of a certain general type.

It is possible to expand this general function by repeated integration by parts. However, the resulting series will usually have a limited region of convergence or semiconvergence.

$$e^{-\varphi}\int_{-\infty}^{t}e^{\varphi}dT\cong\frac{1}{j\omega_0-p_\nu}-j\frac{f'(t)}{(j\omega_0-p_\nu)^2}-\frac{f'(t)^2+f''(t)}{(j\omega_0-p_\nu)^3}+j\frac{f'(t)^3+3f'(t)f''(t)+f'''(t)}{(j\omega_0-p_\nu)^4}+\cdots. \tag{35}$$

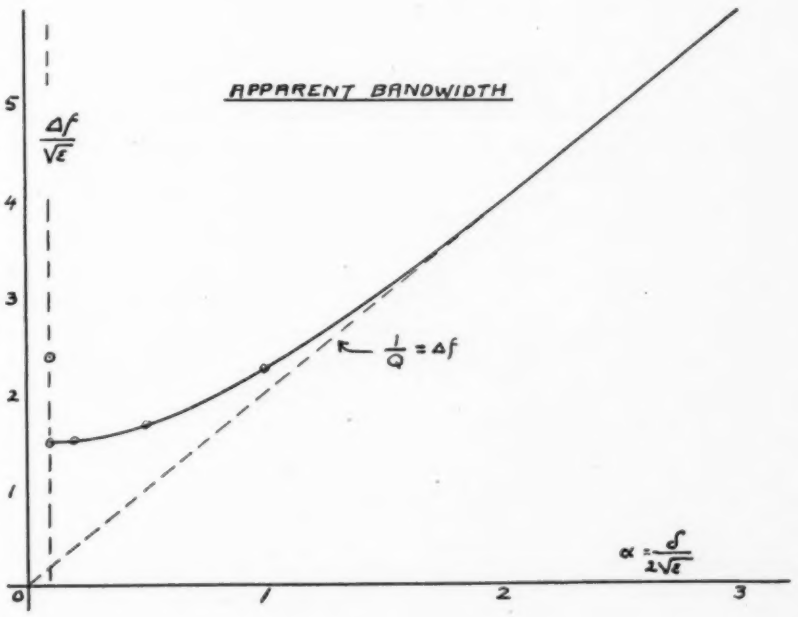

FIG. 8. The apparent band width of a resonant circuit to excitation of linearly varying frequency.

If $f(t)$ is an even function of t the response of a resonant circuit will have many common features with the previous problem where $f(t)=\epsilon t^2$.

In the extreme case of zero resistance the integral is again simplified and

$$\int_{-\infty}^{0}\exp[jf(T)]dT=\int_{0}^{\infty}\exp[jf(T)]dT=A. \quad (36)$$

We assume, as before, $\omega_0=\omega_1$ and "steady-state resonance" at $t=0$. Then there is a transient

$$=2A\exp(p_1 t) \quad (37)$$

generated at $t=0$, and one objective of design is usually to adjust the Q of the circuit so that this transient is negligible. Other objectives may concern the phase angle between excitation and response, which depends not only on the circuit constants and on the instantaneous frequency of the excitation but also on the rate of change of the latter. Numerical evaluation of the complex function or an experimental investigation would be required to obtain detailed information on these questions.

The author acknowledges gratefully the helpful interest of Dr. K. S. Van Dyke throughout the time this work has been in progress, as well as a stimulating discussion of the subject with Dr. H. Ekstein of the Armour Research Foundation.

APPENDIX

The basic expansion of the Fresnel function, convergent for all values of γ, is

$$\begin{aligned}Fr(\gamma)&=\exp(j\gamma^2)\left\{\frac{(j\pi)^{\frac{1}{2}}}{2}-j\gamma\right.\\&\left.-\frac{\gamma^3}{3}+j\frac{\gamma^5}{2!5}+\frac{\gamma^7}{3!7}-\cdots\right\}\\&=\exp(j\gamma^2)\left\{\tfrac{1}{2}(\pi/2)^{\frac{1}{2}}+r\sin\theta\right.\\&-\frac{r^3}{3}\cos3\theta-\frac{r^5}{2!5}\sin5\theta+\cdots\\&+j(\tfrac{1}{2}(\pi/2)^{\frac{1}{2}}-r\cos\theta\\&\left.-\frac{r^3}{3}\sin3\theta+\frac{r^5}{2!5}\cos5\theta+\cdots)\right\}, \quad (38)\end{aligned}$$

where $\gamma=r\exp(j\theta)$.

For large values of γ the number of terms that have to be included to get a satisfactory approximation becomes prohibitive. A semiconvergent series in falling powers of γ can then be used.

$$\begin{aligned}Fr(\gamma)&\cong\frac{1}{2\gamma}-j\frac{1}{4\gamma^3}-\frac{3}{8\gamma^5}+j\frac{3\cdot5}{16\gamma^7}+\frac{3\cdot5\cdot7}{32\gamma^9}-\cdots\\&\cong\frac{1}{2r}\cos\theta-\frac{1}{4r^3}\sin3\theta-\frac{3}{8r^5}\cos5\theta+\cdots\\&+j\left(-\frac{1}{2r}\sin\theta-\frac{1}{4r^3}\cos3\theta\right.\\&\left.+\frac{3}{8r^5}\sin5\theta+\cdots\right). \quad (39)\end{aligned}$$

Other expressions obtained by contour integration, Taylor's expansion, etc, have also been used, but the two given above have been found the most satisfactory.

Simple Relations for Calculating Certain Transient Responses

W. J. CUNNINGHAM
*Cruft Laboratory, Harvard University, Cambridge, Massachusetts**
(Received August 15, 1947)

The response of a linear transmission system to a step or an impulse is related directly to its steady-state response to a sinusoidal signal of variable frequency. Several very simple relations between these two types of response for low pass systems are collected here. These equations are empirical in nature, but generally may be expected to be in error no more than ±25 percent. Such equations may be useful in preliminary design work where great accuracy is not required, or in checking the results of exact but tedious calculations.

I. INTRODUCTION

THE response of a linear four-terminal transmission system to a sudden change in its driving signal is of considerable interest in any over-all analysis of the system. This response may be found mathematically by any of several standard methods,[1] but if the system is not exceedingly simple, such a calculation is complicated and tedious. In order to simplify the analysis so far as possible, very simple forms for the driving signal are commonly used. The step function and its time derivative, the impulse function, are convenient for this purpose, since they are mathematically relatively simple but provide a severe test for the system. These two functions are shown in Fig. 1, a and c. The impulse function is approximated by a physical pulse of finite duration, but short compared with the reciprocal of the highest frequency transmitted by the system.

There exist several very simple relations between the steady-state response of a system to a sinusoidal driving signal of variable frequency and its response to a step or an impulse. These relations are usually strictly true only for an idealized system or a limited class of physical systems. However, they often apply to any unknown system with sufficient accuracy as to be very useful, particularly in preliminary design work where a quick answer is needed, even though a reasonable error may be present. The following discussion is a collection of such relations together with a few pertinent remarks about each.

The relations may be obtained in the following way. A standard system (either physical or idealized) having very simple steady-state transmission characteristics is used for a mathematical study. The response of this system to a step or an impulse is calculated by any rigorous method; this process is not difficult because of the simplicity of the system. Significant relations between the steady-state characteristics and the response to the step or impulse are now observed. These relations are taken as empirical equations which may apply to other systems with similar characteristics.

Two systems with identical frequency characteristics must yield identical time responses. Two systems with similar frequency characteristics should yield time responses which are similar. For the latter case it is difficult to predict the difference to be expected in the time responses from a knowledge of the difference in the frequency characteristics. In an attempt to check this point, the empirical equations given here have been tested in a wide variety of typical systems, both through mathematical analysis and experimental measurements. In almost every case, the equations give information which is in error no more than ±25 percent and usually less than this amount. It may be expected that errors occurring in the application of the equations to typical physical systems will lie within these limits.

The equations are directly applicable to low pass systems, in most cases with the requirement of minimum phase shift.[2] Often they may

* Now at Department of Electrical Engineering, Yale University, New Haven, Connecticut.

[1] M. F. Gardner and J. L. Barnes, *Transients in Linear Systems* (John Wiley and Sons, Inc., New York, 1942), Vol. I.

[2] H. W. Bode, *Network Analysis and Feedback Amplifier Design* (D. Van Nostrand Company, Inc., New York, 1945), p. 242.

be applied to situations in which band pass systems are involved, by making use of the analogy which exists between low pass and band pass systems.[3] The steady-state response curve of the low pass system should have only a single pronounced peak, although this peak may occur at zero, or any higher frequency. The equations are most accurate if the curves are relatively smooth.

II. DEFINITIONS OF SYMBOLS

Since the various equations involve many of the same symbols, it is well to define them all at one time. Reference should be made to Figs. 1 and 2, where the meanings of the symbols are illustrated. In most cases it is convenient to express the amplitude characteristic in decibels.

Input signal (Fig. 1, a and c).—E_0—value of input step, E_0t_0—area of input impulse.

Steady-state response curve (Fig. 2).—A_n—amplification at zero frequency, f_a—band width, three decibels below zero-frequency value (c.p.s.), f_d—band width, six decibels below zero-frequency value (c.p.s.), f_n—nominal cut-off frequency (c.p.s.), P—slope of chord connecting points at $f=0$ and $f=f_d$ (db/c.p.s.), Φ—slope (always negative) of tangent at point three decibels below maximum of curve (db/c.p.s.), β—phase shift through system (radians), ω—angular frequency (radians/second).

Response to step (Fig. 1b).—E_n—final value, s—maximum relative overshoot, t_b—build-up time (sec.), t_d—time delay (sec.).

Response to impulse (Fig. 1d).—$\hat{e}_n$—peak of response, t_d—time delay (sec.), t_e—duration at $\hat{e}_n/2$ (sec.), t_f—duration measured at base of main peak (sec.), t_g—duration measured at $0.01\hat{e}_n$, taken to envelope if response oscillates (sec.).

The units in which A_n, E_0, E_n, and $\hat{e}_n$ are measured depend upon the type of system under consideration. For example, if E_0, E_n, and $\hat{e}_n$ are all voltages, then A_n is the voltage amplification of the system and is merely a ratio.

III. TIME DELAY OF OUTPUT SIGNAL

In any system having minimum phase shift, a signal begins to appear at the output just after a signal is applied at the input. The output signal may be exceedingly small for a time, after which it increases rapidly, giving rise to an apparent time delay. This time delay depends primarily upon the slope of the curve of phase shift through the system as a function of frequency. The time delay for the response to a step, or an impulse, is defined as shown in Fig. 1, b and d. The time delay is given by the equation[4]

$$t_d = |d\beta/d\omega|. \tag{1}$$

When the phase curve is not linear, it may be approximated with a straight line at pass band frequencies, and the slope of this line taken for use in Eq. (1).

IV. RESPONSE TO AN IMPULSE

If the input signal is a very short pulse (ideally approaching zero duration) the output signal will be a pulse, more or less broadened and possibly containing oscillations.

The peak value of the output signal, $\hat{e}_n$, is given by the equation

$$\hat{e}_n = A_nE_0t_0(2f_a+7.4/|\Phi|). \tag{2}$$

The basis for this equation is given in the appendix. The equation may not be applicable if the steady-state response curve falls more slowly than $1/f^2$ at frequencies well above the pass band.

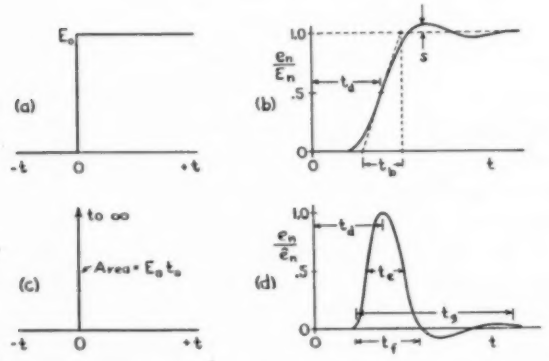

FIG. 1. a—Step function; b—response of low pass system to step function; c—impulse function; d—response of low pass system to impulse function.

[3] E. C. Cherry, "Pulse response, a new approach to a.c. electric network theory and measurement," J. Inst. Elec. Eng. 92, III, 183 (1945).

[4] E. A. Guillemin, *Communication Networks* (John Wiley and Sons, Inc., New York, 1935), Vol. II, Chap. XI, Sections 4 and 5.

If the steady-state curve falls as slowly as $1/f$, a better approximation to the peak is

$$\hat{e}_n = A_n E_0 t_0 (2\pi f_d). \tag{3}$$

This equation is the rule of thumb often quoted to the effect that the peak is proportional to the band width of the system. In case of doubt as to which of these equations, (2) or (3), will give the better results, Eq. (2) is probably the more accurate.

The duration of the output signal may be defined in several ways. If measured at half the peak of the signal, the duration, t_e, is given by the equation

$$t_e = 1/(2f_d). \tag{4}$$

This equation is an extension of the relation, $4f_n t_n = 1$, between the nominal cut-off frequency, f_n, and the nominal duration, t_n, for real symmetrical pulses.[5] The nominal cut-off frequency is that which, when multiplied by the zero-frequency value of the amplitude curve (ratio form) yields the total area under the curve. The nominal duration is similarly defined. The frequency, f_d, corresponds approximately to the nominal cut-off, and the duration, t_e, corresponds approximately to twice the nominal duration.

If only the main part of the output pulse, near zero time, is considered, the duration, t_f, measured near the base of the pulse is given by the equation

$$t_f = 1/f_d. \tag{5}$$

This equation is an extension of Eq. (4), based on the assumption that the output pulse is roughly triangular in shape.

The duration, t_g, measured at one percent of the peak of the output pulse is given by the equation

$$t_g = 0.16|\Phi|. \tag{6}$$

The basis for this equation is given in the appendix. For an oscillatory response, t_g is measured to the envelope of the oscillations rather than to the response itself.

If the damping of the system is large, the output signal will have no oscillations, and t_f and t_g will be approximately the same. If the damping is small, the response will be oscillatory, and t_g will be larger than t_f. The intensity of the oscillations is indicated by the amount t_g exceeds t_f. Since the slope, P, is $|P| = 6/f_d = 6t_f$, and the slope, Φ, is $|\Phi| = t_g/0.16 = 6t_g$, oscillations are indicated if slope $|\Phi|$ exceeds slope $|P|$.

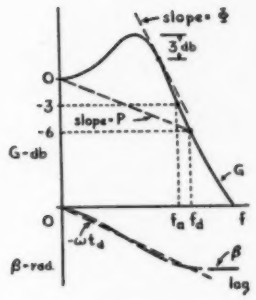

FIG. 2. Important parameters in the shape of the steady-state transmission characteristics of a low pass system.

V. RESPONSE TO A STEP

If the input signal is a step, the output signal will rise to its final value more or less rapidly, always requiring a finite time for this build-up. The final value, E_n, is given by

$$E_n = A_n E_0. \tag{7}$$

The build-up time may be defined as the time required for the output signal first to reach its final value if it rises at a rate corresponding to that at half its final value. The build-up time, t_b, is given by the equation[6,7]

$$t_b = 1/(2f_d). \tag{8}$$

A better approximation is to use f_n, rather than f_d, in Eq. (8), although f_n is not easily found from the amplitude curve expressed in decibels.

If the damping of the system is small, the response to the step will overshoot its final value, which will be reached only after a train of oscillations. Such behavior is predicted by the same criterion which indicates oscillations in the response to an impulse. The maximum relative overshoot, s, is expressed as a fraction of the final value, and is given by the equation

$$s = \exp\left(\frac{-21}{f_d|\Phi - P|}\right) = \exp\left(\frac{-21}{f_d|\Phi| - 6}\right), \tag{9}$$

where $|\Phi|$ must be greater than $|P|$.

[5] H. A. Wheeler, "The interpretation of amplitude and phase distortion in terms of paired echoes," Proc. I.R.E. **27**, 359 (1939).

[6] See reference 4, p. 479.

[7] C. C. Eaglesfield, "Transition time and pass band," Proc. I.R.E. **35**, 166 (1947).

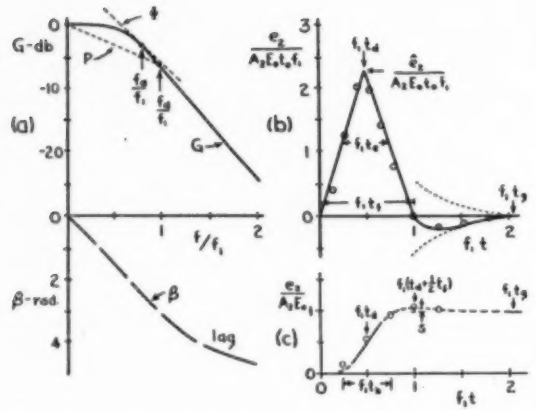

FIG. 3. a—Actual steady-state transmission characteristics of a low pass system; b—output signal due to impulse at input; c—output signal due to step at input. Circles indicate correct values.

Two further observations may be made, based on the fact that the response to an impulse is the time derivative of the response to a step. The time for the maximum overshoot is the time of the first zero of the impulse response, and is approximately $(t_d+t_f/2)$. The interval needed for the step response to begin its rise and then to settle very nearly to its final value is approximately t_g.

VI. APPLICATION TO EXAMPLE

As an example of their use, some of the foregoing equations are here applied to the problem of finding the response of a typical low pass system to an input step or impulse. The steady-state transmission characteristics of the system to be studied are shown in Fig. 3a. These are the actual characteristics of two sections of a circuit of the type shown in Fig. 4a.

The necessary quantities may easily be evaluated from the curves of Fig. 3a, and are as follows:

$$f_a=0.8f_1, \qquad |\Phi|=12.7/f_1,$$
$$f_d=1.0f_1, \quad |d\beta/d\omega|=0.5/f_1.$$

For convenience, these quantities are expressed in terms of a reference frequency, f_1, which is here equal to f_d.

If an impulse is applied to the input of the system, important factors in the shape of the output signal are found as follows:

$$t_d=0.5/f_1, \quad t_f=1/f_1,$$
$$t_e=0.5/f_1, \quad t_g=2.04/f_1,$$
$$\frac{\hat{e}_2}{A_2E_0l_0f_1}=2.2.$$

These factors are used to predict the shape of the output signal in Fig. 3b. Since the time t_g is greater than the time t_f, oscillations in the response are predicted. The envelope of the oscillations decays almost exponentially, and may be assumed to have the form $k_1\exp(-k_2f_1t)$. Evaluation of the constants k_1 and k_2 by making use of the known points, t_d and t_g, gives for the envelope, $11.6\exp(-3.07f_1t)$, which is plotted in the figure. The predicted response passes through the points located from the equations and lies inside the envelope. It oscillates with a period about twice the time t_f.

So long as t_f is at least twice t_d, it is measured from zero time as in this example. However, if t_f is less than twice t_d (as will be true for systems with large time delay) t_e and t_f will be approximately equally distributed on either side of t_d. In such a case, t_g will be measured from the beginning of the output signal, and not from zero time.

If a step is applied to the same system, the build-up time is $t_b=0.5/f_1$. The maximum relative overshoot is $s=0.043$ and occurs approximately at $(t_d+t_f/2)=1/f_1$. The shape of the output signal is predicted in Fig. 3c.

Points found from exact mathematical analysis are plotted as circles in Fig. 3, b and c. The agreement between the predicted curves and the correct points is fairly good.

VII. ACKNOWLEDGMENT

The original work reported here was done under the able guidance of Professor E. L. Chaffee, and his helpful comments and suggestions are gratefully acknowledged.

APPENDIX

Source of Equations

Equations (2), (3), (6), (8), and (9) may be obtained from studies of the sort now to be described. The build-up time is found as follows.

At half the final value of the response to a step, the slope is E_n/t_b, following the definition of t_b. For a low pass system with zero phase shift, the response to a step is given by the Fourier integral[8]

$$e(t)=2\int_0^\infty (E_0/j\omega)A_n g(f)\exp(j\omega t)df.$$

In this equation, $(E_0/j\omega)$ is the frequency spectrum of the step, and $A_n g(f)$ is the amplitude characteristic of the system. The resulting response is symmetrical about zero time, under the assumptions made, so that the slope of the response at half its final value is

$$(de(t)/dt)_{t=0}=2A_nE_0\int_0^\infty g(f)df=2A_nE_0f_n=E_n/t_b.$$

Therefore, $t_b=1/(2f_n)$, and if it is assumed that f_n is approximately the same as f_d, Eq. (8) results.

Consider now the circuit shown in Fig. 4a. This is a simple low pass filter which is driven by a pentode current source. The amplitude characteristic for this circuit may be written as

$$g=\left|\frac{E_a}{A_1E_b}\right|=\frac{1}{[(1-x^2)^2+d_1^2x^2]^{\frac{1}{2}}},\qquad (A\ 1)$$

where E_a is the r.m.s. voltage at the input, E_b is the r.m.s. voltage at the output, A_1 is the voltage amplification at zero frequency, $(A_1=g_mR)$, g_m is the transconductance of the tube, d_1 is the dissipation factor for the circuit $d_1=R/(L\omega_1)=R(C/L)^{\frac{1}{2}}$, x is a normalized frequency variable $(x=\omega/\omega_1)$, and $\omega_1=(1/LC)^{\frac{1}{2}}$. At the point $(x=x_a)$, where g is equal to $2^{-\frac{1}{2}}$ times the zero frequency value, the slope of the curve of g *vs.* x is

$$\left(\frac{dg}{dx}\right)_{x=x_a}=(-1/4)[(4+h^2)(h+[4+h^2]^{\frac{1}{2}})]^{\frac{1}{2}},\qquad (A\ 2)$$

where

$$h=(2-d_1^2).$$

If $d_1<2^{\frac{1}{2}}$, the curve of g has a peak at other than zero frequency. At the point $(x=x_b)$, where g is equal to $2^{-\frac{1}{2}}$ times its maximum value at this peak, the slope of the curve is

$$\left(\frac{dg}{dx}\right)_{x=x_b}=\mp\left[\frac{2(h\pm[4-h^2]^{\frac{1}{2}})^{\frac{1}{2}}}{4-h^2}\right].\qquad (A\ 3)$$

The voltage ratio, g, may be expressed in decibels as

$$G=20\log_{10}g,$$

in which case the slope relation is

$$\frac{dG}{dx}=\frac{20\log_{10}e}{g}\frac{dg}{dx}.\qquad (A\ 4)$$

The value of dG/dx, at x_a for $d_1>2^{\frac{1}{2}}$ and at x_b for $d_1<2^{\frac{1}{2}}$, is given the symbol Ψ. The response of this circuit to an impulse of area E_0t_0, when $d_1<2$, may be written as

$$\frac{e_b}{A_1E_0t_0\omega_1}=\frac{\exp(-d_1\omega_1t/2)}{(1-d_1^2/4)^{\frac{1}{2}}}\sin[\omega_1t(1-d_1^2/4)^{\frac{1}{2}}],\qquad (A\ 5)$$

where e_b is the instantaneous voltage at the output. The peak, $\hat{e}_b$, occurs at the time, t_p, given by

$$\tan[\omega_1t_p(1-d_1^2/4)^{\frac{1}{2}}]=[(4/d_1^2)-1]^{\frac{1}{2}}.$$

Similar equations may be obtained for the cases of $d_1=2$ and $d_1>2$.

The quantities ω_1t_g and Ψ may be determined from the preceding equations. The ratio ω_1t_g/Ψ as calculated for a wide range of values of d_1 is plotted in Fig. 4b. It is evident that this ratio is surprisingly constant, and that to a good approximation it may be set equal to unity. A little algebraic juggling then leads to

$$t_g=0.16|\Phi|,\qquad (A\ 6)$$

which is the same as Eq. (6).

A second type of circuit which is easy to study is the low pass analog of stagger-tuned circuits. The amplitude characteristic for such circuits is

$$g_n=\left|\frac{E_n}{A_nE_a}\right|=\frac{1}{(1+y^{2r})^{n/2}},\qquad (A\ 7)$$

where E_n is the r.m.s. output voltage, r is the number of circuits in the stagger-tuned unit, n is the number of units in the system, y is a normalized frequency variable $(y=f/f_c)$, and f_c is the frequency at which $g_1=2^{-\frac{1}{2}}$ (i.e., $n=1$). For the present discussion it is not necessary to go into detail about the actual circuit, but merely to take Eq. (A 7) as a mathematical response to be studied. Maximum value (unity) for g_n occurs at $y=0$. At the point $(y=y_a)$, where g_n equals $2^{-\frac{1}{2}}$, the slope of the curve is

$$\gamma=\left(\frac{dg_n}{dy}\right)_{y=y_a}=\frac{nr(2^{1/n}-1)^{(1-1/(2r))}}{2^{(\frac{1}{2}+1/n)}}.\qquad (A\ 8)$$

This quantity, γ, may be expressed in decibels, and the symbol, Γ, defined as

$$\Gamma=\left(\frac{dG_n}{dy}\right)_{y=y_a}.\qquad (A\ 9)$$

For the case of $r=1$, the response of the system to an impulse of area E_0t_0 is

$$\frac{e_n}{A_nE_0t_0\omega_c}=\frac{(\omega_ct)^{(n-1)}}{(n-1)!}\exp(-\omega_ct),\qquad (A\ 10)$$

where e_n is the instantaneous voltage at the output.

For the case of $r=2$ and $n=1$, the response to the

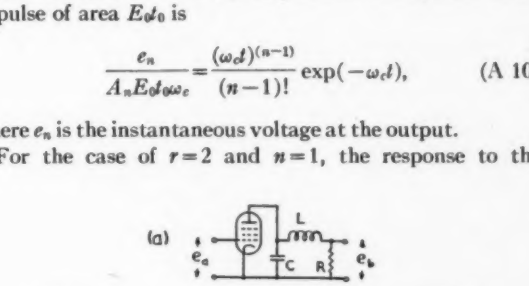

FIG. 4. a—Low pass system for analysis; b—curve showing the constancy of the ratio $\omega_1t_g/|\Psi|$; c—curves showing the region of application of the empirical equations.

[8] See reference 4, Chapter XI.

TABLE I.

r	n	$\omega_c t_g$	$\frac{f_a}{f_b}$	γ	Γ	$\frac{\omega_c t_g}{\lvert\Gamma\rvert}$	Correct $\frac{\hat{e}_n}{A_n E_0 t_0 \omega_c}$	Eq. (A 13) $\frac{\hat{e}_n}{A_n E_0 t_0 \omega_c}$
1	1	4.6	1.0	−0.35	−4.3	1.06	1.0	0.59
1	2	7.6	0.64	−0.64	−7.9	0.96	0.37	0.35
1	4	11.4	0.44	−1.03	−12.5	0.91	0.23	0.24
1	6	14.2	0.35	−1.33	−16.3	0.87	0.18	0.18
1	10	18.6	0.27	−1.77	−28.6	0.86	0.13	0.14
2	1	8.1	1.0	−0.71	−8.6	0.94	0.46	0.45
2	2	10.8	0.80	−1.03	−12.5	0.86	0.34	0.35
2	3	13.2	0.71	−1.23	−15.1	0.86	0.29	0.31

impulse is

$$\frac{e_1}{A_1 E_0 t_0 \omega_c} = 2^{\frac{1}{2}} \exp(-\omega_c t/2^{\frac{1}{2}}) \sin(\omega_c t/2^{\frac{1}{2}}). \qquad \text{(A 11)}$$

Similar expressions apply for other values of r and n.

The quantities $\omega_c t_g$ and Γ, and their ratio, may be calculated from the preceding equations and collected in Table I. From this table it is apparent that the ratio $\omega_c t_g/|\Gamma|$ is always near unity in value, and, with some algebra, Eq. (6) may be obtained again.

A study of Eq. (A 5) shows that if d_1 is very small or very large, the peak of the response is given by

$$\frac{\hat{e}_n}{A_n E_0 t_0} = 2\pi f_a \quad \text{or} \quad 2\pi f_b, \qquad \text{(A 12)}$$

where f_a or f_b (as the case may be) is the frequency at which g is $2^{-\frac{1}{2}}$ times its maximum value. This is the same as Eq. (3).

A similar study of the data of Table I shows that Eq. (A 12) does not apply there with very good accuracy, and, further, that the following equation is better.

$$\frac{\hat{e}_n}{A_n E_0 t_0 \omega_c} = 0.3(f_a/f_c) + 0.1/|\gamma|. \qquad \text{(A 13)}$$

Values found from this equation are tabulated and may be compared with the correct values obtained from equations of the type of Eq. (A 10) and (A 11). If expressed in terms more convenient for ordinary use, Eq. (A 13) becomes

$$\frac{\hat{e}_n}{A_n E_0 t_0} = 2f_a + 7.4/|\Phi|, \qquad \text{(A 14)}$$

which is the same as Eq. (2).

The values of $\hat{e}_n$ for the low pass circuit as calculated from Eqs. (A 5), (A 12), and (A 14) are plotted in Fig. 4c. For values of d_1 in the order of unity (i.e., values commonly used in filter circuits) Eq. (A 14) is evidently more accurate; for other values of d_1, Eq. (A 12) is better. For the case of $r=1$, $n=1$, in Table I, Eq. (A 12) is better than Eq. (A 14) for finding $\hat{e}_n$. By correlating the shape of the output signal with the applicable equation, it is observed that Eq. (A 12) is better when the output signal (or its envelope) begins with a discontinuity; otherwise Eq. (A 14) is better. In general, only those circuits whose steady-state characteristics fall as $1/f$ above the pass band yield a pulse response with a discontinuity, so that Eq. (A 12) is to be preferred only in those cases.

Equation (9), for calculating the relative overshoot in the response to a step, may be set up through empirical methods similar to those just described.

Calendar of Meetings

March

19 Institute of Aeronautical Sciences (Flight Propulsion Meeting), Cleveland, Ohio

22–24 American Chemical Society (Minnesota Section) and the Institute of Technology of the University of Minnesota, Symposium "Modern Instrumental Methods of Analysis," Minneapolis, Minnesota

22–25 Institute of Radio Engineers, New York, New York

26 American Physical Society (Metropolitan Section), Brookhaven National Laboratories, New York

29–30 Conference on Electron Tubes for Instrumentation and Industrial Use, Philadelphia, Pennsylvania

30–April 1 Society of Automotive Engineers (National Transportation Meeting), Philadelphia, Pennsylvania

April

1–3 American Institute of Electrical Engineers (Great Lakes District Meeting), Des Moines, Iowa

7–9 American Society of Civil Engineers, Pittsburgh, Pennsylvania

8–10 Geological Society of America, Pasadena, California (Cordillera Section)

13–15 Society of Automotive Engineers (National Aeronautic and Air Transport Meeting), New York, New York

16–17 American Mathematical Society, New York, New York, Ann Arbor, Michigan, and Berkeley, California

19–23 American Chemical Society, Chicago, Illinois

21–23 American Geophysical Union, Washington, D. C.

22–24 Acoustical Society of America, Washington, D. C.

22–24 American Philosophical Society, Philadelphia, Pennsylvania

25–30 American Ceramic Society, Inc., Chicago, Illinois

26–28 National Academy of Sciences, Washington, D. C.

26–28 International Radio Engineers and the Institute of Radio Engineers (Spring Meeting), Syracuse, New York

28–30 American Institute of Electrical Engineers (Northeastern District Meeting), New Haven, Connecticut

29–May 1 American Physical Society, Washington, D. C.

30–May 1 Canadian Institute of Radio Engineers, Toronto, Ontario, Canada

May

3–5 International Scientific Radio Union and the Institute of Radio Engineers, Washington, D. C.

9–12 American Institute of Chemical Engineers, Cleveland, Ohio

17–21 Society of Motion Picture Engineers, Santa Monica, California

22 Institute of Radio Engineers (North Atlantic Region), Cambridge, Massachusetts

27–29 Canadian Association of Physicists, Ottawa, Canada

30–June 2 American Society of Refrigerating Engineers, Swampscott, Massachusetts

30–June 4 American Society of Mechanical Engineers (Semi-annual Meeting), Milwaukee, Wisconsin

On Creep and Relaxation. II.*

B. Gross
National Institute of Technology, Rio de Janeiro, Brazil
(Received August 20, 1947)

A phenomenological theory of the elastic aftereffect can be formulated with the aid of the principle of superposition. In a previous paper the theory of the transient effects, caused by the sudden application of a constant load or a constant deformation, has been developed. In the present paper the theory of the steady-state behavior under alternating load and deformation is given. Relations are established between the loss factor, the storage factor, the distribution functions, and the Laplace transforms of the creep—and the relaxation—function.

IN an experimental study of the behavior of the visco-elastic body one may choose two ways of attack; they are: (a) The measurement of the transient phenomena caused by the sudden application of a constant load (creep or strain retardation under constant stress) or a constant deformation (stress relaxation under constant strain). (b) The measurement of the steady-state behavior under alternating load or deformation. The transient is measured easily for times of about 1 minute or longer; the steady-state behavior involves measurements with technical and higher frequencies, corresponding to periods smaller than 1 second. The two methods therefore complete themselves mutually; the first one is suitable for the study of the processes with the long relaxation times and the second one for those with the short relaxation times.

The ultimate aim of the measurement is the acquisition of information that may conduce to a general picture of visco-elastic behavior and the knowledge of the nature of the relaxation process. Its realization depends on additional evidence beyond the simple experimental fact. This may be provided (a) by an interpretative theory of the fundamental relaxation process,[1] or (b) by a general phenomenological principle that allows for the coordination of the multiplicity of experimental facts under one point of view. Such a principle is the assumption of the linear superposition of effects, which, since Boltzmann, has guided research in this field. Many years of experience have shown that Boltzmann's principle is correct for a wide variety of materials at low and medium stress and strain; even when it breaks down, it still remains a first approximation to the true fact.[2]

In a previous paper[3] the phenomenological theory of the elastic after effect has been developed, the treatment being mainly concerned with the transient effects. In the present paper these considerations shall be extended so as to include the steady-state behavior under alternating load and deformation. Mathematically speaking, while the former treatment has been by Laplace transforms, the present one is by Fourier transforms. Irreversible effects shall again not be taken into account. Now this is certainly of very little consequence, because, at least when loads or deformations near the yield values are excluded, the time constant of the irreversible effects is many times greater than that of the reversible phenomena, which play a role in the range of frequencies that concern us here.[4]

The transient solution for constant load is characterized by one function of direct physical significance, the creep function; the steady-state solution for alternating load is characterized by two such functions, the loss factor, giving the energy dissipation per cycle, and the storage factor which is a measure of the reversible

* Publication assisted by the Committee on Inter-American Scientific Publication.

[1] Such a theory has been given for instance, by M. S. Green and A. V. Tobolsky, J. Chem. Phys. **14**, 80 (1946).

[2] Recently, the principle of superposition has been extended so as to include non-linear effects by H. Leaderman ("Elastic and creep properties of filamentous materials," J. Text. Found. Washington, D. C., 159 (1944)) and E. Guth, Paul E. Wack, and Robert L. Anthony, J. App. Phys. **17**, 350 (1946). One of these generalizations applies to creep, the other one to relaxation. It is not yet clear how far these laws are compatible. Here we confine ourselves entirely to the linear problem.

[3] B. Gross, J. App. Phys. **18**, 212 (1947). In the following this paper will be quoted as I.

[4] A treatment of the transient effects which includes plastic deformations has recently been given by Charles Mack, J. App. Phys. **17**, 1086 (1946).

storage of energy due to the time-dependent mechanism. An analogous situation exists for given deformation. Thus for one relation in the transient treatment there appear two relations in the steady-state treatment. In theory, all these functions and relations are equivalent;[5] in practice it usually is just one way of treatment that fits adequately for a given problem. In particular, in the study of the interdependence of creep and relaxation phenomena the use of the Laplace transform is generally preferable to that of the Fourier transform.

The theories of the elastic after effect, of dielectric absorption, and of linear electric circuits are formally equivalent, only names have to be changed. Load corresponds to voltage, deformation to quantity of electricity; rate of creep and elastic modulus function correspond to *indicial* admittance and steady-state impedance. Thus results obtained in one branch of the general theory are usually significant for the other branches too. The steady-state solution in circuit theory has been worked out in great detail. Thus, many of the relations presented in this paper are contained in some form or other in the existing literature, but their systematic coordination, forming a consistent description of the various aspects of visco-elastic behavior, is not easily found, yet to our belief it is of interest.

In measurements with constant loads or deformations, oscillations do occur immediately after the application or suppression of the load, but usually observations start only after these oscillations have died away. Then the displacement proceeds so slowly that inertia reactions and viscous friction losses can be neglected and the experiment be considered as a static one. Under such conditions the measured values of load and deformation give direct indication of the values of stress and strain. It then becomes irrelevant, if the principle of superposition is stated in a form in which it correlates load and deformation (as has been preferred in I), or stress and strain. In measurements with alternating load and deformation, inertia reaction can be no longer generally neglected. Thus, for the sake of obtaining the relation between load and deformation, the dynamic equation of motion of the vibrating body must be established. It can be written down, when one knows (a) the mechanical properties of the system and (b) the stress-strain relation. It is this relation that is governed by the principle of superposition. In the present paper we do not consider the dynamic equation but study exclusively the stress-strain relations, which follow from the substitution of Hook's law by the more complicated expression represented by the principle of superposition. For the sake of simplicity and to keep in line with the former paper, we employ the same terminology as in I, calling attention to the fact that our steady-state solution does not contain the inertia terms.

[5] Many correlations between these functions have been considered by A. Gemant, Physics, **7**, 311 (1936); R. Simha, J. App. Phys. **13**, 201 (1942); T. Alfrey and P. Doty, J. App. Phys. **16**, 700 (1945).

I. THE STEADY-STATE ADMITTANCE

The deformation (strain) $y(t)$ produced by a given load (stress) $P(t)$ in a visco-elastic body is given by

$$y(t)=\frac{F}{E}\left[P(t)+\int_{-\infty}^{t}P(\tau)\varphi(t-\tau)d\tau\right]. \quad (1)$$

E is the elastic modulus (instantaneous value), F a form factor, and $\varphi=d\psi/dt$ the rate of creep, ψ being the creep function.[6] The steady-state solution for alternating load is obtained by putting

$$P(t)=P_0e^{i\omega t}. \quad (2)$$

Substitution in (1) gives

$$y(t)=G(i\omega)P(t). \quad (3)$$

$G(i\omega)$ is the steady-state admittance of the system:

$$G(i\omega)=(F/E)[1+L(i\omega)], \quad (4)$$

where $L(i\omega)$ is the Fourier transform of $\varphi(t)$. Decomposition into real and imaginary component gives

$$L(i\omega)=A(\omega)-iB(\omega), \quad (5)$$

and A and B are, respectively, the cosine and the sine transform of $\varphi(t)$.

$$A(\omega)=\int_0^\infty \cos\omega\tau\varphi(\tau)d\tau, \quad (6a)$$

$$B(\omega)=\int_0^\infty \sin\omega\tau\varphi(\tau)d\tau. \quad (6b)$$

[6] The deduction of this equation, also used in I, may be found in H. Leaderman, reference 2, p. 23; the above equation follows from Leaderman's Eq. (8) by partial integration.

Both A and B have direct physical significance. The energy dissipation per cycle is given by $B\pi P_0^2F/E$; the amount of energy, which twice in every cycle is alternately stored and returned, is $(1+A)0.5P_0^2F/E$; only the term $0.5P_0^2F/E$ would be observed, if creep were absent. We call B the *loss factor* and A the *storage factor* for a given load. It follows from (6) that

$$A(0)=\int_0^\infty \varphi(\tau)d\tau=\psi(\infty), \tag{7a}$$

$$B(0)=B(\infty)=0. \tag{7b}$$

The zero-frequency value of the storage factor is therefore a measure of the total amount of creep.

II. THE STEADY-STATE IMPEDANCE

The load (stress) $P(t)$ necessary to produce a specified deformation (strain) $y(t)$ is given by

$$P(t)=\frac{E}{F}\left[y(t)-\int_{-\infty}^{t} y(\tau)\bar{\varphi}(t-\tau)d\tau\right]. \tag{8}$$

$\bar{\varphi}(t)$ is the rate of relaxation.[7] The steady-state solution for alternating deformation is gotten from

$$y(t)=y_0e^{i\omega t}. \tag{9}$$

Substitution in (8) gives

$$P(t)=Z(i\omega)y(t), \tag{10}$$

where $Z(i\omega)$ is the impedance function,

$$Z(i\omega)=\frac{E}{F}[1-\bar{L}(i\omega)]. \tag{11}$$

$\bar{L}(i\omega)$ is the Fourier transform of $\bar{\varphi}(t)$,

$$\bar{L}(i\omega)=\bar{A}(\omega)-i\bar{B}(\omega), \tag{12}$$

and $\bar{A}$ and $\bar{B}$ are again given by integrals of the type.[6] $\bar{A}$ and $\bar{B}$ are, respectively, the storage factor and the loss factor for given deformation. The amount of elastic energy storage is given by $(1-\bar{A})0.5y_0^2E/F$. It is worth while mentioning the asymmetry existing between this expression and the former expression $(1+A)0.5P_0^2F/E$, which has been given above and refers to given load (stress). *In the former case* the contribution of the time-dependent mechanism increases the energy storage beyond the value, which would be observed without creep. *In the present case* the time-dependent effect diminishes the energy storage below the value, which would be observed without relaxation. We observe, finally, that the first mention of the integrals (6) has apparently been made by E. v. Schweidler.[8]

[7] For the deduction of (8) see reference 6, p. 24, Eq. (11).

Complex Elastic Modulus

In the foregoing the expressions steady-state admittance and impedance have been used with a view on the close analogy existing between the elastic and the electric relaxation theory. But again attention is called to the fact that these functions do not represent the total mechanical admittance or impedance of an oscillating system because they contain neither the mass reaction of the vibrating body nor possible friction losses. If one prefers, one may therefore define a complex elastic modulus function $E^*(-i\omega)=E_1+iE_2$, where $E_1=E(1-\bar{A})$ and $E_2=E\bar{B}$. This complex elastic modulus corresponds with the impedance function, and its reciprocal with the admittance function.

III. RELATIONS BETWEEN LOSS FACTOR AND STORAGE FACTOR

An inspection of the Eqs. (6) clearly reveals the fact, that $A(\omega)$ and $B(\omega)$ are mutually dependent. An inversion of the Fourier transform (6a) yields φ in function of A; substitution of the result in (6b) gives B in function of A. There follows finally:

$$B(\omega)=\frac{2}{\pi}\int_0^\infty A(\beta)\frac{\omega}{\omega^2-\beta^2}d\beta, \tag{13a}$$

$$A(\omega)=\frac{2}{\pi}\int_0^\infty B(\beta)\frac{\beta}{\beta^2-\omega^2}d\beta. \tag{13b}$$

The integrals are principal values. A deduction and discussion of these equations has recently been given by Gross[9,10] and, independently, by Cole.[11] Very detailed information is given by Bode.[12] In view of the numerous literature exist-

[8] E. v. Schweidler, Ann. d. Physik **24**, 711 (1905).
[9] B. Gross, Phys. Rev. **59**, 748 (1941).
[10] B. Gross, Am. Math. Monthly **50**, 89 (1943), contains further bibliography.
[11] R. H. Cole, Phys. Rev. **60**, 172 (1941).
[12] H. W. Bode, *Network Analysis and Feedback Amplifier Design* (D. Van Nostrand Company, Inc., New York, 1945).

ing about these relations, there is here no need for further discussion. We only observe that putting $\omega=0$ one obtains the relation

$$A(0)=\frac{2}{\pi}\int_0^\infty \frac{B(\beta)}{\beta}d\beta, \tag{14}$$

mentioned already by Kronig.[13] It connects an integral over the loss factor with the zero-frequency value of the storage factor, or, according to Eq. (7a), with the total amount of creep. It is obvious, that the same relations hold between $\bar{A}$ and $\bar{B}$.

IV. RELATIONS BETWEEN IMPEDANCE AND ADMITTANCE FUNCTION

The very definition of the impedance function makes it obvious that this function must be the reciprocal of the admittance function, and *vice versa*. Thus

$$G(i\omega)=1/Z(i\omega). \tag{15}$$

In the present treatment, the deduction of the expression for G has started with Eq. (1), and that of Z with Eq. (8). Thus, from our point of view, the relation between G and Z is more than a pure definition; it represents a condition of compatibility between the Eqs. (1) and (8) and results ultimately in a relation between the creep and the relaxation function. Indeed, substitution of (4) and (11) in (15) gives

$$\bar{L}(i\omega)+\bar{L}(i\omega)L(i\omega)-L(i\omega)=0. \tag{16}$$

Since $L(i\omega)$ is the Fourier transform of the rate of creep and $\bar{L}(i\omega)$ is the Fourier transform of the rate of relaxation, Eq. (16) permits the calculation of one of these functions when the other one is given. The substitution $i\omega=p$ converts the Fourier transforms $L(i\omega)$ into the Laplace transforms $L(p)$, and the relation (16), between the Fourier transforms, into the corresponding relation between the Laplace transforms (I, Eq. (8)). This illustrates well the fact that the description in terms of steady-state admittance and impedance signifies treatment by Fourier transforms and that the description in terms of the transient effects signifies treatment by Laplace transforms. But while $L(p)$ is a real function, $L(i\omega)$ is a complex one; therefore Eq. (16) implies the existence of two relations between the real and imaginary components of L and $\bar{L}$. After algebraic transformations one gets

$$\bar{A}=\frac{A(1+A)+B^2}{(1+A)^2+B^2}, \tag{17a}$$

$$\bar{B}=\frac{B}{(1+A)^2+B^2}. \tag{17b}$$

A similar set of equations is obtained for A and B in terms of $\bar{A}$ and $\bar{B}$. Thus when A and B are known, $\bar{A}$ and $\bar{B}$ can be calculated, and *vice versa*. Furthermore, it is sufficient that *either A or B* is known, and $\bar{A}$ and $\bar{B}$ may still be calculated. This follows from the existence of the direct relations (13) between A and B. Here only the relations between B and $\bar{B}$ shall be considered in detail. For reasons of the following we make the substitutions

$$\beta=\sqrt{s}, \tag{18a}$$

$$B(\sqrt{\omega})=\pi b(\omega), \quad \bar{B}(\sqrt{\omega})=\pi\bar{b}(\omega), \tag{18b}$$

and get

$$\bar{b}=\frac{b}{\left[1+\int_0^\infty b(s)\frac{ds}{s-\omega}\right]^2+\pi^2b^2}, \tag{19a}$$

$$b=\frac{\bar{b}}{\left[1-\int_0^\infty \bar{b}(s)\frac{ds}{s-\omega}\right]^2+\pi^2\bar{b}^2}. \tag{19b}$$

These relations allow for an interesting interpretation. In I the distribution functions for creep (ρ) and for relaxation ($\bar{\rho}$) have been introduced. Now it is well known from the analogous electrical case, that the shape of the loss factor curve is similar to that of the corresponding distribution function. This similarity may have appeared to be somewhat fortuitous; now it becomes evident that it must exist of necessity. Indeed, a comparison of the above relations with Eqs. I (27), which give the relations between ρ and $\bar{\rho}$, shows the 2 sets of equations to be formally identical. It follows that every pair of functions b and $\bar{b}$ must serve as a pair of distribution functions, and conversely every pair of distribution functions ρ and $\bar{\rho}$ must fulfill the condition necessary for being considered as a pair of loss-factor functions.

[13] R. L. de Kronig, J. Opt. Soc. Am. **12**, 547 (1926).

V. RELATIONS BETWEEN THE LOSS FACTOR, THE STORAGE FACTOR, AND THE LAPLACE TRANSFORM

For many problems, the knowledge of the Laplace transforms $L(p)$ and $\bar{L}(p)$ is of interest. When both A and B are known, $L(i\omega)=A-iB$ can be calculated and $L(p)$ follows by the substitution $i\omega=p$. But again it can be shown that $L(p)$ can still be calculated if *either* A *or* B is known. In the following a very simple deduction shall be given. For more detailed considerations we refer to a paper by Nijenhuis and Stumpers.[14] Multiplying Eq. (6a) on both sides by $1/(\omega^2+p^2)$, integrating over ω from 0 to ∞, and changing on the right side the order of integration, one gets

$$\int_0^\infty \frac{A(\omega)d\omega}{\omega^2+p^2}=\int_0^\infty \varphi(\tau)d\tau\int_0^\infty \frac{\cos\omega\tau}{\omega^2+p^2}d\omega. \quad (20)$$

The cosine integral is known, giving

$$\int_0^\infty \frac{\cos\omega\tau}{\omega^2+p^2}d\omega=\frac{\pi e^{-p\tau}}{2p}.^{15} \quad (21)$$

Substitution of (21) in (20) shows, that the right-side term is identical with $\pi L(p)/2p$, and therefore

$$L(p)=\frac{2}{\pi}\int_0^\infty A(\omega)\frac{p}{\omega^2+p^2}d\omega, \quad (22a)$$

$$L(p)=\frac{2}{\pi}\int_0^\infty B(\omega)\frac{\omega}{\omega^2+p^2}d\omega, \quad (22b)$$

the second equation being obtained in a way analogous to that given above. A set of analogous equations connects $\bar{A}$ and $\bar{B}$ with $\bar{L}$.

These equations may find various applications. It has already been mentioned, that in the short time interval the measurement of the storage factor and loss factor is performed with much less difficulty than that of the creep or relaxation function. The result of the measurements with alternating load or deformation may then conveniently be used for computation of the creep or relaxation function in the short time interval. An inversion of the Fourier transforms (6) gives directly $\varphi(t)$. But when the analytic expressions for A or B are not simple, then it may become more advantageous to calculate first the Laplace transform $L(p)$ by means of one of the Eqs. (22). The inversion of the Laplace transform can be carried out by modern operational methods and become less difficult than the Fourier inversion.

The Eqs. (22) can supplant the direct relations (13) in computations of the storage factor from loss-factor measurements or *vice versa*. To this purpose we observe that these equations obviously are equivalent to

$$L(pe^{\pm i\pi/2})=A(p)\mp iB(p), \quad (23)$$

or, written differently

$$A(p)=\mathrm{Re}L(pe^{\pm i\pi/2}), \quad (24a)$$

$$B(p)=\pm\mathrm{Im}L(pe^{\pm i\pi/2}). \quad (24b)$$

(23) is really identical with Eq. (5), with which we have introduced the factors A and B, only for $\pm i$ now we have substituted $e^{\pm i\pi/2}$. This substitution becomes necessary because in making transformations between $L(p)$ and $L(i\omega)$ we really consider one function, $L(z)$, of a complex variable z; taken along the positive real axis, $L(z)$ gives what here has been called the Laplace transform and taken along the imaginary axis it gives what has been called the Fourier transform. In the complex plane $L(z)$ is found to have ramification points. To avoid ambiguities one has to chose one determination of the function. Along the positive real axis, $L(z)$ must be real. Thus one is led to chose the phase of z in the interval between $-\pi$ and π. An example for such an application of Eqs. (22) is given at the end of the paper.

The technique of measurement frequently allows for the simultaneous determination of loss factor and storage factor. One may then perhaps doubt the usefulness of formulae containing only one of these functions as compared with the much simpler relations containing their sum or difference. Now the result of the measurement is a set of numerical data which may be represented analytically by suitable expressions $A(\omega)$ and $B(\omega)$. But if these expressions shall constitute the starting point for further mathematical developments, the functions $A(\omega)$ and $B(\omega)$ cannot be chosen independently of each other because then

[14] W. Nijenhuis and F. L. Stumpers, Physica **8**, 289 (1941).

[15] See F. Hurwitz and R. Courant, *Funktionentheorie* (Julius Springer Verlag, Berlin, 1929), p. 312. The integral (21) is obtained by integrating the integral given by Hurwitz and Courant.

they would not satisfy the relations (13), the sum and difference $A \pm iB$ not being a function of the argument $i\omega$ and not constituting a function $L(i\omega)$. It follows, that one is free in the choice of *one* function only, and for this reason one needs the "single" relations of the theory.

VI. DETERMINATION OF THE DISTRIBUTION FUNCTIONS

In I, the distribution functions $\rho(p)dp$ for creep and $\bar{\rho}(p)dp$ for relaxation have been formally introduced by the relations

$$\varphi(t) = \int_0^\infty e^{-pt}\rho(p)dp, \tag{25a}$$

$$\bar{\varphi}(t) = \int_0^\infty e^{-pt}\bar{\rho}(p)dp. \tag{25b}$$

A method has been given for the determination of ρ and $\bar{\rho}$ from creep and relaxation data. From the present point of view, $A(\omega)$ and $B(\omega)$ are the given function. Thus the problem arises how to calculate the distribution functions from the loss-factor and storage-factor data. This problem has first been considered and solved by Fuoss and Kirkwood.[16] Here we shall give a different deduction based on the foregoing developments. For this purpose multiply both sides of Eq. (25a) by $\cos\omega t$ and integrate over t from 0 to ∞. Changing the order of integration on the right side, it follows that

$$\int_0^\infty \varphi(t)\cos\omega t dt = \int_0^\infty \rho(p)dp \int_0^\infty e^{-pt}\cos\omega t dt. \tag{26}$$

The left-hand integral is equal to $A(\omega)$, the integral over the exponential function is known. Making a similar integration with $\sin t$, there is

$$A(\omega) = \int_0^\infty \rho(p)\frac{p}{\omega^2+p^2}dp, \tag{27a}$$

$$B(\omega) = \int_0^\infty \rho(p)\frac{\omega}{\omega^2+p^2}dp.^{17} \tag{27b}$$

A comparison of these equations with the Eqs. (22) shows the formal identity of (27a) and (22b), and (27b) and (22a). But in the former case, the functions under the integral were known and the left-hand functions unknown; now the contrary happens, Eqs. (27) representing integral equations for $\rho(p)$. The method of solution is indicated by the analogy existing between the sets (22) and (27). It has been shown, that (22) is equivalent with the relations (23) and (24), in which the connection between A and B on one side and $L(ip)$ on the other side is given. Thus we now suppose the existence of 2 functions $A(z)$ and $B(z)$ of a complex variable z, such that along the positive real axis $A(z)$ coincides with the given $A(\omega)$ and $B(z)$ with the given $B(\omega)$. Then in analogy with (24) one gets

$$\rho(\omega) = \frac{2}{\pi}\,\mathrm{Im}A(\omega e^{-i\pi/2}) = -\frac{2}{\pi}\,\mathrm{Im}A(\omega e^{+i\pi/2}), \tag{28a}$$

$$\rho(\omega) = \frac{2}{\pi}\,\mathrm{Re}B(\omega e^{-i\pi/2}) = \frac{2}{\pi}\,\mathrm{Re}B(\omega e^{+i\pi/2}).^{18} \tag{28b}$$

The solution obviously implies the principle of analytic continuation.

The functions ρ and $\bar{\rho}$ are not normalized; they are related to the normalized distribution function, $F(\tau)d\tau$, of retardation times of strain and, $\bar{F}(\tau)d\tau$, of relaxation times of stress by the Eqs. I (14):

$$\beta F(\tau)d\tau = -\rho(p)dp/p, \quad p = 1/\tau, \tag{29}$$

and an analogous relation for $\bar{F}$ and $\bar{\rho}$. The normalization constant β can be determined from the condition that the integral over F must be equal to 1 (I, Eq. (12)). But frequently another method of determination may be found convenient. Integrating (25a) from 0 to ∞ and taking into account (29) there results

$$\beta = \int_0^\infty \varphi(t)dt = \psi(\infty) = A(0). \tag{30}$$

An analogous relation holds for $\bar{\beta}$.

[16] R. Fuoss and J. G. Kirkwood, J. Am. Chem. Soc. **63**, 385 (1941).

[17] Equations of this type have been already derived by E. v. Schweidler, reference 8. Compare W. A. Yager, Physics **7**, 434 (1936), Eqs. (5b) and (6b).

[18] This solution is easily seen to be identical to the formulae of Fuoss-Kirkwood, reference 16. It can be arrived at in many different ways; f.i., by the substitution $p^2 = s$ the Eqs. (27) can be transformed into Stieltjes' integral equation, the solution of which is known; c.f., I (16).

VI. APPLICATIONS

We now shall apply some of the formulae given above to the discussion of a problem which has appeared primarily in dielectric theory but which, to our belief, is of interest also for the treatment of visco-elastic behavior. Fuoss and Kirkwood, in their paper frequently referred to,[19] have represented their loss-factor data by the law

$$B(\omega)=\frac{1}{\omega^{\alpha}+\omega^{-\alpha}}. \tag{31}$$

The coincidence between measured and calculated values is good. A little later, Cole and Cole[20] formulated another law, that represents equally well many experimental data of loss-factor and storage-factor measurements and therefrom deduced an expression for the corresponding function $\varphi(t)$.[21] The measurements of Fuoss and Kirkwood have been made with high polymers; in consequence of the close analogy existing between the electric and the elastic relaxation effects for these materials, their results are significant not only for the electrical effect where they originally have been established, but also for the elastic effect. Therefore it seems to us worth while trying to get the function $\varphi(t)$, that belongs to the expression (31). Its knowledge may facilitate a comparison between the theories of Fuoss and Kirkwood and Cole and Cole. Unfortunately a treatment based on (31) is more complicated than one based on Cole's expression. So we shall confine ourselves to the particular case

$$\alpha=\tfrac{1}{2}, \tag{32}$$

which admits of an easy solution in terms of known transcendents. We shall start with the calculation of the Laplace transform, because once this function is given, the other characteristic functions are obtained relatively easily.

The *Laplace transform* $L(p)$ belonging to (31) and (32) is gotten from (22b); integration gives

$$L(p)=\frac{2}{1+p^2}\left[1+\left(\frac{p}{2}\right)^{\frac{1}{2}}(p-1)\right]. \tag{33}$$

The *Fourier transform* $L(i\omega)$ is obtained from (33) by the substitution $p=\omega e^{i\pi/2}$; there results

$$L(i\omega)=\frac{1}{1-\omega^2}[2-(\omega)^{\frac{1}{2}}(\omega+1)]-i\frac{1}{\omega^{\frac{1}{2}}+\omega^{-\frac{1}{2}}}. \tag{34}$$

The *storage factor* is given by the real component of $L(i\omega)$;

$$A(\omega)=\frac{1}{1-\omega^2}[2-(\omega)^{\frac{1}{2}}(\omega+1)]. \tag{35}$$

The *loss factor* is given by the coefficient of the imaginary component of $L(i\omega)$;

$$B(\omega)=\frac{1}{\omega^{\frac{1}{2}}+\omega^{-\frac{1}{2}}}. \tag{36}$$

This expression coincides with the given function (31); the coincidence constitutes a proof of the correctness of the foregoing because there can exist only *one* function $L(i\omega)$, the imaginary part of which gives (31).

The *distribution functions* are most easily gotten from the Laplace transform by the method given in I. Along the negative real axis we have

$$L(pe^{-i\pi})=\frac{2}{1+p^2}\left[1+i\left(\frac{p}{2}\right)^{\frac{1}{2}}(1+p)\right]. \tag{37}$$

The imaginary component, according to I, Eq.

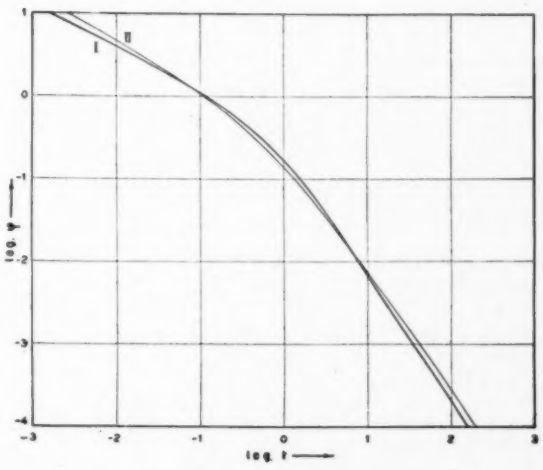

FIG. 1. I—Eq. (42) (Fuoss-Kirkwood).
II—Eq. (45) (Cole-Cole).

[19] Reference 16, Eq. (43). For the sake of rendering as simple as possible the following expressions we shall omit the factor $H(0)$ and, instead of ω/ω_m, write simply ω.

[20] K. S. Cole and R. H. Cole, J. Chem. Phys. **9**, 341 (1941).

[21] K. S. Cole and R. H. Cole, J. Chem. Phys. **10**, 98 (1942).

(23) gives the distribution function for creep

$$\rho(p)dp=\frac{(2p)^{\frac{1}{2}}}{\pi}\frac{1+p}{1+p^2}dp; \tag{38}$$

the real component, according to I, Eqs. (21a) and (27a), gives for the distribution function for relaxation

$$\tilde{\rho}(p)dp=\frac{\rho(p)dp}{(1+2/1+p^2)^2+\pi^2\rho^2(p)}. \tag{39}$$

The distribution functions F and $\bar{F}$ are obtained making the substitution (29), but there is no need for explicitely writing down the results; one may only add that the normalization constant β, according to (30), is equal to 2, and $\bar{\beta}=\frac{2}{3}$.

The *creep function* $\varphi(t)$ is obtained by inverting the Laplace transform (33). Consider first the last term $(p/2)^{\frac{1}{2}}/(1+p^2)$. Since $1/(1+p^2)$ is the transform of $\sin t$ and $(2p)^{-\frac{1}{2}}$ is the transform of $(2\pi t)^{-\frac{1}{2}}$, there is, by Borels theorem,[22]

$$p\frac{1}{(2p)^{\frac{1}{2}}(1+p^2)}=\frac{d}{dt}\int_0^t\frac{\sin(t-\tau)}{(2\pi\tau)^{\frac{1}{2}}}d\tau. \tag{40}$$

The integral can easily be expressed in terms of Fresnel's integrals

$$S(t)=\int_0^t\frac{\sin t}{(2\pi t)^{\frac{1}{2}}}dt, \tag{41a}$$

$$C(t)=\int_0^t\frac{\cos t}{(2\pi t)^{\frac{1}{2}}}dt.[23] \tag{41b}$$

It is interesting to note, that the expression (40) also appears in the theory of the transmission line; in this connection it has been discussed by McLachlan[24] with the aid of the complex inversion theorem. The second term in (33), obtained from the foregoing one by multiplication with p, obviously is equal to the derivative of (40), the identification of p with d/dt being justified because the expression to which it applies disappears for $t=0$. Therefore the final result is

$$\varphi(t)=\frac{2}{(2\pi t)^{\frac{1}{2}}}+2\sin t[1-C(t)-S(t)]+2\cos t[S(t)-C(t)]. \tag{42}$$

For small values of t there is

$$t\to 0:\quad \varphi(t)=2/(\pi t)^{\frac{1}{2}}. \tag{43a}$$

For very great values of t the asymptotic expansion formula for the Fresnel integrals[23] gives

$$t\to\infty:\quad \varphi(t)=1/t(2\pi t)^{\frac{1}{2}}. \tag{43b}$$

The behavior of the function (42) at very small and at very great values of t is up to a constant *identical* with that of the corresponding Cole function (I (40), (41)). It can be shown, that this is not restricted to the value $\alpha=\frac{1}{2}$, but happens for all values of α. Figure 1 gives in a logarithmic scale the function $\varphi(t)/2$ given by (42).

In I, it has been shown, how the generalization of the simple power law can lead to a very general type of creep function which is identical with the function indicated by Cole. It can be expressed in terms of the Mittag-Leffler function $E_m(-t)$. For $m=\frac{1}{2}$ the Mittag-Leffler function reduces to the expression[25]

$$E_{\frac{1}{2}}(-t)=\exp(t^2)[1-\Phi(t)], \tag{44}$$

where $\Phi(t)$ is the error integral; this gives for the creep function

$$\varphi(t)=\frac{1}{(\pi t)^{\frac{1}{2}}}-e^t[1-\Phi(\sqrt{t})]. \tag{45}$$

This function has also been plotted in Fig. 1. Clearly the difference between the two functions is small.

For α of the form $\alpha=n/m$, where n and m are integers, the integral (22b) can still be evaluated, but with increasing values of n and m the calculus becomes increasingly tiresome. The creep function can without difficulty be obtained in series form, which allows for numerical computation.

I am very much indebted to the Director of the Institute, Professor E. L. da Fouseca Costa, who made this study possible.

[22] See R. V. Churchill, *Modern Operational Mathematics in Engineering* (McGraw-Hill Book Company, Inc., New York, 1944), p. 37.

[23] Tables and expansions for the Fresnel integrals are given by E. Jahnke and F. Emde, *Funktionentafeln* (B. G. Teubner, Leipzig, 1923), p. 24.

[24] N. W. McLachlan, *Complex Variable and Operational Calculus* (Cambridge University Press, Teddington, England, 1939), p. 92.

[25] F. M. de Oliveira Castro, Zeits. f. Physik **114**, 116 (1939), Eq. (37).

A Determination of the Elastic Constants for Beta-Quartz

E. W. Kammer, T. E. Pardue,* and H. F. Frissel**
Naval Research Laboratory, Washington, D. C.

(Received September 2, 1947)

The complete set of adiabatic elastic constants for beta-quartz have been obtained for a series of temperatures ranging from 580°C to 800°C. The elastic moduli were computed from the elastic constants and are compared with the adiabatic and isothermal values which have been determined by others.

INTRODUCTION

An experimental method for determining the adiabatic elastic constants for beta-quartz has been described by Kammer and Atanasoff[1] and values for the constants were reported at a single temperature of 600°C. The data contained in the present report are an extension of their work using the same experimental method to cover most of the temperature range in which beta-quartz is known to exist.

GENERAL CONSIDERATIONS

The general theory of wave propagation in homogeneous aeolotropic media as developed by Christoffel and others (for example, see Cady[2]) achieves a desirable simplicity when applied to thickness vibrations in plane-parallel crystal plates of infinite area. In order to employ this method of analysis on the vibrations generated in small plates of alpha-quartz, Atanasoff and Hart[3] demonstrated experimentally that the perturbing effect of the finite plate edges on the resonance frequencies, f_n, diminishes as the number of nodal planes between two opposite surfaces of a vibrating plate are increased, where f_n is the observed frequency and n the order of the harmonic. When the order n of the harmonic was made sufficiently large, the ratio f_n/n approached an asymptotic value which was found to depend only on the thickness of the plate, the mode of vibration, and the elastic properties of the medium. Under these conditions the plate behaves essentially as a two-dimensionally infinite plate, and it is permissible to apply the Christoffel method.

The theoretical treatment used in this report is identical with that outlined in the work of Atanasoff and Hart[3] on alpha-quartz modified as explained in the paper of reference 1 so as to apply to the hexagonal holoaxial symmetry (D_6 Schoenflies) present in beta-quartz.[4,5] This crystal class has a single sixfold axis and six twofold axes perpendicular to it so that there are five independent elastic constants. The matrix in Voigt's[6] notation has the following form:

$$\begin{matrix} c_{11} & c_{12} & c_{13} & 0 & 0 & 0 \\ c_{12} & c_{11} & c_{13} & 0 & 0 & 0 \\ c_{13} & c_{13} & c_{33} & 0 & 0 & 0 \\ 0 & 0 & 0 & c_{44} & 0 & 0 \\ 0 & 0 & 0 & 0 & c_{44} & 0 \\ 0 & 0 & 0 & 0 & 0 & \frac{1}{2}(c_{11}-c_{12}). \end{matrix}$$

The secular equation for the plate orientations used in this study becomes:

$$\begin{vmatrix} c_{11}'-K^2 & 0 & c_{15}' \\ 0 & c_{66}'-K^2 & 0 \\ c_{51}' & 0 & c_{55}'-K^2 \end{vmatrix} = 0. \qquad (1)$$

In this expression $K^2=4\rho d^2(f_n/n)^2$, where ρ is the density and d is the thickness of the plate. Here a double-subscript notation for the elastic constants has replaced the four-subscript notation used in reference 3. The primes indicate that the constants are referred to the rotated axes. The rotated axes, $x_1'x_2'x_3'$, are related to the principal

* Now at the University of North Carolina.
** At Cornell Aeronautical Laboratory, Buffalo, New York.
[1] E. W. Kammer and J. V. Atanasoff, Phys. Rev. **62**, 395 (1942).
[2] W. G. Cady, *Piezoelectricity* (McGraw-Hill Book Company, Inc., New York, 1946), pp. 104–106.
[3] J. V. Atanasoff and P. J. Hart, Phys. Rev. **59**, 85 (1941).
[4] W. Bragg and R. E. Gibbs, Proc. Roy. Soc. London **A109**, 414 (1925).
[5] R. W. G. Wyckoff, Am. J. Sci. **11**, 112 (1926).
[6] W. Voigt, Lehrbuch der Kristallphysik (Teubner, Leipzig, 1928), pp. 585–586 and 830–831.

TABLE I. Dimensions and orientations of the quartz plates at room temperature. The angle, theta, is measured between the x_1 and x_1' axes, being a rotation about a common x_2 axis for both coordinate systems except for the Y-cut. The x_1' axis is in the thickness direction through the plate. Lateral dimensions of all the plates were nearly alike, averaging about 2.3 centimeters.

θ	30°	45°	60°	90° (Z-cut)	Y-cut
Thickness in cm	0.4549	0.4549	0.4549	0.4333	0.4445

crystal axes, $x_1x_2x_3$, by the scheme:

	x_1	x_2	x_3
x_1'	a_{11}	0	a_{13}
x_2'	0	1	0
x_3'	$a_{31}=-a_{13}$	0	$a_{33}=a_{11}$

where a_{11} etc. are the direction cosines. Equation (1) is limited to plate orientations for which the x_2' axis is parallel to the x_2 direction. The x_1' axis is along the thickness direction. The primed constants can then be expressed in terms of the principal elastic constants by the following equations:

$$c_{11}'=a_{11}^4c_{11}+a_{13}^4c_{33}+2a_{11}^2a_{13}^2c_{13}+4a_{11}^2a_{13}^2c_{55}, \quad (2)$$

$$c_{66}'=a_{13}^2c_{44}+a_{11}^2c_{66}, \quad (3)$$

$$c_{55}'=a_{11}^2a_{13}^2c_{11}+a_{11}^2a_{13}^2c_{33}-2a_{11}^2a_{13}^2c_{13}+(a_{11}^2-a_{13}^2)^2c_{55}, \quad (4)$$

$$c_{15}'=c_{51}'=-a_{11}^3a_{13}c_{11}+a_{11}a_{13}^3c_{33}+(a_{11}^3a_{13}-a_{11}a_{13}^3)c_{13}+2(a_{11}^3a_{13}-a_{11}a_{13}^3)c_{55}. \quad (5)$$

In the above equations the equality between c_{44} and c_{55} has not been used since c_{44} and c_{55} are coupled differently by means of the piezoelectric constants to the applied fields. In this way it is possible to identify the modes which are excited if the direction of the field is known, as will be explained below. Also c_{66} is measured as a single constant and the equality $c_{66}=\frac{1}{2}(c_{11}-c_{12})$ is not used until later.

When the expressions for the c' constants are substituted into Eq. (1) and expanded, the relation between the elastic constants, direction cosines, and K^2 becomes:

$$[a_{13}^2c_{44}+a_{11}^2c_{66}-K^2]\times[a_{11}^2a_{13}^2c_{13}^2+2a_{11}^2a_{13}^2c_{55}c_{13}-a_{11}^2a_{13}^2c_{11}c_{33}+(a_{11}^2K^2-a_{11}^4c_{55})c_{11}+(a_{13}^2K^2-a_{13}^4c_{55})c_{33}-(K^2-c_{55})K^2]=0. \quad (6)$$

There are five independent unknown elastic constants in this equation and three predicted modes of vibration indicated by the three possible values for K^2. The process of determining the unknown constants in Eq. (6) is begun by selecting one plate with the direction cosines $a_{11}=0$, and $a_{13}=1$. This has been called a Z-cut. Under these conditions terms with c_{44} and c_{55} are factorable, giving

$$(c_{44}-K^2)(c_{55}-K^2)(c_{33}-K^2)=0. \quad (7)$$

The two piezoelectric constants for beta-quartz,[7] $e_{14}=-e_{25}$, permit modes involving the c_{44} elastic constant to be excited by a field in a direction x_1, and, correspondingly, the field must have a component in the direction x_2 when driving modes dependent upon the c_{55} elastic constant. Hence it is not possible to excite the mode for c_{33} in Eq. (7) by means of coupling

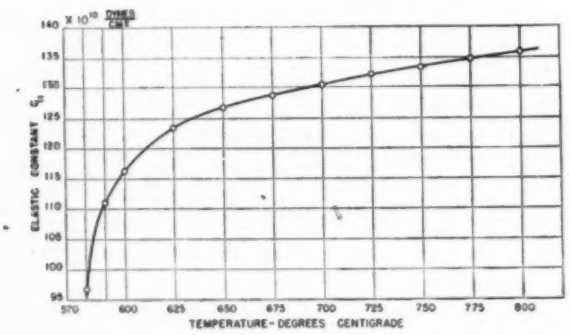

FIG. 1. The c_{11} adiabatic elastic constant for beta-quartz as a function of temperature.

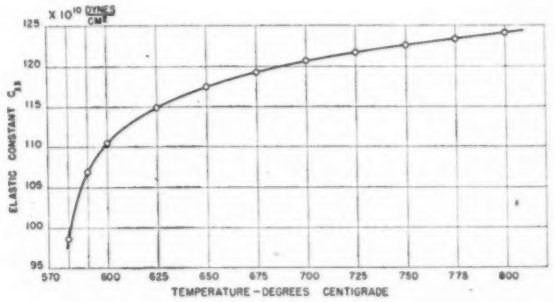

FIG. 2. The c_{33} adiabatic elastic constant for beta-quartz as a function of temperature.

[7] W. Voigt, *Lehrbuch der Kristallphysik* (Teubner, Leipzig, 1928), pp. 830–831.

through a piezoelectric effect. The remaining two modes can be driven by this means. Additional verification of the value for c_{44} was obtained from a Y-cut. For a plate of this orientation the x_1' axis is directed parallel to a principal x_2 axis and the secular equation reduces to:

$$(c_{66}-K^2)(c_{11}-K^2)(c_{44}-K^2)=0. \qquad (8)$$

The value of c_{44} now being known, it is possible to determine c_{66} from the linear factor of Eq. (6). However, it is necessary to select the proper mode of vibration for computation of the K^2 which occurs in this factor. This can be done by choosing the direction of the applied alternating field so as to utilize the appropriate piezoelectric constant for coupling with c_{44}. The frequency of vibration associated with the factor containing c_{66} in Eq. (6), will appear when the field is applied so as to have a component along the x_1 principal axis. The constant c_{55} which occurs in the quadratic factor requires that the field be applied along the x_2 principal axis in order to excite the modes associated with this factor.

The terms in the quadratic factor of Eq. (6) can be rearranged as is shown below:

$$a_{11}^2a_{13}^2\{c_{13}^2+2c_{55}c_{13}-c_{11}c_{33}\} +(a_{11}^2K^2-a_{11}^4c_{55})c_{11} +(a_{13}^2K^2-a_{13}^4c_{55})c_{33}=(K^2-c_{55})K^2. \qquad (9)$$

If three or more independent equations of this form can be found it is possible to eliminate the terms in the braces and solve for c_{11} and c_{33}. The elastic constant c_{13} can then be obtained from any one of the original quadratic factors by use of the quadratic formula or numerical approximation after substituting the values for c_{11} and c_{33}. The

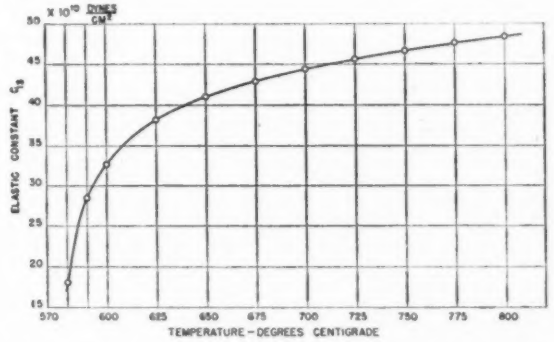

FIG. 3. The c_{13} adiabatic elastic constant for beta-quartz as a function of temperature.

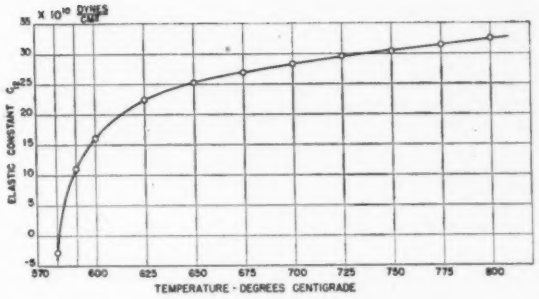

FIG. 4. The c_{12} adiabatic elastic constant for beta-quartz as a function of temperature.

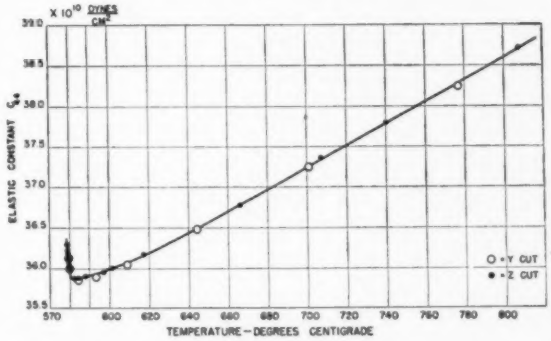

FIG. 5. The c_{44} adiabatic elastic constant for beta-quartz as a function of temperature.

elastic constant, c_{66}, is related to c_{11} and c_{12} by the equation:

$$c_{66}=\tfrac{1}{2}(c_{11}-c_{12}). \qquad (10)$$

Since c_{66} and c_{11} are now available, c_{12} can be computed. This completes the solution of Eq. (6).

EXPERIMENTAL

The apparatus used in the present experiment was improved in several respects over that employed for the earlier work.[1] A General Radio Type LR frequency standard with interpolation oscillator gave greater precision and speed in the

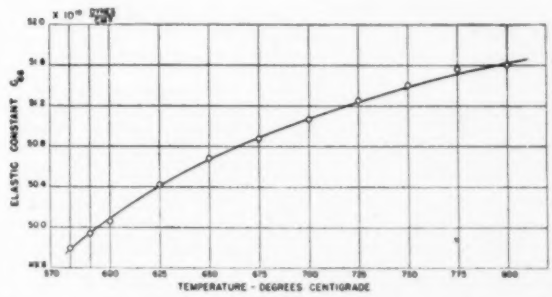

FIG. 6. The c_{66} adiabatic elastic constant for beta-quartz as a function of temperature.

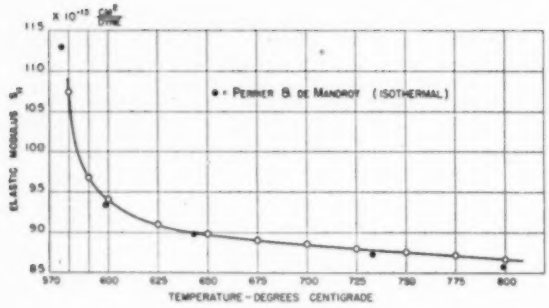

FIG. 7. The s_{11} adiabatic elastic modulus for beta-quartz as a function of temperature. Isothermal values determined by Perrier and de Mandrot are also shown.

measurement of the frequencies of the plates. Changes were made in the construction of the furnace to permit closer control of the temperature. The electrode assembly holding the quartz plate in the furnace was redesigned so as to have greater resistance between the electrodes at high temperatures. This increased the sensitivity of the detector and permitted measurements to be made on harmonic resonances of higher order than previously attainable.

Five plates were used to obtain the frequency data. These plates were prepared by the National Bureau of Standards. The orientations were measured with an x-ray goniometer. The quartz material was examined for flaws and twinning by optical methods developed at the Bureau and the final surfaces were etched. No conducting material was deposited on any of the surfaces. The dimensions and orientations are given in Table I.

The uncertainty in the orientation angle θ as given in Table I is about 2 minutes of arc. These specifications apply to the plates at room temperature. The orientation and thickness change slightly when the plates are elevated to the temperatures necessary for beta-quartz. Corrections for these changes in orientation and thickness were made in the same manner as is described in reference 1. They are based on the thermal expansion coefficients measured by Jay.[8] The maximum correction in orientation angle is encountered with the 45° plate and is about 12 minutes of arc

The density of beta-quartz used in the calculations for the elastic constants was estimated from the density of alpha-quartz at room temperature, 2.648 g/cm³, and the expansion coefficients $\gamma_y = 0.01733$ and $\gamma_z = 0.00998$. Thus:

$$\rho_\beta = \rho_\alpha/(1+\gamma_y)^2(1+\gamma_z). \qquad (11)$$

This yields a value of 2.533 g/cm³ at 600°C. According to the expansion coefficient data obtained by Jay and also the direct measurements of Day, Sosman, and Hostetter,[9] the density of beta-quartz may be considered to remain constant for the temperature range under consideration in this experiment without introducing serious error.

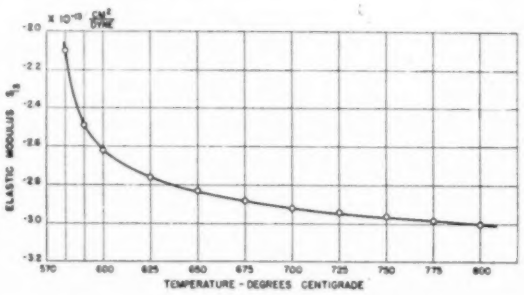

FIG. 9. The s_{13} adiabatic elastic modulus for beta-quartz as a function of temperature.

Beta-quartz is abnormal in that the density increases slightly with increasing temperature.

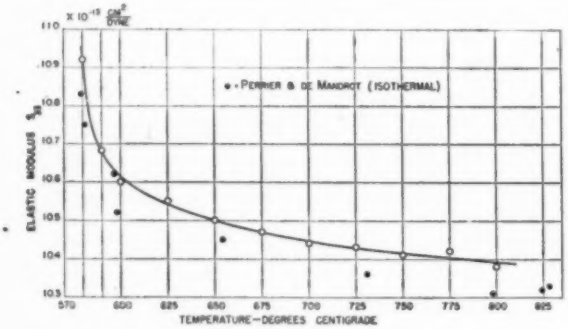

FIG. 8. The s_{33} adiabatic elastic modulus for beta-quartz as a function of temperature. Isothermal values determined by Perrier and de Mandrot are also shown.

RESULTS

Frequencies for ten modes of vibration were measured for the five plates. One mode from each of the Z- and Y-cuts was used to determine c_{44}. The 30°, 45°, and 60° plates each furnished one mode from which c_{66} could be computed with the c_{44} constant being known. Five more modes were observed in the same three plates to furnish an over-determination of c_{11}, c_{33}, and c_{13}.

[8] A. H. Jay, Proc. Roy. Soc. London **A142**, 237 (1933).
[9] A. L. Day, R. B. Sosman, and J. C. Hostetter, Am. J. Sci. **37**, 16 (1914).

A numerical check on the consistency of the experimental results was made by evaluating c_{13} from each of the five equations after c_{11} and c_{33} were known. At 580°, four equations yielded values of c_{13} consistent to within 0.5 percent while the fifth gave a value about 20 percent higher than the mean of the other four. For temperatures above 600°C, the variation of any value from the average at the temperature in question was less than 0.5 percent. The change in frequency of vibration of the plates was large for small temperature variations near the transition point.

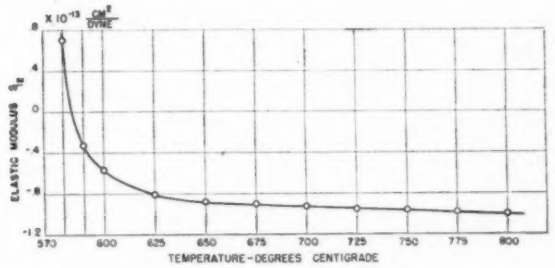

FIG. 10. The s_{12} adiabatic elastic modulus for beta-quartz as a function of temperature.

This increases the difficulty in ascertaining the frequencies in this region and perhaps largely accounts for the major inconsistency in the results for c_{13} at 580°C.

The values of the elastic constants are presented in graphical form in Figs. 1 through 6. Since the crystal plates were not coated with conducting material and were excited in an air gap, the measurements were made under "open circuit" electrical conditions and strictly speaking should be denoted by c^D. Because of the small piezoelectric coupling in beta-quartz, the difference between the "open circuit" (constant charge) constants c^D and the "short circuit" (constant field) constants c^E is less than experimental error so the superscripts are omitted in this paper.

During the measurement of the frequencies of vibration for each mode no attempt was made to set the furnace at the temperatures for which values of the constants are shown. Instead, the furnace was permitted to come to equilibrium at a series of arbitrary temperatures. Interpolation on a graph of these frequencies permitted the selection of values for use in computing the K^2 terms for each mode at the same temperature.

It is possible to compute the elastic moduli

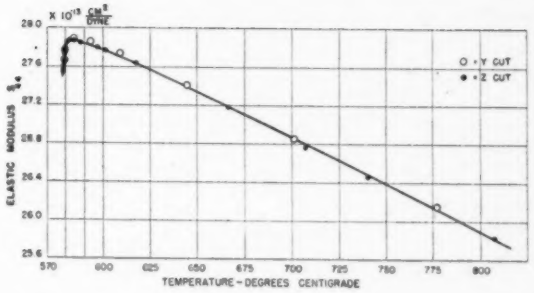

FIG. 11. The s_{44} adiabatic elastic modulus for beta-quartz as a function of temperature.

from the elastic constants, as shown, for example, by Wooster.[10] The values for the moduli obtained in this way are shown in Figs. 7 through 11.

Perrier and de Mandrot[11] measured by isothermal methods the s_{11} and s_{33} moduli as well as a modulus at 50° with respect to the optic axis for beta-quartz. Their values for s_{11} and s_{33} are plotted without correction to adiabatic conditions beside the adiabatic values in Fig. 7 and Fig. 8 respectively.

The elastic constant c_{12}, shown in Fig. 4, becomes negative near the transition temperature. In this connection reference is made to the data in Table V of Atanasoff and Hart.[3] They have tabulated data for c_{11}, c_{66}, c_{44}, and c_{14} for alpha-quartz up to the transition temperature. Using Eq. (10), c_{12} can be computed from their values given for the constants c_{11} and c_{66}. Table II was obtained in this manner and shows the way c_{12} changes with temperature. Apparently the elastic constant, c_{12}, is negative during the transition and changes sign in the beta-state at a temperature a little above 580°C. It is also of interest to note that all of the elastic constants for beta-quartz become stiffer as the temperature increases.

Lawson[12] has measured the adiabatic Young's modulus for beta-quartz along a direction at 45° to the optic axis. This was done by setting up longitudinal vibrations in a rod-shaped specimen. The modulus was computed from the relation:

$$1/s_{33}' = 4f^2L^2\rho(1+k), \qquad (12)$$

[10] W. A. Wooster, *A Text Book on Crystal Physics* (Cambridge University Press, Teddington, England, 1938), pp. 235–237.

[11] A. Perrier and B. de Mandrot, *Memoires de la Société Vaudoise des Sciences Naturelles* (Imprimeries Réunies S. A., Lausanne, 1923), No. 7, pp. 333–363.

[12] A. W. Lawson, Phys. Rev. 59, 608 (1941).

TABLE II. Values for c_{12} as computed from the data for c_{11} and c_{66} of Atanasoff and Hart. ($c_{12}=c_{11}-2c_{66}$.)

Temp. °C	$c_{12}\times10^{10}$ dynes/cm²	Temp. °C	$c_{12}\times10^{10}$ dynes/cm²
0	6.70	500	−13.8
100	4.90	540	−19.3
200	2.60	550	−21.8
300	−0.70	562	−25.8
400	−5.40	573	−32.9

where f is the frequency, L the length of the rod, ρ the density, and k is a Rayleigh correction to compensate for the depression in frequency due to the loading effect of the finite rod cross section. The magnitude of the correction term k for 600°C was estimated to be 0.003. The density for quartz at 600°C used by Lawson was 2.518 g/cm³. If this be changed to 2.533 g/cm³ to permit comparison with the data being presented here, Lawson's determination of the s_{33}' modulus is reduced from 1.067×10^{-12} cm²/dyne to 1.061×10^{-12} cm²/dyne.

The s_{33}' adiabatic modulus at 45° to the optic axis can be computed from the elastic moduli,[13] shown in Figs. (7) to (11), by means of the relation:

$$s_{33}'=s_{11}(1-\alpha_3^2)^2+s_{33}\alpha_3^4+(2s_{13}+s_{44})(1-\alpha_3^2)\alpha_3^2. \quad (13)$$

Since the direction cosine, α_3, is equal to $\sqrt{2}/2$ for the 45° orientation, expression (13) reduces to:

$$s_{33}'=\tfrac{1}{4}(s_{11}+s_{33}+s_{44}+2s_{13}). \quad (14)$$

[13] W. Voigt, reference 5, p. 740.

The values to be used for the moduli on the right-hand side of Eq. (14) at 600°C are:

$$s_{11}=0.941,\quad s_{44}=2.773,$$
$$s_{33}=1.062,\quad s_{13}=-0.262,$$

each multiplied by the factor 10^{-12} cm²/dyne. When these constants are substituted into Eq. (14), s_{33}' becomes 1.062×10^{-12} cm²/dyne, to be compared with Lawson's modified result of 1.061×10^{-12} cm²/dyne. At higher temperatures, the 45° modulus, as computed from the elastic moduli, deviates in a uniform manner from the 45° modulus as computed from Lawson's data, the former being about 5 percent lower at 800°C.

ACKNOWLEDGMENTS

The authors are grateful for this opportunity to record their sincere appreciation to Dr. Irwin Vigness for constructive criticism and encouragement throughout the course of the experimental work. They also wish to thank Mr. Leland T. Sogn in charge of the quartz processing laboratory at the National Bureau of Standards for his generous cooperation, and in particular to thank Miss Catherine Barclay who was responsible for the orientation measurements on the plates used in this experiment. Grateful acknowledgment is made to Dr. Paul L. Smith of the Naval Research Laboratory Crystal Section for his many helpful suggestions. Mr. Fred Havercroft gave valuable aid in preparing the figures presented here as well as numerous graphs of the frequency data necessary for computation purposes.

Dark-Field Electron Microscopy

II. Studies of colloidal carbon

C. E. HALL
Massachusetts Institute of Technology, Cambridge, Massachusetts
(Received September 8, 1947)

Several commercial carbon blacks were examined with dark-field illumination in the electron microscope. Anomalous intensities in the dark-field images are interpreted as resulting from coherent scattering by parallel layer groups of graphitic planes, which were previously identified by Biscoe and Warren using x-ray diffraction. The dark-field micrographs indicate that in a non-reinforcing and a semireinforcing black, the parallel layer groups near the surface of the roughly spherical particles are oriented with their representative vector approximately normal to the surface. No definite evidence was obtainable for such an arrangement in a reinforcing channel black with average particle diameter about 300A. After prolonged heat treatment to the point where graphitization occurs the channel black exhibits numerous diffraction images in dark-field, indicating the presence of crystals with dimensions in the range 20 to 90A.

INTRODUCTION

CARBON black produced by incomplete combustion of gaseous hydrocarbons is widely used as a pigment in inks and lacquers and is of particular importance as an ingredient in rubber compounding. There are many grades, differing from one another in ultimate particle size and other properties. Average particle size may be from 50A up to several thousand A. Biscoe and Warren[1] have shown through x-ray analysis that carbon black is not finely divided graphite. The structure is one of true graphite layers arranged roughly parallel and equidistant, but otherwise completely random as to orientation about an axis normal to the layers. The interplanar spacing is somewhat larger than that for graphite. Dimensions of the parallel layer groups in different blacks were found to be from 12.1 to 26.6A for the axis perpendicular to the graphite planes (L_c) and from 18.6 to 47.5A parallel to the planes (L_a). These results indicate that a carbon particle is a mesomorphic solid, neither crystalline nor amorphous, for which class of substances they suggest the term "turbostratic." When carbon black is heated to about 1000°C and higher, the graphite layers grow and thermal agitation allows orientation of the graphite planes over limited regions to produce small graphite crystals. At the same time there is a decrease in the interplanar spacing. From measurement of the x-ray line breadths, Biscoe and Warren have estimated the average dimensions of these graphite crystallites to be up to 40.0A for L_c and up to 65.2A for L_a.

Further evidence concerning the structure of carbon black comes from the calorimetric determination of heats of adsorption reported by Beebe, Biscoe, Smith, and Wendell.[2] Experiments on the same black with and without devolatilization, indicate that it is the state of the underlying solid rather than the presence of a chemisorbed layer which determines the magnitude of the binding energy for the adsorbed molecules of nitrogen. The binding energy for a monolayer is considerably higher than the heat of liquefaction. In the initial stages of adsorption, the binding energy is abnormally high, indicating that the first fraction of a monolayer is bound at active centers. When the black is heat-treated to the point where graphitization occurs as in the x-ray experiments, there is a marked decrease in the heat of adsorption in the initial stage, indicating disappearance of the active centers as a more ordered structure is produced. Although the role of the active centers in rubber reinforcement remains to be determined, the surface activity as determined by heat measurements closely parallels the rubber-reinforcing properties of the black.[3]

[1] J. Biscoe and B. E. Warren, J. App. Phys. **13**, 364 (1942).

[2] R. A. Beebe, J. Biscoe, W. R. Smith, and C. B. Wendell, J. Am. Chem. Soc. **69**, 95 (1947).

[3] W. R. Smith, F. S. Thornhill, and R. I. Bray, Ind. Eng. Chem. **33**, 1304 (1941).

The electron microscope is widely used to measure the particle size of carbon blacks and to observe their state of aggregation. The literature contains many papers on the subject of which the work of Ladd and Wiegand[4] and Watson[5] may be cited as examples. Although the ultimate particles are in most cases roughly spherical, Hofmann and Höper[6] have shown that after prolonged heat treatment at 3000°C the particles develop angularities in outline. In a recent note[7] the author included a dark-field micrograph in which images of carbon particles exhibited regions of enhanced intensity at their edges. The reason for this appearance was not obvious, but it was suggested that the enhanced intensities were in some way related to the crystal structure near the particle surface. It appeared that the dark-field method was capable of showing structural features that are not visible in bright-field. These phenomena have been studied further with techniques described in Part I and are the subject of the present report.

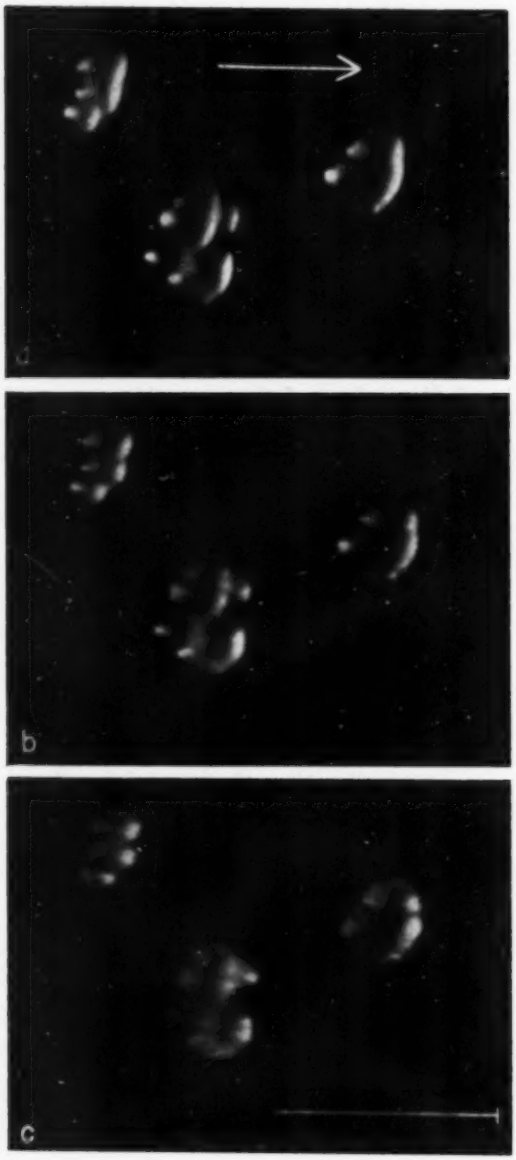

FIG. 1. Dark-field images with tilted beam of carbon particles (P33), objective current decreasing from (a) to (c). Arrow indicates direction of aperture.

OBSERVATIONS OF CARBON PARTICLES IN DARK-FIELD

The bright spots which appear at the edges of dark-field images of certain relatively large carbon particles,[7] exhibit peculiarities in the manner of their occurrence and in their appearance in a through-focus sequence. They occur only on edges directly toward or directly away from the aperture (the region of bright-field illumination) and never at edges whose tangent is in the aperture direction. In some instances, enhanced spots have been observed apparently in this latter position, but further study has established that these come from smaller particles, sometimes poorly resolved, at the edge of a larger one. Spots away from the aperture which are produced by pencils bent under the particle, are not in focus at the same objective setting as those toward the aperture, which are produced by pencils reflected away from the particle. This anomaly is shown in the three micrographs reproduced in Fig. 1. The material, consisting of relatively large particles, is known as P33 and is classified as non-reinforcing in rubber. The objective current was decreased in steps from (a) to (c) and the aperture direction is indicated by an arrow. In (a) the spots are visible on edges away from the aperture, but the edges toward the aperture appear as a broad, bright line. As the objective current is decreased from (a) to (c) the images away from the aperture go out of focus and those toward the aperture come into focus. For these micrographs, the

[4] W. A. Ladd and W. B. Wiegand, Rubber Age **57**, 299 (1945).
[5] J. H. L. Watson, J. App. Phys. **17**, 121 (1946).
[6] U. Hofmann and W. Höper, Naturwiss. **32**, 225 (1944).
[7] C. E. Hall, J. App. Phys. **18**, 588 (1947).

incident beam was tilted with respect to the lens axis to minimize the displacement of the enhanced images that normally occurs when the objective current is altered. The fact that the two sets of images are not in focus at the same objective setting indicates either that observed structures are at different levels, or that the respective imaging pencils make quite different angles with the lens axis.

In Fig. 2 is reproduced a typical micrograph for which the objective current was decreased slightly below the value for best focus so that the object plane is above the object. In this case the incident beam is closely parallel to the lens axis. The scattered intensity toward the aperture is displaced into the particle, while the enhanced spots sway from the aperture are displaced away from the particles. The displacements indicate that the scattered pencils make relatively large angles with the lens axis, and the coherency of the displaced images indicates that the pencils are confined to narrow relative aperture. These are just the characteristics of pencils produced by Bragg reflections. It is therefore concluded that the enhanced intensities at the particle edges are owing to the presence of crystalline structure. However, the enhanced images have diameters in the range 100 to 900A and the images are quite diffuse compared to dark-field images of single crystals in this range of dimensions. This particular carbon black was studied by Biscoe and Warren[1] who give the values, $L_c = 16.8$ and $L_a = 28.0$A. Obviously, single crystals of these dimensions could not account for images of the size and intensity observed at the edges. The diffraction images must consist of the superimposed images of assemblies of parallel layer groups. The fact that the diffraction images are deflected approximately as a unit indicates that within an assembly the individual crystallites are oriented with their reflecting planes nearly parallel to one another.

That enhanced intensities never occur on edges whose tangent is the aperture direction can mean one of two possibilities, (a) diffracted rays are prevented from leaving the particles with an appreciable component tangential to the image periphery by refraction or some other factor, or (b) reflecting planes responsible for the principal scattered intensity do not occur near the surface

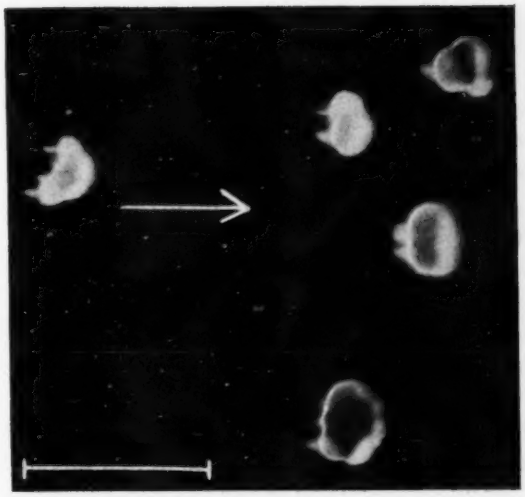

FIG. 2. Dark-field images of carbon particles (P33), objective current lower than for best focus. Arrow indicates direction of aperture.

except with their representative vector approximately normal to the surface. Possibility (a) is discounted because there appears to be no reason why, if the particles contain a random assembly of crystallites, rays should not leave at all azimuths. Possibility (b) is therefore proposed as the explanation. To identify the planes most probably responsible for the diffraction images, we refer to the x-ray diagram of Biscoe and Warren.[1] Their Fig. 1(a) shows that almost all the diffracted intensity is contained in the rather broad (002) ring. Since relative electron diffraction intensities follow those in x-ray diagrams rather closely, it is assumed that the diffraction spots in the dark-field electron microscope images result mainly from the (002) spacing. This would mean that the (002) vector is, near the surface, always approximately normal to the surface. The conclusion then follows that in carbon particles of this particular sample the parallel layer groups originally determined from x-ray analysis are, near the surface, all oriented with the graphite layers approximately parallel to the surface of the particles, but are otherwise randomly disposed with respect to one another so that there is lack of coherency between the individual groups.

The P33 carbon black shown in Figs. 1 and 2 has an average particle diameter of about 1400A and is classified as non-reinforcing in rubber. Several other types of black were examined, one

of which is classified as semireinforcing and is known under the trade name of Sterling R. The average diameter in this case is about 800A. Dark-field micrographs exhibit phenomena similar to those described above and typical micrographs of a group of particles are reproduced in Fig. 3. For (a) the objective current is at, or a little higher than, that for best focus and the scattered intensity from edges away from the aperture is imaged as diffuse spots which taper inward. In (b) the intensity from edges away from the aperture is deflected away from the particles to form brush-like streaks, while the intensity on edges toward the aperture appears as spots. (Different exposure times were used for the upper and lower parts of the print in (b) in order to show the intensity distribution to better advantage.) This effect is like that shown in Fig. 2, but the resolution of the deflected intensity into narrow streaks indicates inhomogeneities in the surface of 100A and less. That fine structure was not observed in the deflected intensity as shown in Fig. 2, may mean either that the structure for P33 is too small to be resolved, or that there is too much overlapping in the image.

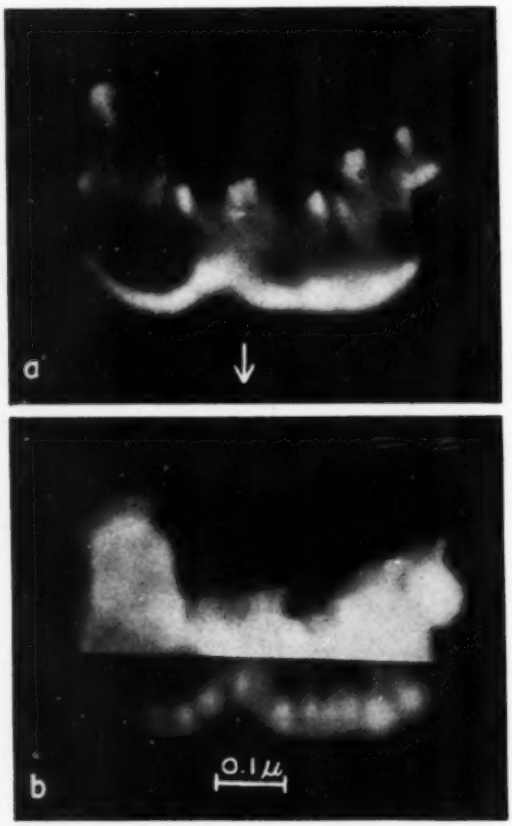

FIG. 3. Dark-field images of carbon particles (Sterling R), (a) objective current close to best focus, (b) objective current lower than for best focus. In (b), upper and lower portions of the print have been given different exposure times. Arrow indicates direction of aperture.

A few comments should be made on the curious alterations that take place in the image with alterations in objective current as illustrated in Figs. 1, 2, and 3. It is to be noted that the distribution of intensity seen in the image is a cross section, real or virtual, of the scattered beam at a plane determined by the objective current. There is a notable difference between the two sets of images, those on edges toward the aperture and those at edges away from the aperture. In an image which is in best focus, edges away from the aperture exhibit diffuse spots which taper inward, while the structures at edges toward the aperture tend to fuse together along the periphery as seen in Figs. 1(a) and 3(a). When the objective current is decreased from best focus, the typical behavior is as shown in Figs. 2 and 3(b). (Figure 1 is not typical of this condition since the incident beam was tilted.) At edges away from the aperture the scattered intensity fans out normal to the periphery in fine streaks which may or may not be resolved and at edges toward the aperture the intensity occurs as diffuse spots which are in the nature of a virtual crossover above the object plane (Fig. 3(b)). These differences indicate that the scattering mechanism is quite different at the opposite edges. Although it is not possible to give a quantitative explanation of these phenomena, some of the factors involved may be mentioned. If, as has been concluded, the parallel layer groups near the surface are oriented with their graphite planes approximately parallel to the surface, the scattered beam is reflected at edges away from the aperture as if from a concave surface, while the scattered beam at edges toward the aperture is reflected as from a convex surface. Also, in considering the possible factors contributing to the difference in appearance and behavior of the two sets of images, the effect of refraction at the particle surface must be considered. As was pointed out in Part I, when rays are incident at small angles to a surface, the refraction deflection

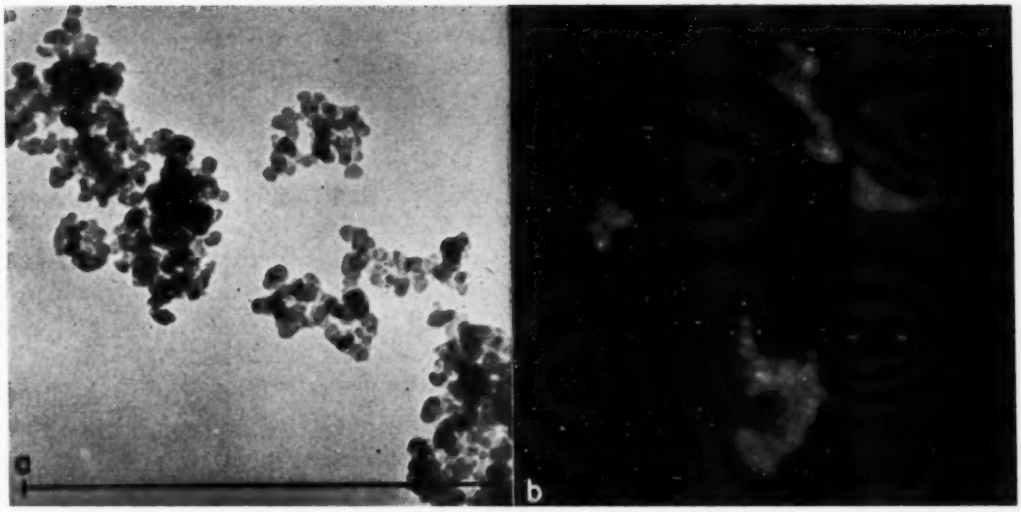

FIG. 4. Reinforcing channel black (Spheron Grade 6), (a) bright-field, (b) dark-field.

may be of the same order of magnitude as that given by the simple Bragg law. Furthermore, refraction effects would be quite different according to whether the scattered pencils were bent under the particle or reflected away from the particle. In view of these differences in the scattering mechanism, it is not surprising that images at opposite edges appear different at a given objective setting, or that the cross sections of the scattered beams undergo anomalous changes in intensity and shape with variations in objective current. Qualitatively, rays can be traced through particles near the edges to account for the observed anomalies in the images, but without more specific information on the structure of the particles or the magnitude of refraction effects, a rigorous treatment of the problem is not possible at present.

Probably the most interesting carbon blacks are those classified as reinforcing for rubber. Particle diameters are about 300A for this type. Unfortunately, the particles occur in aggregates which are difficult to separate and this, together with the small particle size, makes them difficult to study in dark-field. An example, shown in Fig. 4, is known commercially as Spheron Grade 6. In the bright-field micrograph may be seen the usual clusters of particles about 300A in diameter. In dark-field the individual particles are poorly resolved. Superimposed on the images of the clumps are weak spots, difficult to observe because of the diffuse intensity, but which are probably to be associated with assemblies of the parallel layer groups because they exhibit slight displacement with changes in objective current. Evidence, however, is lacking for any high degree of order as has been described for the larger blacks. As far as the electron microscope can show at present, the parallel layer groups are too small to be resolved individually and are randomly disposed. The x-ray results for this material are, $L_c = 12.7$ and $L_a = 20.0$A.

A sample of Spheron 6 which had been graphitized in commercial production was examined in dark-field in order to determine whether the changes observed in the x-ray work[1] could be detected with the electron microscope. Micrographs of the heat-treated sample (known commercially as Graphon) are shown in Fig. 5. The material had been heated in commercial production for about 24 hours at about 2500°C. In bright-field, (a), the particles appear to be sintered together and some show internal structure. In dark-field, (b), the aggregates exhibit numerous, sharp diffraction images with minimum dimensions of about 50A. The relation between image diameter and crystal dimensions is presumably like that estimated in Part I, Fig. 14. The largest diffraction images in Fig. 5 are about 90A and where they are intense, they probably represent crystals of about this size. The weak images probably represent crystals of

the minimum detectable dimensions which were estimated in Part I to be about 20A. Although there is some uncertainty in estimating crystal dimensions from such small dark-field images, it is concluded that the graphite crystals are present with dimensions between 20 and 90A. Biscoe and Warren give $L_c = 40.0$A and $L_a = 65.2$A for a sample heated at 2800°C for two hours, which was the longest heating time used at comparable temperatures. Of the x-ray samples, this one most closely approximates the conditions of preparation of the commercial sample used in the electron microscope work. Since it would be expected that crystals would be present on either side of the average x-ray values, it is apparent that the electron microscope observations are quite consistent with what would be expected from the x-ray results.

Another carbon black examined in dark-field was Shawinigan Standard Black (acetylene black). Watson[5] has studied this material in bright-field and has observed, attached to the spherical particles, rod-like elements which are apparently platelets oriented with their faces approximately parallel to the incident beam. Similar structures have been observed in this work, but only with this particular black. The rods are not very numerous and the bulk of the material appears to consist of roughly spherical particles of about 500A average diameter. In bright-field the particles exhibit considerable internal structure. In dark-field, numerous faint streaks about 75A wide, appear superimposed on the images of the particle aggregates and project around the edges. This structure has been seen only with this particular black and seems to indicate the presence of single, relatively large parallel layer groups. The streaks are like those which fan out from the edges of the Sterling black described above, but in the Shawinigan black they occur around the edges and throughout the aggregates. It is concluded that the parallel layer groups are relatively large in this black and occur in less orderly arrangement near the surface than in P33 or Sterling. The conclusion that the parallel layer groups are unusually large is consistent with Watson's observation of platelets in bright-field and it is also consistent with the observations of Biscoe and Warren, who calculate that the average dimensions of the parallel layer groups in this material are almost twice as large as those in the other blacks examined in the x-ray study.

CONCLUSIONS

The anomalous intensities appearing in dark-field micrographs of carbon particles are interpreted as originating in assemblies of the parallel layer groups originally determined through x-ray analysis. From the assumption that most of the coherently scattered intensity is in the (002)

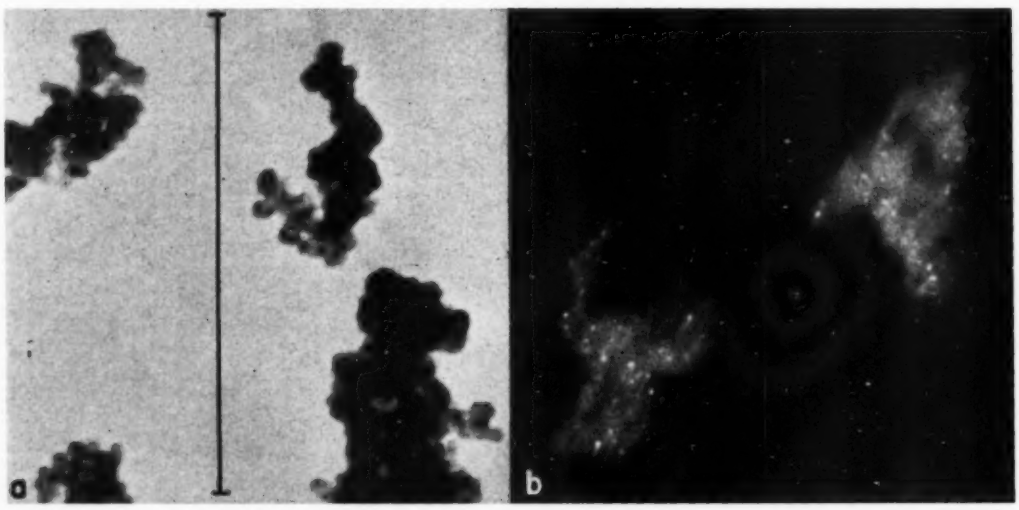

FIG. 5. The same type of black as shown in Fig. 4 after heat-treatment (Graphon), (a) bright-field, (b) dark-field.

reflection, it is concluded that for a sample of nonreinforcing black and another classified as semireinforcing, the parallel layer groups are oriented, near the particle surface, with the graphite planes approximately parallel to the surface. Evidence for structure of this type is lacking for a reinforcing channel black of much smaller particle size. Whether the absence of such evidence for the reinforcing black is owing to lack of resolution or contrast, or whether it represents a significant difference in the structure, it is not possible at present to say. After prolonged heating at elevated temperatures, a sample of channel black exhibited numerous sharp diffraction images indicating the presence of graphite crystallites with estimated dimensions between 20 and 90A. The absence of this type of image in the unheated samples is confirmation of the mesomorphic nature of colloidal carbon as determined from x-ray analysis. Observations on a sample of acetylene black indicate that in this material the parallel layer groups are relatively large. Evidence for preferential orientation is much less marked for this material than for the nonreinforcing and semireinforcing samples.

It is concluded that the size and relative orientation of the parallel layer groups vary from one type of black to another. No correlation has been made between the observed structures and the properties of carbon blacks in rubber compounding and other applications, but the results are strongly suggestive that some correlations may be possible with the acquisition of more and improved data. Although the resolution in dark-field is generally inferior to that in bright-field, the dark-field method appears to be useful in providing information concerning the crystalline structure of small colloidal particles.

SAMPLES.

Sample	Manufacturer
P33	Thermatomic Carbon Company, New York
Sterling R	Godfrey L. Cabot, Inc., Boston
Spheron Grade 6	Godfrey L. Cabot, Inc., Boston
Graphon	Godfrey L. Cabot, Inc., Boston
Shawinigan Standard	Shawinigan Products Corporation, New York

ACKNOWLEDGMENTS

The author is indebted to Professor G. G. Harvey and Professor B. E. Warren for advice and assistance during the course of this work and to Dr. W. R. Smith of Godfrey L. Cabot, Inc. who contributed samples of material and helpful discussions of the results.

Mass Emissivity of Powder Gases in Solid Fuel Rockets[1]

S. S. PENNER*
Allegany Ballistics Laboratory, Cumberland, Maryland
(Received October 3, 1947)

An analysis has been carried out to determine an upper limit for the effective mass emissivity of the radiating gases in a solid fuel rocket motor. The calculations depend upon a comparison between experimentally observed performance data relating to a rocket motor and theoretical results based on a theory for the effect of radiation on the performance of solid fuel rocket motors. A simplified treatment is developed for correlating the rate of burning of the powder with the temperature rise of a powder grain caused by the absorption of radiant energy.

INTRODUCTION

A SOLID fuel rocket motor is powered by a charge of combustible material. The power output of the motor depends upon the rate of generation of gaseous combustion products from the burning solid, on the temperature of the combustion products, the dimensions of the rocket chamber, etc. One of the factors which determines the rate of gas generation and, therefore, the performance of the rocket motor is the temperature of the powder before burning. This, in turn, is related to the absorption of radiant energy from the hot gases surrounding the solid fuel.[2]

The surface of a burning powder grain recedes in a direction normal to itself. As the grain burns, heated gases are evolved which may or may not undergo chemical reactions in the gas phase. Radiant energy is assumed to be emitted uniformly in all directions from the gaseous envelope surrounding the burning powder. A portion of this energy is absorbed by the gases separating the emitting layer from the powder surface. The light which is not reflected from the powder surface is absorbed by the powder grain. The decrease in intensity per unit distance depends on the absorption coefficients of the powder grain and on the wave-length distribution of the incident radiation. The burning rate of the powder grain, in turn, depends on the temperature rise accompanying the absorption of radiation.

The preceding physical picture requires several restrictive assumptions before useful calculations can be carried through, *viz.*,

(1) The gaseous envelope radiates like a graybody, i.e., the emissivity of the gases is the same for all wave-lengths. This implies that the temperature dependence of the radiation intensity is the same as that of a blackbody. It is recognized that this simplification cannot correspond to fact. However, it is necessitated by the absence of more detailed information.

(2) All of the radiant energy striking the powder surface is assumed to be incident in a direction normal to the surface of the powder grain. More general treatments without this simplifying assumption are quite complex and have been carried through in only a few selected cases.[3,4]

A complete treatment of the effect of radiation

[1] This is the first of three articles abstracted from OSRD report No. 5251 which was written in 1945 at the Allegany Ballistics Laboratory. The work was carried out under OSRD Contract OEMsr-273 with the George Washington University, Washington, D. C. The original paper was reissued as Part IV of OSRD report No. 5817.

A summary of the original paper is given in the Bibliography of Scientific and Industrial Reports, Office of Technical Service, Department of Commerce, Vol. 3, No. 4, Oct. 1946. The PB number is 34764.

The radiation program at the Allegany Ballistics Laboratory was initiated by the Director of Research, Dr. R. E. Gibson. Dr. W. H. Avery, to whom the author is indebted for advice throughout the course of the work, directed the radiation studies.

The author wishes to acknowledge the aid of the Editorial Staff of the Jet Propulsion Laboratory, California Institute of Technology, in preparing this paper for publication.

* Present address: Jet Propulsion Laboratory, California Institute of Technology, Pasadena, California.

[2] W. H. Avery, OSRD report No. 3880, July 1944; J. Beek, Jr., W. H. Avery, M. J. Dresher, F. T. McClure, and S. S. Penner, OSRD report No. 5817, 1946.

[3] B. L. Crawford, Jr. and R. G. Parr, University of Minnesota Report No. 27, February 1945. This memorandum is available in the files of Division 3, Section H, NDRC.

[4] J. Beek, Jr., Armor and Ordnance Report No. A-287, OSRD No. 4033, Aug. 1944. An abstract of this report appears in the Bibliography of Scientific and Industrial Reports **2**, 883 (1946), PB 34774.

on the performance of solid fuel rockets requires study of the following phenomena:

(1) Absorption of radiation by powder grains, necessitating determination of absorption coefficients as a function of wave-length. The required experimental work was carried out by F. Daniels and co-workers[5] at the University of Wisconsin and by B. L. Crawford, Jr., *et al.*[6] at the University of Minnesota.

(2) Emission of radiation from the hot gaseous products of combustion of a solid fuel rocket motor. The radiation emitted from the gaseous envelope has been studied experimentally by R. S. Craig[7] who employed an experimental technique developed by F. Kracek and W. S. Benedict.[8] The present treatment obviates the necessity for experimental emissivity determinations by allowing calculation of an effective emissivity from observed performance data.

(3) Calculation of the temperature rise associated with the absorption of radiant energy and determination of the change in burning rate associated with the temperature rise. Avery's theory for calculation of temperature rise and its effect on performance has been used in the present paper.

I. AVERAGE TEMPERATURE RISE IN A POWDER GRAIN, CAUSED BY THE ABSORPTION OF RADIANT ENERGY

Avery[2] has shown how to calculate the average temperature rise in a powder grain resulting from the absorption of radiant energy. An extended treatment, utilizing Avery's method, is given here for a solid cylindrical powder grain which is restricted by the use of inert material so that it can burn from one end in only one direction, namely, parallel to the cylinder axis. Application of the theory developed in the following sections to experimentally determined performance data permits direct evaluation of the mass emissivity which makes theoretical calculations consistent with experimental observations.

If ϵ_λ represents the emissivity in the wave-length region between λ and $\lambda+d\lambda$ of the hot gases, produced as the result of powder burning, then

$$\log(1-\epsilon_\lambda) = -k_\lambda g \rho, \tag{1}$$

where k_λ represents the mass emissivity for the corresponding wave-length region, ρ is the density of the powder gases, and g stands for the path length in a given direction throughout which emitters of radiant energy are uniformly distributed between the energy receiving powder surface and the rocket chamber wall.

The wave-length dependence of k_λ is neglected in all of the following calculations in accord with the assumption of gray body emission. With this simplification Eq. (1) may be written as

$$I_\lambda = I_{0\lambda}(1-e^{-k\rho g}) \tag{2}$$

after replacing ϵ_λ by $I_\lambda/I_{0\lambda}$, where $I_{0\lambda}$ represents the energy radiated by a blackbody emitter at the temperature of the powder gas per sq. cm of area per sec. over an angle of 2π steradians in the wave-length region under consideration.

A cylindrical rocket chamber of length $L+L_0$, containing a powder grain of length L, is shown in Fig. 1. The powder grain may be divided into small sections which are not necessarily of the same width: $\Delta L_1, \Delta L_2, \cdots \Delta L_n$. The average rate of burning of the slab of width ΔL_1 is designated as r_1 and corresponds to an average gas density ρ_1, etc. Thus, the slab of width ΔL_j burns with an average rate r_j at an average gas density ρ_j.

It is desired to determine the temperature rise of the section of width a as the result of the absorption of radiant energy. This section is located at a distance b from the original surface of the powder grain.

The distance from the right-hand surface of the slab of width a to the burning powder surface at any time is designated as X. While the powder burns over a distance ΔL_1,

$$X = b - r_1 t;$$

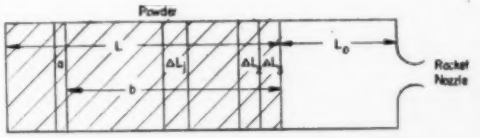

FIG. 1. Cylindrical motor chamber containing a powder grain which burns from one end only.

[5] S. S. Penner and F. Daniels in NDRC Report No. A-485, OSRD Report No. 6559, Dec. 1945.
[6] B. L. Crawford, Jr. and R. Gledhill in OSRD Report No. 6374, Dec. 1945.
[7] R. S. Craig, OSRD Report No. 5832, 1945.
[8] F. C. Kracek and W. S. Benedict, Armor and Ordnance Report No. A-252, OSRD No. 3291, 1944.

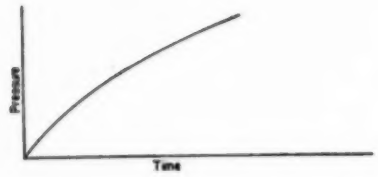

FIG. 2. Progressive pressure *vs.* time curve.

while burning occurs over the distance ΔL_2,

$$X=(b-\Delta L_1)-r_2t;$$

while burning occurs over the distance ΔL_j,

$$X=b-(\Delta L_1+\Delta L_2+\cdots+\Delta L_{j-1})-r_jt, \text{ etc.} \quad (3)$$

Only radiant energy incident in a direction normal to the burning powder surface is considered, as a first approximation.** With this simplification Eq. (2) becomes

$$I_\lambda=I_{0\lambda}(1-e^{-k\rho_1 L_0}) \quad (4)$$

while the powder burns through the distance ΔL_1. Equations similar to Eq. (4) hold for the incident intensities of radiation while the powder burns through other selected distances.

The decrease in radiation intensity per unit length of powder is strongly dependent on the wave-length distribution of the incident light since the absorption coefficients of the powder vary from one wave-length to another.

The average absorption coefficient of the powder for light in the wave-length region between λ and $\lambda+d\lambda$ is designated as K_λ in the following, and defined by the relation

$$I_\lambda'=I_\lambda e^{-K_\lambda x}, \quad (5)$$

where I_λ' is the radiant energy in the wave-length region between λ and $\lambda+d\lambda$ transmitted through a length x of powder when the incident radiant energy is I_λ for the same wave-length region.

The preceding physical picture leads to Eq. (6) for the radiant energy $E_{a\lambda}$ absorbed by the powder grain in the wave-length region between λ and $\lambda+d\lambda$ (see Appendix for details).

$$E_{a\lambda}=I_{0\lambda}(1-e^{-K_\lambda a})\sum_{j=1}^{n}\frac{\exp\{-K_\lambda(b-\sum_{i=1}^{j-1}\Delta L_i\}}{r_j}$$
$$\times\left\{\frac{1}{K_\lambda}\left[\exp\left\{K_\lambda r_j\sum_{i=1}^{j}\frac{\Delta L_i}{r_i}\right\}-\exp\left\{K_\lambda r_j\sum_{i=1}^{j-1}\frac{\Delta L_i}{r_i}\right\}\right]\right.$$
$$-\frac{\exp\{-k\rho_j[L_0+\sum_{i=1}^{j-1}\Delta L_i]\}}{K_\lambda-k\rho_j}$$
$$\left.\times\left[\exp\left\{(K_\lambda-k\rho_j)r_j\sum_{i=1}^{j}\frac{\Delta L_i}{r_i}\right\}-\exp\left\{(K_\lambda-k\rho_j)r_j\sum_{i=1}^{j-1}\frac{\Delta L_i}{r_i}\right\}\right]\right\}. \quad (6)$$

The temperature rise, ΔT_λ, produced by the absorption of $E_{a\lambda}$ cal./sq.cm/sec. is given by the relation

$$\Delta T_\lambda=E_{a\lambda}/C\rho_p a,$$

where C represents the heat capacity in cal./degree/gram of the powder, and ρ_p is the powder density. When a is very small the approximation may be made that

$$(1-e^{-K_\lambda a})/a\simeq K_\lambda.$$

The temperature rise of the powder grain associated with the absorption of radiant energy in the wave-length region between λ and $\lambda+d\lambda$ is, therefore, given by Eq. (7):

$$\Delta T=\frac{I_{0\lambda}}{C\rho_p}\sum_{j=1}^{n}\frac{\exp\{-K_\lambda(b-\sum_{i=1}^{j}\Delta L_i)\}}{r_j}$$
$$\times\left\{\left[\exp\left\{K_\lambda r_j\sum_{i=1}^{j}\frac{\Delta L_i}{r_i}\right\}-\exp\left\{K_\lambda r_j\sum_{i=1}^{j-1}\frac{\Delta L_i}{r_i}\right\}\right]\right.$$
$$\frac{\exp\{-k\rho_j(L_0+\sum_{i=1}^{j-1}\Delta L_i)\}}{K_\lambda-k\rho_j}\cdot K_\lambda$$
$$\left.\times\left[\exp\left\{(K_\lambda-k\rho_j)r_j\sum_{i=1}^{j}\frac{\Delta L_i}{r_i}\right\}-\exp\left\{(K_\lambda-k\rho_j)r_j\sum_{i=1}^{j-1}\frac{\Delta L_i}{r_i}\right\}\right]\right\}. \quad (7)$$

** Neglect of radiant energy incident in a direction other than the normal to the powder surface is justified by the large absorption coefficient of the propellant charge. The contribution of radiant energy from directions other than the normal to the powder surface is relatively small for a strongly absorbing powder at some distance below the powder surface.

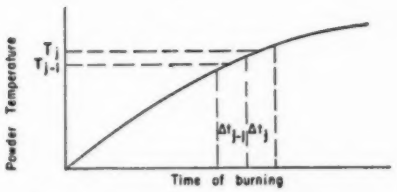

FIG. 3. Temperature *vs.* time curve.

For accurate calculations the temperature rise must be computed for each individual wavelength interval $\Delta\lambda=\Delta\lambda_m$ for which an average value $K_\lambda=K_m$ can be assigned to the absorption coefficient of the powder. It is then necessary to sum over m in order to obtain the total temperature rise.

Equations (6) and (7) require more detailed information than is usually available. For this reason it is necessary to assume an average burning rate at an average pressure for reasonably long distances. For each of these distances Eq. (7) reduces to Eq. (8):

$$\frac{\bar{r}\Delta TC\rho_p}{I_{0\lambda}}=(1-e^{-K_\lambda b})+\frac{K_\lambda\exp\{-k\bar{\rho}L_0\}}{K_\lambda-k\bar{\rho}}\times(\exp\{-K_\lambda b\}-\exp\{-k\bar{\rho}b\}), \quad (8)$$

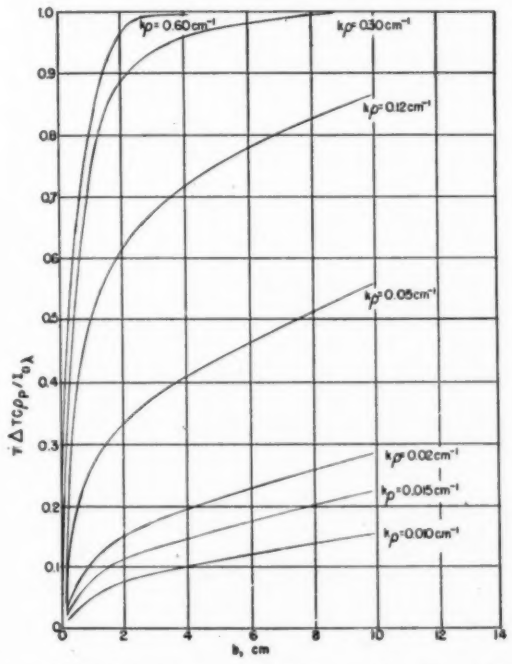

FIG. 4. Radiation temperature rise at various distances for $K=2$ cm^{-1}, $0.5\mu\leq\lambda\leq1.0\mu$, $L_0=7.00$ cm.

where $\bar{r}$ represents the average burning rate in cm/sec. and $\bar{\rho}$ is the average gas density in grams/cc.

II. APPROXIMATE METHOD FOR THE CALCULATION OF PROGRESSIVENESS OF PRESSURE-TIME CURVES

Experimental techniques have been evolved which permit the determination of the pressure in a rocket chamber as a function of time.[9] A pressure *vs.* time curve of the type shown in Fig. 2 is said to be progressive. One of the factors which determines the degree of progressiveness is the depth of the hot radiating gas layer which increases continuously in a motor chamber of the type shown in Fig. 1.

In order to correlate the effect of radiation with progressiveness of the pressure *vs.* time curve, it is necessary to develop a relation between instantaneous powder temperature and instantaneous burning rate.

The product $\bar{r}\Delta T$ can be calculated from Eq. (8) for a definite powder temperature with fixed path length and constant pressure. The actual temperature rise is obtained by dividing $\bar{r}\Delta T$ by $\bar{r}$

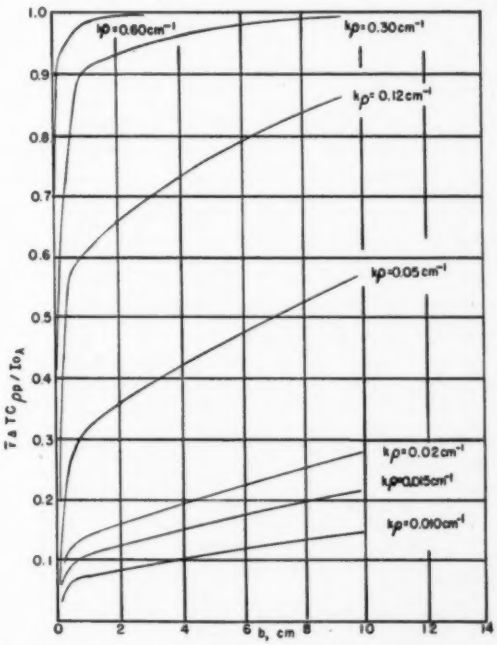

FIG. 5. Radiation temperature rise at various distances for $K=10$ cm^{-1}, $1.0\mu\leq\lambda\leq2\mu$, $L_0=7.00$ cm.

[9] W. H. Avery, R. E. Hunt, and M. N. Donin, OSRD report No. 5827, January 1946; W. H. Avery, R. E. Hunt, and L. D. Sachs, OSRD report No. 5824, March 1946.

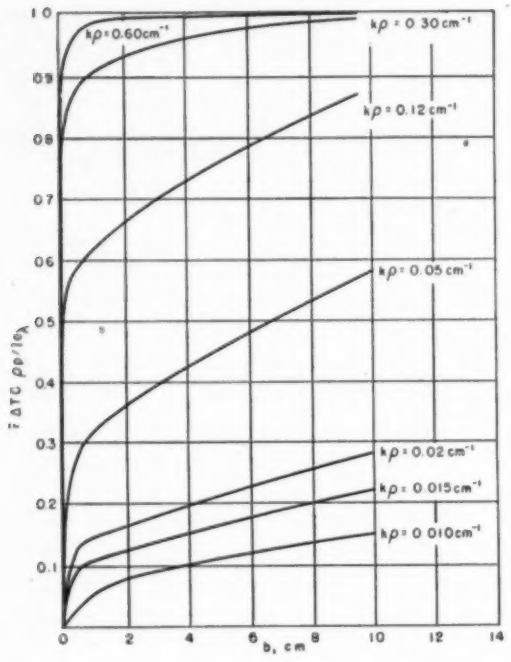

FIG. 6. Radiation temperature rise at various distances for $3\ \text{cm}^{-1} \leq K \leq 60\ \text{cm}^{-1}$, $2\mu \leq \lambda \leq 10\mu$, $L_0 = 7.00$ cm.

where an approximate average value is used for $\bar{r}$. Dividing b, the initial distance of a from the burning powder surface, by $\bar{r}$ gives the time at which burning occurs at the right-hand plane of the section of width a (cf. Fig. 1). Addition of the initial powder temperature to the values of ΔT gives the necessary data for the construction of Fig. 3.

The ordinate of Fig. 3 represents the powder temperature at which burning occurs and the abscissa the time at which the indicated powder temperature is reached.

Let T_{j-1} represent the average temperature during the time interval Δt_{j-1}, and T_j the average temperature during the time interval Δt_j. Assuming the validity of the relation[9]

$$r = c' P^n / (T_1 - T), \tag{9}$$

it follows that

$$dr/r = n dP/P + dT/(T_1 - T). \tag{10}$$

Here c', n, and T_1 are constants characteristic of the powder under investigation, P represents the pressure, and T is the powder temperature. During the early stages of burning[10]

$$S\rho_p r = C_D A_t P + d(\rho V)/dt, \tag{11}$$

where S = surface area of the burning powder, A_t = throat area of the rocket nozzle, C_D = discharge coefficient, V = chamber volume, and r, ρ, and P have their previous meaning. After the very rapid initial temperature rise, which occurs immediately after ignition of the rocket powder, the value of $d(\rho V)/dt$ is small compared with $C_D A_t P$. Therefore,

$$r = C_D A_t P / S\rho_p \tag{12}$$

or

$$dr/r = dP/P. \tag{13}$$

Combining Eqs. (10) and (13),

$$dP = [P/(1-n)][dT/(T_1 - T)]. \tag{14}$$

Let $dT_{j-1,j}$ represent the average temperature rise occurring between the Δt_j'th and the Δt_{j-1}'rst second, i.e., $dT_{j-1,j} = T_j - T_{j-1}$; if $dP_{j-1,j} = P_j - P_{j-1}$ is the corresponding pressure rise, then, from Eq. (14),

$$dP_{j-1,j} = [(P_j + P_{j-1})/2(1-n)] \times [dT_{j-1,j}/(T_1 - \tfrac{1}{2}T_j - \tfrac{1}{2}T_{j-1})]. \tag{15}$$

But $P_j = P_{j-1} + dP_{j-1,j}$ and, therefore,

$$dP_{j-1,j} = \frac{\dfrac{P_{j-1}}{1-n} \cdot \dfrac{dT_{j-1,j}}{T_1 - \frac{1}{2}T_j - \frac{1}{2}T_{j-1}}}{1 - \dfrac{1}{2(1-n)} \cdot \dfrac{dT_{j-1,j}}{T_1 - \frac{1}{2}T_j - \frac{1}{2}T_{j-1}}}. \tag{16}$$

A pressure *vs.* time curve can be constructed from Eq. (16) provided one value of $P = P_0$ at a definite time $t = t_0$ is known. Since Eq. (16) is based on the assumption that nearly steady state conditions exist, an experimental pressure value, after the rapid initial pressure rise, is chosen as starting point for the calculations. The remaining pressure *vs.* time curve may then be constructed by use of Eq. (16). Calculation of T_j requires the selection of a definite value for the mass emissivity of the powder gases. If the assumed value for the mass emissivity does not lead to a pressure-time curve which agrees with the experimental curve, a different mass emissivity is

[10] Rocket Fundamentals, OSRD Report No. 3711, May 1944; PB Report No. 50835, Chapter 3 by R. B. Kershner.

chosen, and the calculations are repeated. The effective mass emissivity is the value at which theoretical and experimental pressure-time curves agree with one another.

III. CALCULATION OF MASS EMISSIVITY BY TRIAL AND ERROR

Calculations of mass emissivity from the progressive pressure-time curves observed experimentally are made on the assumption that all of the observed increase in pressure with time is caused by radiation. Other factors than increased radiant energy incident on the powder surface may be responsible for causing progressiveness of the pressure-time curve. For example, the vaporization of the inert material which prevents burning of the powder grain in a direction normal to the cylinder axis may be responsible for a continuous increase in pressure during burning. Nevertheless, a calculation which assumes that the only important factor is radiation is of interest since the result of this study gives an upper limit for the mass emissivity.

Some of the data required for calculation are summarized in a series of graphs. The dimensionless factor $\bar{r}\Delta TC\rho_p/I_{0\lambda}$ is plotted against initial distance from the powder surface for various wave-length regions for which average absorption coefficients have been assigned to representative double base rocket powders*** (see Figs. 4 to 6). Experimentally determined absorption coefficients for powders which do not contain added darkening agents are given for the required wave-length regions in each of the figures. Absorption coefficient data are taken from the work of Daniels,[5] Crawford,[6] and their co-workers.

The term $\bar{r}\Delta TC\rho_p/I_{0\lambda}$ is effectively independent of K_λ for $K_\lambda b \geq 10$, as can be seen from Eq. (8). For this reason the entire wave-length interval from 0.50 to 10.0 microns, which is of interest in radiation calculations on rockets, can be summarized for all wave-lengths by the plot shown in Fig. 7 for a darkened grain for which $12 \leq K \leq 56$. In Fig. 7, b has been chosen to be greater than or equal to 1 cm.

An experimental pressure *vs.* time curve is shown in Fig. 8 for a double base powder which did not contain added darkening agent such as finely divided carbon. The average pressure during burning was $\bar{P} = 209$ p.s.i. and the average rate of burning $\bar{r} = 0.447$ cm/sec. Also shown in Fig. 8 are the calculated pressure-time curves for a powder gas temperature $T = 2400°K$ at $k\rho = 0.02$ cm^{-1} and $k\rho = 0.05$ cm^{-1}, and for a powder gas temperature $T = 3000°K$ at $k\rho = 0.02$ cm^{-1}.

It can be seen from Fig. 8 that reasonably good agreement exists between experimental and theoretical data for $k\rho = 0.05$ cm^{-1} at a flame temperature of 2400°K. At this temperature and a pressure of 209 p.s.i., ρ has the value 0.00204 g/cc.* Therefore $k = 24.5$ cm^2/g for the given conditions. This value of the mass emissivity is in good agreement with approximate experimental findings for powders of the type investigated.[7]

The theoretical pressure *vs.* time curves do not flatten out in the same manner as the experimental curve, as can be seen from Fig. 8. This may be caused by the fact that the emitting layer of hot gases does not increase uniformly in depth during burning.

The method of determining mass emissivity from the progressiveness of the pressure *vs.* time

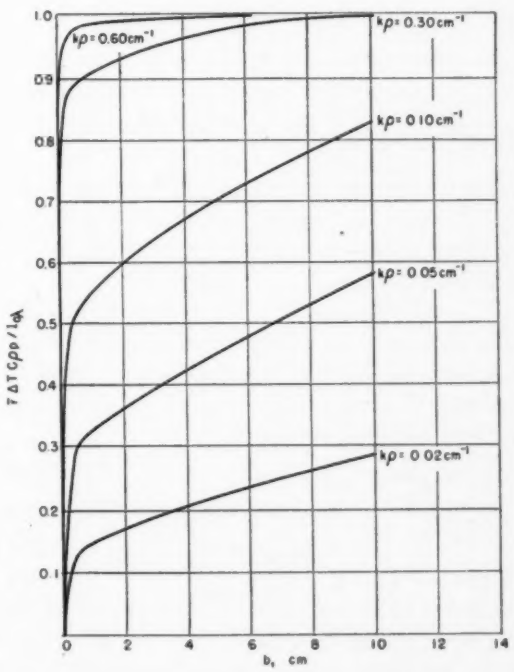

FIG. 7. Radiation temperature rise at various distances for $12 \text{ cm}^{-1} \leq K \leq 56 \text{ cm}^{-1}$, $0.5\mu \leq \lambda \leq 10\mu$, $L_0 = 7.00$ cm.

*** A double base rocket powder consists of approximately 60 percent nitrocellulose and 40 percent nitroglycerin, compounded with various other ingredients.

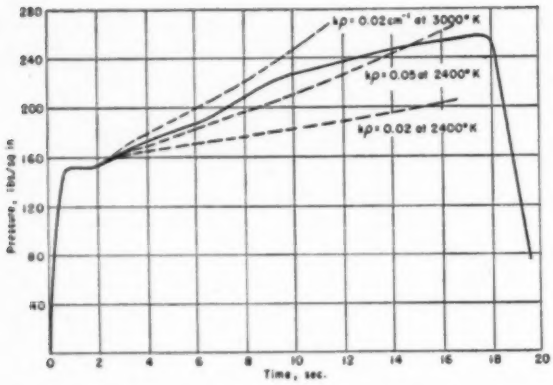

FIG. 8. Experimental and calculated pressure *vs.* time curves for a restricted rocket propellant ($L_0=8.8$ cm., $P=209$ lbs./in.^{2}, $r=0.447$ cm/sec., initial powder temperature = 62°C).

curve requires knowledge of the flame temperature. The calculated mass emissivities do not respond to slight variations in flame temperature. Nevertheless, it is necessary to use a value for the flame temperature within 100 degrees of the correct value in order to obtain calculated mass emissivities which are of the correct order of magnitude.

APPENDIX TEMPERATURE RISE IN A CYLINDRICAL POWDER GRAIN BURNING FROM ONE END ONLY, CAUSED BY THE ABSORPTION OF RADIANT ENERGY

The temperature rise in a cylindrical powder grain, caused by the absorption of radiant energy, may be determined by application of Eqs. (3)–(5).

When the powder burns a distance ΔL_1 (see Fig. 1) the total radiant energy received by a is given by

$$E_{i1}=I_{0\lambda}\int_0^{t_{\text{final}}}[1-\exp\{-k\rho_1(L_0+r_1t)\}]\times\exp\{-K_\lambda X\}dt. \quad \text{(A-1)}$$

The transmitted energy is

$$E_{t1}=I_{0\lambda}\int_0^{t_{\text{final}}}[1-\exp\{-k\rho_1(L_0+r_1t)\}]\times\exp\{-K_\lambda(X+a)\}dt. \quad \text{(A-2)}$$

The limits of integration in Eqs. (A-1) and (A-2) are given by the condition that $t=0$ when $X=b$, $t=\Delta L_1/r_1$ when $X=b-\Delta L_1$. In the section of thickness ΔL_1, $X=b-r_1t$. Therefore, the energy absorbed by the section of thickness a while the powder burns through the distance ΔL_1 is given by

$$E_1=I_{0\lambda}(1-\exp\{-K_\lambda a\})e^{-K_\lambda b}\times\int_0^{\Delta L_1/r_1}[1-\exp\{-k\rho_1(L_0+r_1t)\}]\times\exp\{K_\lambda r_1t\}dt. \quad \text{(A-3)}$$

Similarly, when the powder burns through the section of thickness ΔL_2 the incident energy on the section of thickness a is given by the relation

$$E_{i2}=I_{0\lambda}\times\int_{\Delta L_1/r_1}^{t_{\text{final}}}[1-\exp\{-k\rho_2[(L_0+\Delta L_1)+r_2t]\}]\times\exp\{-K_\lambda X\}dt. \quad \text{(A-4)}$$

The transmitted energy is therefore

$$E_{t2}=I_{0\lambda}\times\int_{\Delta L_1/r_1}^{t_{\text{final}}}[1-\exp\{-k\rho_2[(L_0+\Delta L_1)+r_2t]\}]\times\exp\{-K_\lambda(X+a)\}dt, \quad \text{(A-5)}$$

and the absorbed energy becomes

$$E_2=I_{0\lambda}(1-e^{-K_\lambda a})\times\int[1-\exp\{-k\rho_2[(L_0+\Delta L_1)+r_2t]\}]\times\exp\{-K_\lambda X\}dt$$

subject to the boundary conditions $t=\Delta L_1/r_1$ when $X=b-\Delta L_1$; $t=\Delta L_1/r_1+\Delta L_2/r_2$ when $X=b-\Delta L_1-\Delta L_2$, and $X=b-\Delta L_1-r_2t$ at any time while the section of thickness ΔL_2 is burning. The energy absorbed by the section of thickness a while the powder burns through the distance ΔL_2 is, therefore, seen to be

$$E_2=I_{0\lambda}(1-\exp\{-K_\lambda a\})\exp\{-K_\lambda(b-\Delta L_1)\}\times\int_{\Delta L_1/r_1}^{\Delta L_1/r_1+\Delta L_2/r_2}[1-\exp\{-k\rho_2(L_0+\Delta L_1+r_2t)\}]\times\exp\{K_\lambda r_2t\}dt. \quad \text{(A-6)}$$

Repeating the preceding argument, it is found that the energy E_j is absorbed by the section of thickness a while the powder burns through the

distance ΔL_j:

$$E_j = I_{0\lambda}(1-e^{-K_\lambda a}) \times \exp\{-K_\lambda(b-\Delta L_1-\cdots-\Delta L_{j-1})\} \times \int_{\frac{\Delta L_1}{r_1}+\cdots+\frac{\Delta L_{j-1}}{r_{j-1}}}^{\frac{\Delta L_1}{r_1}+\cdots+\frac{\Delta L_j}{r_j}} [1-\exp\{-k\rho_j(L_0+\Delta L_1+\cdots+\Delta L_{j-1}+r_j t)\}] \exp\{K_\lambda r_j t\}\,dt$$

$$= I_{0\lambda}(1-e^{-K_\lambda a}) \exp\{-K_\lambda(b-\sum_{i=1}^{j-1}\Delta L_i)\} \times \int_{\sum_{i=1}^{j-1}\frac{\Delta L_i}{r_i}}^{\sum_{i=1}^{j}\frac{\Delta L_i}{r_i}} [1-\exp\{-k\rho_j(L_0+\sum_{i=1}^{j-1}\Delta L_i+r_j t)\}] \times \exp\{K_\lambda r_j t\}\,dt. \quad \text{(A-7)}$$

In order to obtain the total energy of radiation absorbed by a before the flame front reaches a it is necessary to sum over all of the j's from $j=1$ to $j=n$. The result is

$$E_{a\lambda} = \sum_{j=1}^{n} E_j = I_{0\lambda}(1-e^{-K_\lambda a}) \times \sum_{j=1}^{n} \exp\{-K_\lambda(b-\sum_{i=1}^{j-1}\Delta L_i)\} \times \int_{\sum_{i=1}^{j-1}\frac{\Delta L_i}{r_i}}^{\sum_{i=1}^{j}\frac{\Delta L_i}{r_i}} [1-\exp\{-k\rho_j(L_0+\sum_{i=1}^{j-1}\Delta L_i+r_j t)\}] \times \exp\{K_\lambda r_j t\}\,dt. \quad \text{(A-8)}$$

Equation (A-8) reduces to Eq. (6) after integration.

Viscous Slip Along Grain Boundaries and Diffusion of Zinc in Alpha-Brass*

T'ING-SUI KÊ
Institute for the Study of Metals, The University of Chicago, Chicago, Illinois
(Received October 6, 1947)

The viscous behavior of the grain boundaries in 70–30 alpha-brass was demonstrated by anelastic measurements. It was shown that the grain boundaries cannot sustain permanently a shear stress and have a coefficient of viscosity decreasing with an increase of temperature. Using the same alpha-brass specimen, the activation energy associated with the stress-induced preferential orientation of pairs of zinc atoms in alpha-brass (which is a diffusion process) was determined. This activation energy was found to be identical, within experimental error, to the activation energy associated with the grain boundary slip in alpha-brass. This finding indicates that the grain boundary slip in alpha-brass is a diffusion process and the diffusion mechanism is similar to the volume diffusion in alpha-brass.

I. INTRODUCTION

THE mechanical behavior of grain boundaries in metals has previously been studied by considering the grain boundary as an entity without inquiring into its true nature.[1,2] Thus it has been demonstrated that the grain boundary behaves in a viscous manner in the sense that it cannot sustain permanently a shear stress and has a coefficient of viscosity decreasing with an increase of temperature.[1] The concept of a viscous grain boundary was further elucidated by later experiments[2] where it was shown that when a periodic stress is applied to a polycrystalline metal, the manifestations of the grain boundary viscosity can be expressed as functions of the grain size (G.S.) the frequency of vibration, f, and the absolute temperature, T, only through the parameter $(\text{G.S.})\times f\times\exp(H/RT)$, where R is the gas constant and H the heat of activation.

The viscous behavior of grain boundaries demonstrated above gives no definite information

* This research has been supported by ONR (Contract No. N-6ori-20-IV).
[1] T. S. Kê, Phys. Rev. **71**, 533 (1947).
[2] T. S. Kê, Phys. Rev. **72**, 41 (1947).

regarding the nature or the structure of the boundary region between adjacent crystals. It should be emphasized that the concept of a viscous grain boundary is consistent with both the two principal theories regarding the nature of grain boundaries, e.g., the amorphous cement or irregular intercrystal layer theory and the transitional lattice theory. It can be seen that any region of disturbed crystallinity, when considered as an entity, may behave in a viscous manner. So far, most of the work was done on high purity aluminum. The purpose of this paper is to describe some findings on alpha-brass, which, in addition to the further demonstration of the viscous behavior of grain boundaries in metals, might shed light on the mechanism of the viscous slip along grain boundaries.

II. GRAIN BOUNDARY VISCOSITY IN ALPHA-BRASS

If the grain boundaries behave as if they were viscous and have a coefficient of viscosity decreasing with an increase of temperature, then as the temperature of a polycrystalline specimen is raised, the internal friction associated with the viscous slip along grain boundaries (a convenient measure of this internal friction may be taken as the product of the viscous slip along the boundary and the resistance to slip) must go over a maximum value. The reason for this can be illustrated as follows. At low temperatures, the viscous slip along the grain boundaries is negligibly small, and therefore the internal friction is small. At high temperatures, the resistance to slip along the grain boundaries is negligibly small, so again the internal friction is small. Only in an intermediate temperature range, when both the viscous slip and the resistance to slip are appreciable, will the internal friction be appreciable. Such a maximum has been observed in the case of aluminum and magnesium.[1] For alpha-brass, internal friction measurements have been taken by Zener and his associates from room temperature up to 450°C at a frequency of transverse vibration of between 600 and 900 cycles per second.[3] It has been found that the internal friction increases with the grain size of the specimen. However, a maximum was never attained. According to the proposition that an increase of the frequency of vibration will shift the internal friction curve (*versus* temperature) to higher temperatures,[2] apparently still higher temperatures were needed to reach the maximum unless a lower frequency of vibration is used.

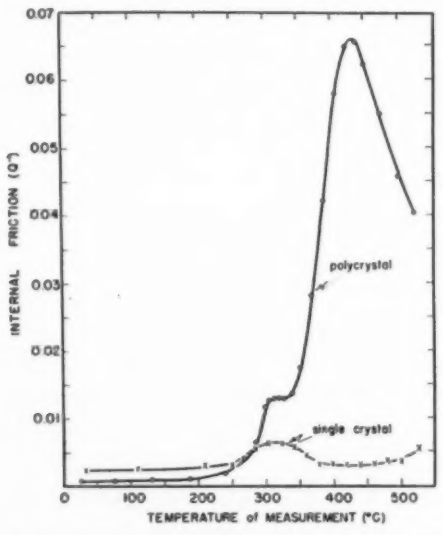

FIG. 1. Variation of internal friction with temperature in polycrystalline and single-crystal alpha-brass. (Frequency of vibration is about half a cycle per second.)

In the present experiment, the internal friction (logarithmic decrement divided by π) and the shear modulus were determined using a simple torsional pendulum. The frequency of vibration was about one cycle per second so that the measurements could be made by visual observation. The apparatus used was practically identical with that described before.[1] The alpha-brass used was similar to that used by Burke and Shiau in their study on the grain growth in alpha-brass.[4] It was prepared by melting cathode copper and commercially pure zinc together in an induction heated graphite crucible. The copper content of the final alloy was 70.14 percent, and the percentages of the impurities as determined by spectrographic analysis were: Fe, 0.005; Pb, 0.002; Ag, 0.001; Cd, 0.001; As, 0.005; Sb, 0.002. A three-inch piece of this specimen, having a diameter of one-quarter inch was cold-swaged and drawn to a final diameter of 0.035 inch with several intermediate anneals at 650°C. The final cold-work was about 70 percent reduction in area

[3] C. Zener, D. van Winkle, and H. Nielson, Trans. A.I.M.E. **147**, 96 (1942).

[4] J. E. Burke and Y. G. Shiau, Metals Tech. **14**, No. 6 (September, 1947).

(70 percent R.A.). A wire 12 inches long was mounted up in the furnace and all the measurements on internal friction and shear modulus were taken in an atmosphere of argon having a purity of 99.8 percent. The temperature of the wire specimen was controlled and measured within ± 1°C with a Tag Celectray indicating temperature controller. The torsional stress applied to the specimen was very small and the maximum shearing strain on the surface of the wire was of the order of magnitude of 10^{-5}. Under such a small stress, the internal friction and shear modulus were found to be independent of stress.

A. Variation of Internal Friction with Temperature

The alpha-brass wire described above was annealed at 600°C for five hours in an argon atmosphere, and it has been found that the recrystallized grains have an average grain diameter of about 0.03 cm. Measurements on internal friction and shear modulus were taken from room temperature up to 525°C and then coming down again to room temperature. The variation of internal friction and shear modulus with temperature are shown, respectively, in Fig. 1 and Fig. 4. It can be seen from Fig. 1 that the expected internal friction maximum occurs at a temperature of 415°C and at this temperature the natural frequency of vibration is 0.482 cycle per second. In order to determine the heat of activation associated with the grain boundary slip, two different frequencies of vibration were used and the corresponding internal friction curves were plotted against the reciprocal of absolute temperature ($1/T$) in Fig. 2. It can be shown that the internal friction obtained in measurements with different frequencies of vibration should be identical if the frequency, f, and the temperature of measurement, T, be related through the heat of activation, H, according to the relation

$$d \ln f/d(1/T) = -H/R,$$

or

$$H = R \ln(f_2/f_1)/(1/T_1 - 1/T_2),$$

when two frequencies, f_2 and f_1, are involved. The horizontal shift in $1/T$ required to bring the two internal friction curves in Fig. 2 to superpose on each other is 0.055×10^{-3}. As the average ratio of these two frequencies in the temperature range

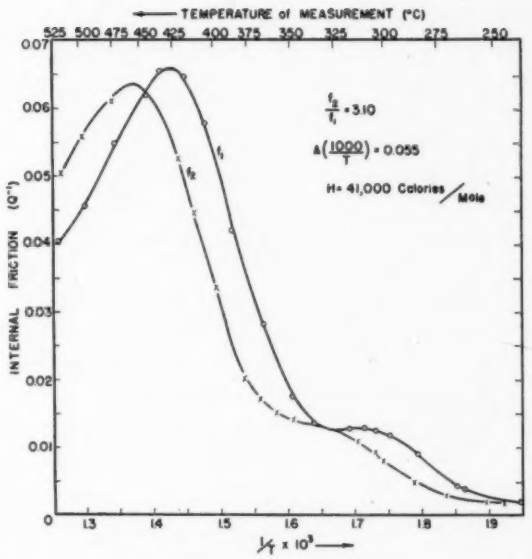

FIG. 2. Effect of frequency of vibration on internal friction associated with grain boundary slip in alpha-brass. Frequency of vibration: ⊙, about 0.5 c.p.s.; ×, about 1.5 c.p.s. (see Fig. 3).

studied is, from Fig. 3, 3.10, this gives a heat of activation of $H = 41{,}000$ calories per mole, which should be accurate to within five percent.

It can be seen from Fig. 1 that this internal friction peak does not occur in alpha-brass single

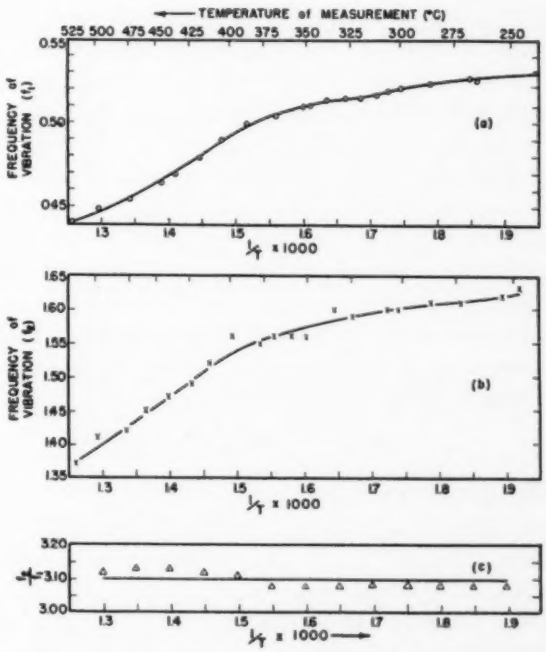

FIG. 3. Ratio of two natural frequencies of vibration over a wide temperature range.

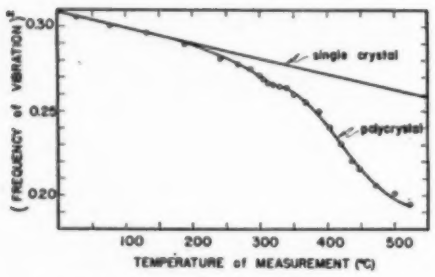

FIG. 4. Variation of shear modulus with temperature in polycrystalline alpha-brass.

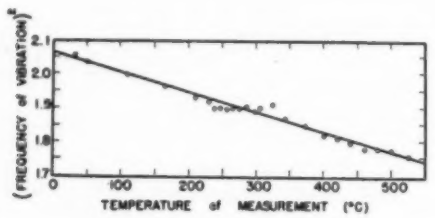

FIG. 5. Variation of shear modulus with temperature in alpha-brass crystal.

crystal. This indicates that the internal friction observed can be ascribed only to the grain boundaries in alpha-brass. However, it is to be noticed that there is a smaller internal friction peak around 300°C in both polycrystalline and single-crystal alpha-brass. These will be discussed in some detail in the next section.

From the data given in Figs. 1 and 3, we can estimate the thermal variation of the viscosity coefficient associated with the grain boundaries in alpha-brass. It has previously been shown that the coefficient of viscosity can be estimated from the formula[1]

$$\eta_T = (G_U)_T \tau_T d/(\text{G.S.}),$$

where G_U is the unrelaxed shear modulus, τ the relaxation time, d the effective thickness of the grain boundary, and (G.S.) the average grain diameter of the specimen. Following similar procedures as in the case of aluminum, we get

$$\tau_T = 8.20\times10^{-15}\exp(20{,}500/T),$$

utilizing the facts that the internal friction is maximum at 688°K when the frequency of vibration is 0.482 cycle per second and the heat of activation is 41,000 calories per mole.

The unrelaxed shear modulus is of the order of magnitude of 10^{11} dynes per cm² for all metals and d may be taken as of the order of magnitude of 10^{-8} cm. Since the average grain diameter for the alpha-brass specimen is about 0.03 cm, we have

$$\eta_T \sim 10^9 \exp(20{,}500/T).$$

At the melting point of alpha-brass, which is 940°C, the coefficient of viscosity is, according to the above relation, of the order of magnitude of 10^{-2} poise, which is of the same order as the coefficient of viscosity of most molten metals.

B. Temperature Variation of Shear Modulus

When an over-all stress, however small, is applied to a polycrystalline specimen, the shear stress across all grain boundaries, because of their viscous behavior, will gradually relax. The locking effect of the grain edges and corners will insure that the over-all stress relaxation will be of limited extent for a fixed over-all strain. The theoretical maximum shear stress relaxation in metals is,[5]

$$1-G_R/G_U = 1-2(7+5\sigma)/5(7-4\sigma),$$

where G_R is the shear modulus of a polycrystalline specimen in the case where the grain boundaries are viscous and the relaxation of shearing stress across the grain boundaries has been complete, G_U the shear modulus where no slip occurs across the grain boundaries, and σ the Poisson's ratio.

The temperature variation of the shear modulus (which is proportional to the square of the natural frequency of vibration) in polycrystalline and single-crystal alpha-brass are, respectively, shown in Figs. 4 and 5. The straight line in Fig. 4 was converted from Fig. 5. Let $G(T)$ be the shear modulus in polycrystalline alpha-brass at temperature T, then we have

$$G(T)/G_U = (f_p/f_s)^2,$$

where f_p and f_s are, respectively, the frequency of vibration in polycrystalline and single-crystal alpha-brass at the temperature T. The ratio $G(T)/G_U$ is plotted as a function of the temperature of measurement in Fig. 6. It can be seen that the grain boundary relaxation has not been completed at the highest temperature of measurement but we can infer that G_R/G_U is smaller than but close to 0.73. The over-all stress relaxation across

[5] C. Zener, Phys. Rev. 60, 906 (1941); see also reference 1.

the grain boundaries in the alpha-brass specimen is thus greater than, but close to 27 percent. This lies within the range of theoretical value of from 24 to 45 percent when σ covers the range from $\frac{1}{2}$ to $\frac{1}{4}$ for metals.

III. ANELASTIC RELAXATION IN ALPHA-BRASS ARISING FROM ATOMIC DIFFUSION

It has been mentioned above that there is a smaller internal friction peak around 300°C in both polycrystalline and single-crystal alpha-brass (Fig. 1). The frequency of vibration used was of the order of one cycle per second. It is believed that this internal friction peak has the same physical origin as that observed by Zener in 70–30 alpha-brass crystal.[6] The optimum temperature observed by Zener was around 420°C using a frequency of vibration of 620 cycles per second. The origin of this internal friction has been recently determined by Zener as the stress-induced preferential orientation of pairs of zinc atoms in alpha-brass.[7] This mechanism is formally similar to that arising from the stress-induced preferential distribution of the interstitial solute atoms in alpha-iron (solute atoms: carbon or nitrogen)[8] and in tantalum (solute atoms: carbon or oxygen).[9]

In a copper crystal which has a face-centered cubic structure, there are twelve closest neighbors for each individual atom and these neighbors are so arranged as to form a cubic symmetry. When zinc atoms are dissolved in copper to form a substitutional solid solution or alpha-brass, an elastic distortion of the lattice will take place since the zinc atom is larger than the copper atom it replaced. If another zinc atom happens to become one of the twelve closest neighbors of a zinc atom, then distortion of the lattice will no longer have cubic symmetry and the lattice will be extended more along the axis of the pair of zinc atoms than along any other directions. In a stress-free alpha-brass specimen the pair axes will be distributed at random along various permissible crystallographic directions. But when a tensile stress is applied to the specimen, the zinc pairs will tend to be oriented preferentially along those permissible axes which make the least angle with the direction of the applied stress. Some time is required for the establishment of this preferential orientation of the zinc pairs and, consequently, strain lags behind the applied stress. This will cause all kinds of anelastic effects including internal friction.

It can be seen that if the above picture is correct, then the activation energy associated with the observed internal friction should be identical with the activation energy for the diffusion of zinc atoms in alpha-brass. An estimation of this activation energy has been made by Zener[6] from the slope of the internal friction curve plotted against $1/T$ and he obtained a value of 33,600 calories per mole, which is much smaller than the value of 41,700 calories per mole for the diffusion of zinc (29.08 percent) in alpha-brass.[10] A careful determination of the activation energy using the standard procedure of measuring internal friction with various frequencies of vibration is thus desirable.

The alpha-brass single crystals used in the present experiment were kindly prepared by Mr. Harold Hirsch of the metallurgy section of this institute. They were grown from the melt in a graphite mould. The crystals so prepared, $\frac{5}{32}''$ in diameter and about 6″ in length, are quite homogeneous in composition throughout the whole length, but the internal friction background of such a crystal is unusually high. Subsequent annealing at 800°C has the effect of reducing partly the internal friction background, but it was still several times higher than that of the polycrystalline specimen (see Fig. 1). It was thus decided to use polycrystalline specimens having very large grain size with the hope that

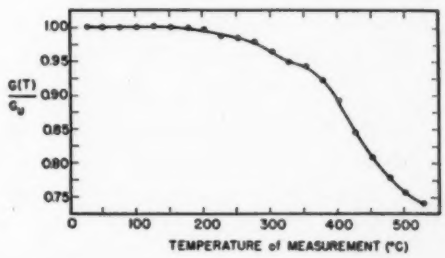

FIG. 6. Relaxation of shear modulus in polycrystalline alpha-brass.

[6] C. Zener, Trans. A.I.M.E. **152**, 122 (1943).
[7] C. Zener, Phys. Rev. **71**, 34 (1947).
[8] J. Snoek, Physica **8**, 711 (1941).
[9] T. S. Kê, communicated to the Physical Review.
[10] A. E. Arkel, Metallwirtschaft **7**, 656 (1928); see also R. F. Mehl, Trans. A.I.M.E. **122**, 11 (1936).

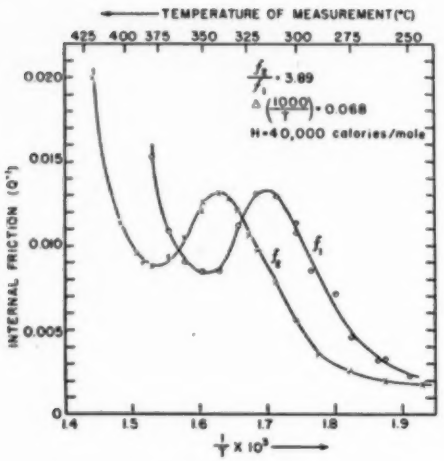

FIG. 7. Effect of frequency of vibration on internal friction associated with the preferential orientation of zinc atom pairs in alpha brass. Frequency of vibration: ⊙, about 0.6 c.p.s.; ×, about 2.3 c.p.s.

the internal friction due to the grain boundary slip will be shifted sufficiently to higher temperatures and be separated from the internal friction due to the preferential orientation. The alpha-brass wire used in the study of grain boundary relaxation (Section I) was sealed in a thin quartz tube filled with ¼-atmosphere of argon (99.8 percent pure). This was annealed at 800°C for 5 hours. After such a treatment the grains in the wire specimen were much larger than the diameter of the wire and most of them were extended clear across the specimen. The concentration of zinc in the specimen after such a treatment was found by chemical analysis to be 29 percent, indicating that little zinc was lost by this treatment. The internal friction curve of this wire is shown in Fig. 7, in which the internal friction concerned is fairly well separated from the internal friction due to grain boundary slip. Using two frequencies of vibration having a ratio of 3.89 (average value over the temperature range studied), it was found that the heat of activation associated with the preferential orientation of zinc atom-pairs in alpha-brass is 40,000 calories per mole within 5 percent. This agrees well, within experimental error, with the value of the activation energy for the diffusion of zinc in alpha-brass mentioned above.

IV. GRAIN BOUNDARY SLIP AND ATOMIC DIFFUSION

The activation energy associated with the grain boundary slip in 70–30 alpha-brass has been determined in Section I as 41,000 calories per mole. Using the same specimen, we have also shown in Section II that the activation energy associated with the preferential orientation of pairs of zinc atoms in alpha-brass, which is a diffusion phenomenon, is 40,000 calories per mole. Both values are equal, within experimental error, to the activation energy for the diffusion of zinc atoms in alpha-brass (29.08 percent zinc). It is believed that the experimental accuracy in the determination of the activation energies described in Sections I and II are accurate to 5 percent and, therefore, such a close agreement deserves special attention. This would indicate that the grain boundary slip in alpha-brass as manifested in the anelastic measurements is a process of atomic diffusion. The identity of the activation energies for grain boundary slip and for volume diffusion is somewhat unexpected, because it is a conventional belief that grain boundary diffusion is faster than volume diffusion and the activation energy for the latter is higher, for there the atoms are held in greater restraint and thus a greater energy of activation is required to set them free.[11] However, this finding is consistent with Elam's[12] observation that zinc does not penetrate preferentially along the grain boundaries of copper at a temperature below 500°C.

In conclusion, it is a pleasure to the author to acknowledge his indebtedness to Professors Clarence M. Zener and Cyril S. Smith of this Institute for their constant interest in this problem.

Note added in proof: The identity of the activation energies for grain boundary slip and for volume diffusion has also been found in the case of alpha-iron (T. S. Kê, communicated to Metals Technology). A discussion on the possible inference as to the structure of grain boundaries in metals is lately given by this author.[13]

[11] R. F. Mehl, Trans. A.I.M.E. **122**, 11 (1936).
[12] C. F. Elam, J. Inst. Metals **43**, 217 (1930).
[13] T. S. Kê, Phys. Rev. **73**, 267 (1948).

The Plastic Flow of Thick-Walled Tubes with Large Strains[1]

C. W. MacGregor,[2] L. F. Coffin, Jr.,[3] and J. C. Fisher[4]

(Received October 20, 1947)

The theory for the plastic flow of thick-walled tubes is discussed for a material having an arbitrary true stress-strain curve, loaded by any combination of internal pressure, external pressure, and end load, where the strains may become large necessitating the use of finite true strain definitions.

Comparisons are made of the finite strain theory, the infinitesimal strain theory, and experimental results for the special case of a closed end thick-walled tube of aluminum. The comparison shows that the infinitesimal strain theory is considerably in error even at moderate strain values. The finite strain theory appears to be satisfactory even for strains somewhat beyond the value for the local bulging of thick-walled tubes.

A FINITE strain theory for the plastic flow of thick-walled tubes to large deformations was developed during the War by Bridgman.[5] An independent solution of the same problem was obtained later by the present authors.[6] A comparison of the two solutions now reveals that they are identical save for minor differences of terminology and method of treatment. This duplication of effort resulting from the limited flow of scientific information at the time has only recently been discovered.

The present paper gives experimental data from the expansion of a thick-walled tube under internal pressure indicating the superiority of the finite strain theory over the infinitesimal strain theory with which it is compared. In view of the limited availability of the original references it was felt that an introductory review of the derivation of the finite strain theory would be of value.

REVIEW OF THEORY

In problems concerned with the deformation of materials in the elastic and in the early plastic ranges, the magnitudes of the displacements encountered are small compared to the dimensions of the deforming element. For such problems it is sufficiently accurate to employ the infinitesimal strain concept wherein the deformations are referred to the original dimensions of the element rather than to the instantaneous values. As the magnitude of the plastic deformation increases relative to the dimensions of the element, a condition is soon reached where an analysis of the state of stress and strain requires the application of the finite strain concept.

Such a situation is presented in the problem of the finite plastic deformation of a thick-walled tube subjected simultaneously to an internal pressure, an external pressure, and an end load.* The need for a solution of this problem is threefold: (a) to aid the designer of industrial equipment wherever use is to be made of the added strength available through the heavy cold-working of tubes; (b) to serve as a guide for the pressure *versus* expansion relationship during the cold working operation; and (c) to provide a means for determining the pressure at which failure by local bulging will occur in thick-walled pressure vessels.

The radial equilibrium of an element of ma-

[1] This paper is the result of a portion of a research program carried out at the Massachusetts Institute of Technology for the Bureau of Ordnance, Navy Department. Approval for the release of this information has been received from the Chief of the Bureau of Ordnance. Statements expressed are those of the authors and should in no way be construed as the opinion of the United States Navy.

[2] Professor of Applied Mechanics, Department of Mechanical Engineering, Massachusetts Institute of Technology, Cambridge, Massachusetts.

[3] Assistant Professor of Mechanical Engineering, Department of Mechanical Engineering, Massachusetts Institute of Technology, Cambridge, Massachusetts.

[4] Instructor, Department of Mechanical Engineering, Massachusetts Institute of Technology, Cambridge, Massachusetts.

[5] P. W. Bridgman, Watertown Arsenal Laboratory Report Number WAL 111/7–3, October 8, 1943.

[6] C. W. MacGregor, L. F. Coffin, Jr., and J. C. Fisher, "Project G Report No. 1," submitted to the Chief of the Bureau of Ordnance, Bureau of Ordnance, Navy Department, Washington, D. C., February 10, 1945.

* The cases of the partially yielded tube and the tube just completely yielded have been treated under the assumption of infinitesimal strains (see references 7 and 8).

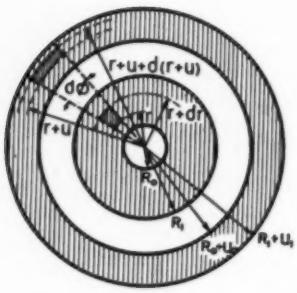

FIG. 1. Expansion of tube to very large deformations.

terial in an expanded tube demands that

$$(r+u)\frac{d\sigma_r}{d(r+u)}=\sigma_t-\sigma_r,^{**} \tag{1}$$

where $r+u$ is the radial distance to the element in the expanded tube.

The cross section of a tube with original inside and outside radii R_0 and R_1 respectively, expanded to internal and external radii R_0+u_0 and R_1+u_1 respectively, is shown in Fig. 1. An arbitrary element at the radius r has moved to the radius $r+u$. The true radial and tangential strains become

$$\left.\begin{aligned}\epsilon_r&=\log_e\frac{d(r+u)}{dr}=\log_e\left(1+\frac{du}{dr}\right)\\ \epsilon_t&=\log_e\frac{(r+u)d\phi}{rd\phi}=\log_e\left(1+\frac{u}{r}\right)\end{aligned}\right\}. \tag{2}$$

After the elimination of u in Eqs. (2), the equation for the compatability of the strains is

$$r\frac{d\epsilon_t}{dr}=e^{\epsilon_r-\epsilon_t}-1. \tag{3}$$

Equation (1) can be rewritten as

$$r\frac{d\sigma_r}{dr}=(\sigma_t-\sigma_r)\frac{1+\dfrac{du}{dr}}{1+\dfrac{u}{r}}=(\sigma_t-\sigma_r)e^{\epsilon_r-\epsilon_t} \tag{4}$$

if use is made of the relationships given in Eqs. (2). Thus Eqs. (3) and (4) are the equations of strain compatability and of equilibrium respectively for the large deformations of a thick-walled tube.

** See Nomenclature for definition of variables.

It is further assumed that (a) the material obeys the distortion energy law of yielding, (b) the volume remains constant, (c) the ratios of principal stress differences to the corresponding principal strain differences are equal,*** and (d) the axial strain is constant over the cross section. These are the commonly accepted laws of plasticity as applied to problems of this type.[7,8]

The distortion energy law of plasticity states that the effective stress

$$\sigma=(\sqrt{2}/2)[(\sigma_1-\sigma_2)^2+(\sigma_2-\sigma_3)^2+(\sigma_3-\sigma_1)^2]^{\frac{1}{2}} \tag{5}$$

required to maintain plastic flow in an element of material is a function of the effective strain

$$\epsilon=(\sqrt{2}/3)[(\epsilon_1-\epsilon_2)^2+(\epsilon_2-\epsilon_3)^2+(\epsilon_3-\epsilon_1)^2]^{\frac{1}{2}} \tag{6}$$

associated with that element, where σ_1, σ_2, σ_3; ϵ_1, ϵ_2, ϵ_3 are the principal stresses and strains, respectively. This relationship can be stated symbolically as

$$\sigma=f(\epsilon). \tag{7}$$

The constants in front of the radicals in Eqs. (5) and (6) were so chosen that for the tension test Eq. (7) reduces to the true stress-strain relationship $\sigma_z=f(\epsilon_z)$.

Since ϵ_1, ϵ_2, and ϵ_3 represent true plastic strains, the constancy of volume can be expressed by the equation

$$\epsilon_1+\epsilon_2+\epsilon_3=0 \tag{8}$$

independently of the magnitude of plastic deformation when there is no rotation of the principal strain axes.

From assumption (c) and Eq. (8) it follows that

$$\left.\begin{aligned}E\epsilon_r&=D[\sigma_r-\tfrac{1}{2}(\sigma_t+\sigma_z)]\\ E\epsilon_t&=D[\sigma_t-\tfrac{1}{2}(\sigma_z+\sigma_r)]\\ E\epsilon_z&=D[\sigma_z-\tfrac{1}{2}(\sigma_r+\sigma_t)]\end{aligned}\right\}, \tag{9}$$

where D is a function of the radius. From Eqs. (5), (6), and (9) it follows that

$$D=\frac{E\epsilon}{\sigma}.$$

*** This is a special case of the more fundamental assumption that the ratios of principal stress differences to the corresponding principal strain rate differences are equal during plastic flow.

[7] A. Nádai, *Plasticity* (McGraw-Hill Book Company Inc., New York, 1931).

[8] C. W. MacGregor, L. F. Coffin, Jr., and J. C. Fisher, *Partially Plastic Thick-Walled Tubes*, to be published shortly.

Inserting this value of D in Eqs. (9) gives

$$\left.\begin{aligned}\epsilon_r&=\frac{\epsilon}{\sigma}[\sigma_r-\tfrac{1}{2}(\sigma_t+\sigma_z)]\\ \epsilon_t&=\frac{\epsilon}{\sigma}[\sigma_t-\tfrac{1}{2}(\sigma_z+\sigma_r)]\\ \epsilon_z&=\frac{\epsilon}{\sigma}[\sigma_z-\tfrac{1}{2}(\sigma_r+\sigma_t)]\end{aligned}\right\}. \tag{10}$$

Let $\epsilon_z=k=$ constant, satisfying the fourth assumption (d) above. Then from Eqs. (10)

$$\sigma_z=\frac{\sigma k}{\epsilon}+\tfrac{1}{2}(\sigma_r+\sigma_t). \tag{11}$$

Substituting this value of σ_z into Eq. (5) for the effective stress,

$$\sigma_t-\sigma_r=\pm\frac{2\sigma}{\sqrt{3}}\left(1-\frac{k^2}{\epsilon^2}\right)^{\frac{1}{2}}, \tag{12}$$

where for a thick-walled tube the upper sign corresponds to an excess of internal over external pressure, and the lower to an excess of external over internal pressure.

The value of $\sigma_t-\sigma_r$ from Eq. (12) can be substituted in the equation of equilibrium (4) which becomes

$$r\frac{d\sigma_r}{dr}=\pm\frac{2\sigma}{\sqrt{3}}\left(1-\frac{k^2}{\epsilon^2}\right)^{\frac{1}{2}}e^{\epsilon_r-\epsilon_t}. \tag{13}$$

Integrating this equation the radial stress is

$$\begin{aligned}\sigma_r&=\int d\sigma_r+c_0=-p_1+\int_{r=R_1}^{r}d\sigma_r\\ &=-p_1\mp\frac{2}{\sqrt{3}}\int_r^{R_1}\sigma\left(1-\frac{k^2}{\epsilon^2}\right)^{\frac{1}{2}}e^{\epsilon_r-\epsilon_t}\frac{dr}{r},\end{aligned} \tag{14}‡$$

where the upper sign applies to an excess of internal pressure and the negative external pressure $-p_1$ appears as the constant of integration.

Expressions for σ_t and σ_z are obtained from Eqs. (11) and (12) as

$$\left.\begin{aligned}\sigma_t&=\sigma_r\pm\frac{2\sigma}{\sqrt{3}}\left(1-\frac{k^2}{\epsilon^2}\right)^{\frac{1}{2}}\\ \sigma_z&=\tfrac{1}{2}(\sigma_r+\sigma_t)+\frac{\sigma k}{\epsilon}\end{aligned}\right\}. \tag{15}$$

‡ The variable of integration could equally well be taken as $r+u$, in which case Eq. (14) would appear as

$$\sigma_r=-p_1\mp\frac{2}{\sqrt{3}}\int_{r+u}^{R_1+u_1}\sigma\left(1-\frac{k^2}{\epsilon^2}\right)^{\frac{1}{2}}\frac{d(r+u)}{r+u}. \tag{14a}$$

Considering now the plastic strains, it follows from Eq. (8) that

$$\epsilon_r=-k-\epsilon_t.$$

Substituting this value of ϵ_r into the compatability Eq. (3)

$$r\frac{d\epsilon_t}{dr}=e^{-(k+2\epsilon_t)}-1.$$

Integrating,

$$\epsilon_t=\tfrac{1}{2}\log_e\left[e^{-k}+\frac{c}{r^2}\right] \tag{16}$$

where c is a constant of integration.

Defining

$$z=\log_e\left[e^{-k}+\frac{c}{r^2}\right],$$

the strains become

$$\left.\begin{aligned}\epsilon_r&=-k-\tfrac{1}{2}z\\ \epsilon_t&=\tfrac{1}{2}z\\ \epsilon_z&=k\end{aligned}\right\}. \tag{17}$$

The value of the effective strain can be computed from the values of ϵ_r, ϵ_t, and ϵ_z in Eqs. (17) according to the definition of ϵ in Eq. (6). Thus

$$\epsilon=(k^2+\tfrac{1}{3}(k+z)^2)^{\frac{1}{2}}. \tag{18}$$

The expressions for the stresses and strains contained in Eqs. (7), (14), (15), (17), and (18) are summarized below:

$$\left.\begin{aligned}\sigma_r&=-p_1\mp\frac{2}{\sqrt{3}}\int_r^{R_1}\sigma\left(1-\frac{k^2}{\epsilon^2}\right)^{\frac{1}{2}}e^{\epsilon_r-\epsilon_t}\frac{dr}{r}\\ \sigma_t&=-p_1\mp\frac{2}{\sqrt{3}}\int_r^{R_1}\sigma\left(1-\frac{k^2}{\epsilon^2}\right)^{\frac{1}{2}}e^{\epsilon_r-\epsilon_t}\frac{dr}{r}\\ &\qquad\pm\frac{2\sigma}{\sqrt{3}}\left(1-\frac{k^2}{\epsilon^2}\right)^{\frac{1}{2}}\\ \sigma_z&=-p_1\mp\frac{2}{\sqrt{3}}\int_r^{R_1}\sigma\left(1-\frac{k^2}{\epsilon^2}\right)^{\frac{1}{2}}e^{\epsilon_r-\epsilon_t}\frac{dr}{r}\\ &\qquad\pm\frac{\sigma}{\sqrt{3}}\left(1-\frac{k^2}{\epsilon^2}\right)^{\frac{1}{2}}+\frac{\sigma k}{\epsilon}\\ \epsilon_r&=-k-\tfrac{1}{2}z\\ \epsilon_t&=\tfrac{1}{2}z\\ \epsilon_z&=k\\ \sigma&=f(\epsilon)\end{aligned}\right\} \tag{19}$$

where

$$\left.\begin{aligned}\epsilon&=(k^2+\tfrac{1}{3}(k+z)^2)^{\frac{1}{2}}\\ z&=\log_e\left[e^{-k}+\frac{c}{r^2}\right]\\ \frac{u}{r}&=e^{\epsilon t}-1\end{aligned}\right\} \tag{20}$$

and where c is constant for a given deformation of the tube.

The integrals in Eqs. (19) can be evaluated readily by numerical methods when the relationship $\sigma=f(\epsilon)$ has been determined from a tension test and when the loading system is specified. In general, several trial solutions are needed in order to determine which pair of values for c and k satisfies the boundary conditions.

A particular loading condition of practical interest occurs when the tube has closed ends, and is subjected to no end load in addition to that due to the internal pressure p_0 and the external pressure p_1. It will be shown that for this loading the axial strain is $\epsilon_z=k=0$.

When $k=0$ Eqs. (19) and (20) reduce to

$$\left.\begin{aligned}\sigma_r&=-p_1\mp\frac{1}{\sqrt{3}}\int_r^{R_1}\frac{\sigma d(r^2)}{r^2+c}\\ \sigma_t&=-p_1\mp\frac{1}{\sqrt{3}}\int_r^{R_1}\frac{\sigma d(r^2)}{r^2+c}\pm\frac{2\sigma}{\sqrt{3}}\\ \sigma_z&=-p_1\mp\frac{1}{\sqrt{3}}\int_r^{R_1}\frac{\sigma d(r^2)}{r^2+c}\pm\frac{\sigma}{\sqrt{3}}\\ \epsilon_r&=-\tfrac{1}{2}z\\ \epsilon_t&=\tfrac{1}{2}z\\ \epsilon_z&=0\\ \sigma&=f(\epsilon)\end{aligned}\right\} \tag{21}$$

where

$$\left.\begin{aligned}\epsilon&=\frac{z}{\sqrt{3}}\\ z&=\log_e\left[1+\frac{c}{r^2}\right]\\ \frac{u}{r}&=e^{\epsilon t}-1\end{aligned}\right\}. \tag{22}$$

The expression $e^{\epsilon r-\epsilon t}$ has been replaced by its value

$$e^{-z}=\frac{1}{1+\dfrac{c}{r^2}}=\frac{r^2}{r^2+c}$$

in determining the above expressions.

From Eqs. (21) it is seen that $2\epsilon_t=z$. Substituting the value of ϵ_t from Eqs. (2) and the value of z from Eqs. (22) in this expression

$$\log_e\left(1+\frac{u}{r}\right)^2=\log_e\left(1+\frac{c}{r^2}\right)$$

from which

$$(r+u)^2=r^2+c \tag{23}$$

and

$$d(r+u)^2=d(r)^2. \tag{24}$$

By means of these relationships the stress Eqs. (21) can be reduced to

$$\left.\begin{aligned}\sigma_r&=-p_1\mp\frac{2}{\sqrt{3}}\int_{r+u}^{R_1+u_1}\frac{\sigma d(r+u)}{r+u}\\ \sigma_t&=-p_1\mp\frac{2}{\sqrt{3}}\int_{r+u}^{R_1+u_1}\frac{\sigma d(r+u)}{r+u}\pm\frac{2\sigma}{\sqrt{3}}\\ \sigma_z&=-p_1\mp\frac{2}{\sqrt{3}}\int_{r+u}^{R_1+u_1}\frac{\sigma d(r+u)}{r+u}\pm\frac{\sigma}{\sqrt{3}}\end{aligned}\right\}. \tag{25}$$

The end load acting on the tube can now be evaluated as

$$F=\int_{R_0+u_0}^{R_1+u_1}2\pi\sigma_z(r+u)d(r+u). \tag{26}$$

Let

$$\rho=r+u, \tag{27}$$

then the expression

$$F-\pi\rho_0^2p_0+\pi\rho_1^2p_1$$

becomes

$$\begin{aligned}F-\pi\rho_0^2p_0+\pi\rho_1^2p_1&=2\pi\int_{\rho_0}^{\rho_1}\left\{-p_1\mp\frac{2}{\sqrt{3}}\int_\rho^{\rho_1}\frac{\sigma}{\rho}d\rho\pm\frac{\sigma}{\sqrt{3}}\right\}\rho d\rho\\ &\quad+\left[-p_1\mp\frac{2}{\sqrt{3}}\int_{\rho_0}^{\rho_1}\frac{\sigma}{\rho}d\rho\right]\pi\rho_0^2+\pi\rho_1^2p_1\\ &=\mp\frac{4\pi}{\sqrt{3}}\int_{\rho_0}^{\rho_1}\left\{\int_\rho^{\rho_1}\frac{\sigma}{\rho}d\rho\right\}\rho d\rho\\ &\quad\pm\frac{2\pi}{\sqrt{3}}\int_{\rho_0}^{\rho_1}\sigma\rho d\rho\mp\frac{2\pi\rho_0^2}{\sqrt{3}}\int_{\rho_0}^{\rho_1}\frac{\sigma}{\rho}d\rho.\end{aligned} \tag{28}$$

Evaluating by parts, the first integral in Eq. (28) becomes

$$\int_{\rho_0}^{\rho_1}\left\{\int_{\rho}^{\rho_1}\frac{\sigma}{\rho}d\rho\right\}\rho d\rho=-\frac{\rho_0^2}{2}\int_{\rho_0}^{\rho_1}\frac{\sigma}{\rho}d\rho+\tfrac{1}{2}\int_{\rho_0}^{\rho_1}\sigma\rho d\rho.$$

Substitution of this value in Eq. (28) results in

$$F-\pi\rho_0^2p_0+\pi\rho_1^2p_1=0$$

or

$$F=\pi(R_0+u_0)^2p_0-\pi(R_1+u_1)^2p_1 \qquad (29)$$

corresponding to a closed end tube, and justifying the original assumption that $\epsilon_z=0$ for such a tube.†

For a material with a constant yield stress $\sigma=\sigma_0$, Eqs. (25) can be integrated directly, yielding

$$\left.\begin{aligned}
\sigma_r&=-p_1\mp\frac{2\sigma_0}{\sqrt{3}}\log_e\frac{R_1+u_1}{r+u}\\
\sigma_t&=-p_1\pm\frac{2\sigma_0}{\sqrt{3}}\left(1-\log_e\frac{R_1+u_1}{r+u}\right)\\
\sigma_z&=-p_1\pm\frac{2\sigma_0}{\sqrt{3}}\left(\tfrac{1}{2}-\log_e\frac{R_1+u_1}{r+u}\right)\\
\epsilon_t&=-\epsilon_r\\
\epsilon_z&=0\\
\frac{u}{r}&=e^{\epsilon_t}-1
\end{aligned}\right\}. \qquad (30)$$

Using the upper signs, the expressions for the stresses are identical with those given by Nádai[7] for the case of internal pressure; except that R_1+u_1 and $r+u$ replace R_1 and r, respectively, and the external pressure p_1 is included. This indicates quite reasonably that Nádai's stress expressions are valid for large deformations of a material exhibiting a constant yield stress if the actual instantaneous radii are used.††

COMPARISON WITH INFINITESIMAL STRAIN THEORY AND EXPERIMENT

It is of interest to compare the predictions of the finite strain theory with those of a theory based upon the assumption of infinitesimal strain. Such a comparison has been made for the pressure *versus* external tangential strain curve of a closed end 17SO aluminum tube with wall ratio $R_1/R_0=2.0$ and outside diameter of 5 inches. A typical stress-strain curve for the aluminum is shown in Fig. 2.

The curve predicted by the new theory was computed by numerical integration of the expression in Eqs. (21) for σ_r, assuming $p_1=0$. The integration was carried out for several values of c, and the corresponding pairs of values of external tangential strain

$$\epsilon_{t1}=\tfrac{1}{2}\log_e\left(1+\frac{c}{R_1^2}\right)$$

and bore pressure $p_0=-\sigma_{r0}$ are plotted in Fig. 3.

The curve predicted by the infinitesimal strain

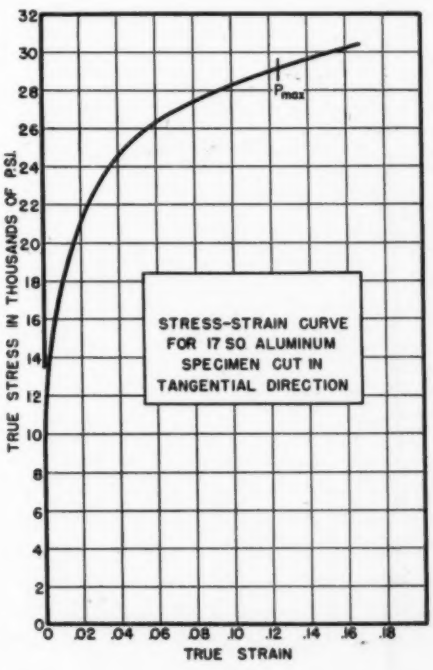

FIG. 2.

† Both Bridgman's tests on the collapsing of closed end steel tubes under external pressure and the tests described below for the expansion of a closed end aluminum tube check experimentally the value $\epsilon_z=0$.

†† For the more common case occurring in practice for large strains, namely, the arbitrary stress-strain curve, it is not sufficient to replace R_1 and r by R_1+u_1 and $r+u$, respectively, in Nádai's infinitesimal strain solution to obtain agreement with the present theory. Agreement is obtained only when $\sigma=\sigma_0$, since for $\sigma=\sigma_0$ the strain distribution is irrelevant; when σ varies with ϵ, however, the infinitesimal strain theory gives incorrect values of the stresses as it bases them on approximate values of ϵ in the relationship $\sigma=f(\epsilon)$. This difficulty is not removed by introducing the actual instantaneous radii.

theory was computed from the equations

$$\sigma_r = -p_1 \mp \frac{1}{\sqrt{3}} \int_r^{R_1} \frac{\sigma d(r^2)}{r^2}$$

$$\sigma_t = -p_1 \mp \frac{1}{\sqrt{3}} \int_r^{R_1} \frac{\sigma d(r^2)}{r^2} \pm \frac{2\sigma}{\sqrt{3}}$$

$$\sigma_z = -p_1 \mp \frac{1}{\sqrt{3}} \int_r^{R_1} \frac{\sigma d(r^2)}{r^2} \pm \frac{\sigma}{\sqrt{3}}$$

$$\epsilon_r = -\frac{c_1}{r^2}$$

$$\epsilon_t = \frac{c_1}{r^2}$$

$$\epsilon_z = 0$$

$$\epsilon = \frac{2}{\sqrt{3}} \frac{c_1}{r^2}$$

$$\sigma = f(\epsilon)$$

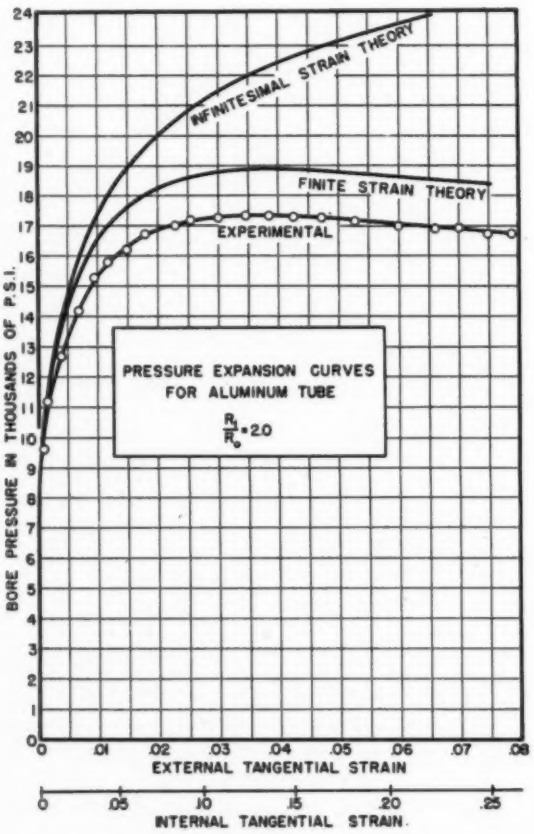

FIG. 3.

which correspond to the infinitesimal strain assumption.[7] In this case as before p_1 was considered zero. A similar method of numerical integration was employed for the determination of the bore pressure corresponding to several values of c_1, and the pairs of p_0, ϵ_{t1} values so found are indicated in Fig. 3.

Figure 3 also gives the experimentally determined curve of pressure *versus* external tangential strain for the aluminum tube. It is evident that the infinitesimal strain theory indicates an indefinitely increasing bore pressure, while the large strain theory and the experimental curve both indicate a maximum pressure corresponding to a strain of about 0.04, after which the tube bulges locally and the pressure falls off. At strains larger than about 0.01 the infinitesimal strain theory departs considerably from the large strain theory and from experiment.

No great significance can be attached to the smaller disagreement between the predictions of the large strain theory and the actual behavior of the aluminum tube. Extensive study of the material of the tube shows it to be highly anisotropic, with substantial differences in the stress-strain curves for axially and tangentially oriented specimens. It is not likely that the simple relationship $\sigma = f(\epsilon)$ as defined in this paper will apply exactly to anisotropic materials.

ACKNOWLEDGMENT

The authors wish to express their appreciation to the following individuals for their interest, support, and encouragement of this work. They are indebted to Captain F. F. Foster, Captain J. S. Champlin, Captain G. L. Schuyler, Commander B. D. Mills, Jr., Mr. C. B. Green, and Mr. J. H. McVay, all of the Bureau of Ordnance, United States Navy.

NOMENCLATURE

c	Constant of integration
c_1	Constant of integration
D	Variable coefficient relating plastic strains and stresses
E	Modulus of elasticity
F	End load
k	Constant value of ϵ_z
p_0	Internal pressure
p_1	External pressure
r	Radial distance to an element in the undeformed tube
R_0	Internal radius of the undeformed tube

R_1 External radius of the undeformed tube

u Radial displacement of an element of initial radius r during plastic yielding of the tube

u_0 Radial displacement of the internal surface of the tube

u_1 Radial displacement of the external surface of the tube

z $\text{Log}_e(e^{-k}+c/r^2)$

$\epsilon_r, \epsilon_t, \epsilon_z$ Radial, tangential, and axial strains, respectively, corresponding to an element at radial distance $r+u$ in the deformed tube

$\epsilon_1, \epsilon_2, \epsilon_3$ Principal strains

ϵ Effective strain, $\epsilon=\frac{\sqrt{2}}{3}((\epsilon_1-\epsilon_2)^2+(\epsilon_2-\epsilon_3)^2+(\epsilon_3-\epsilon_1)^2)^{\frac{1}{2}}$

ρ $r+u$

ρ_0 R_0+u_0

ρ_1 R_1+u_1

$\sigma_r, \sigma_t, \sigma_z$ Radial, tangential, and axial stresses, respectively, corresponding to the radial distance $r+u$ in the expanded tube

σ_{r0} $-p_0$

$\sigma_1, \sigma_2, \sigma_3$ Principal stresses

σ Effective stress, $\sigma=\frac{\sqrt{2}}{2}((\sigma_1-\sigma_2)^2+(\sigma_2-\sigma_3)^2+(\sigma_3-\sigma_1)^2)^{\frac{1}{2}}$

σ_0 Constant yield stress

ϕ Angle

Gyrograms for Simple Harmonic Systems Subjected to External Forces*

V. Rojansky
Department of Physics, Union College, Schenectady, New York

(Received November 17, 1947)

A graphical method is described for the approximate integration of equations of the form $md^2x/dt^2+kx=f(t)$, which arise in several branches of physics and engineering. The graphs, named "gyrograms," are an extension of the familiar "reference circle" used in representing simple harmonic motion. The method is applicable whenever $f(t)$ can be adequately approximated by a step function having a few steps.

INTRODUCTION

OUR purpose is to describe a graphical method for integrating the equation

$$m\frac{d^2x}{dt^2}+kx=f(t), \tag{1}$$

when $f(t)$ is a step function having a few steps, or when it can be adequately approximated by such a step function. For definiteness, we shall regard Eq. (1) as referring to the motion of the frictionless one-dimensional elastic system shown in Fig. 1 and supposed to be so far removed from the earth that the gravitational forces acting on it are negligible, and we shall take m to be the mass of the bob, k the combined restoring constant of the two (massless) springs, x the (vertical) displacement of the bob from its free equilibrium position (that is, the equilibrium position in the absence of external forces, namely, forces other than those that are exerted by the springs), and $f(t)$ the external force acting on the bob and depending explicitly only on the time t. But the method applies to any equation of the form (1), irrespective of its physical interpretation.[1]

The present method is rather elementary and can hardly be new; yet no references to it seem to be available.[2] We shall describe it by examples.

* The author is indebted to the Chief Scientific Adviser, Ministry of Works (London), for permission to publish this material, which was prepared in 1944, when the author was a member of the staff of the Research and Experiments Department of the Ministry of Home Security (London) as a representative of the Princeton University Station of Division 2, NDRC, under OSRD contract OEMsr-260.

[1] An equation of this form governs, for example, the bending moment along an axially compressed uniform beam; for a graphical method of handling the boundary conditions that then arise, see V. Rojansky and R. A. Beth, "Camptograms for beams in compression," Trans Am. Soc. Mech. Eng. **69**, A-202 (1947).

[2] For a recent method for the graphical solution of equations of the form (1), see G. E. Hudson, "A method for estimating equivalent static loads in simple elastic structures," The David W. Taylor Model Basin, U. S. Navy, Report No. 507 (June 1943). Hudson's method is based on a method of Kelvin[3] and of Meissner.[4]

[3] Lord Kelvin, Phil. Mag. **34**, 433 (1892). This method was designed primarily to treat the motion of a particle in a plane.

[4] E. Meissner, Schweizerische Bauzeitung (Zürich) **104**, 35 (1934).

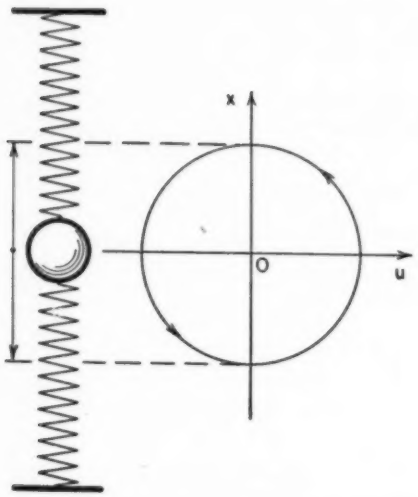

FIG. 1. A simple harmonic system and a reference circle; the circle is drawn for the case of free oscillation between the limits indicated by the dashed lines.

FREE OSCILIATION

We begin with the "reference circle," familiar from the elementary theory of simple harmonic motion. Let no external forces act on the bob in Fig. 1, and let the bob oscillate, about its free equilibrium position, between the limits indicated by the dashed lines. The corresponding reference circle is shown at the right-hand side of the figure. In the coordinate frame accompanying this circle, the ordinate x represents the displacement of the bob from the point $x=0$, and the abscissa u, which has the physical dimensionality of length, is given by the equation

$$u=v/\omega, \tag{2}$$

where v is the velocity of the bob and

$$\omega=(k/m)^{\frac{1}{2}}; \tag{3}$$

that is,

$$u=dx/d\phi, \tag{4}$$

where

$$\phi=\omega t. \tag{5}$$

When expressed in terms of x and u, the energy E of the system, namely, $\frac{1}{2}kx^2+\frac{1}{2}mv^2$, takes a symmetric form:

$$E=\tfrac{1}{2}k(x^2+u^2). \tag{6}$$

The natural period of the system will be denoted by T:

$$T=2\pi/\omega. \tag{7}$$

Each of the quantities x,.v, and presently $f(t)$, will be regarded as positive if it is directed upward. The plane of the reference circle will be called the xu plane.

The basic property of the reference circle is that, while the bob oscillates freely, its displacement x is at all times equal to the vertical component of the displacement of a "representative point," which moves in the xu plane counterclockwise along the circumference of this circle with the constant angular velocity ω.

Let the motion begin at $t=0$ with the initial values $x=x_0$ and $v=v_0$, so that $u_0=v_0/\omega$. Then the initial coordinates of the representative point in the xu plane are x_0 and u_0; hence the appropriate reference circle (whose center lies at O) passes through this point, and therefore the representative point begins its motion as shown by the circular arc in Fig. 2, drawn for a case when x_0 is positive and $u_0=x_0$. This arc we call the "gyrogram" of the motion. The gyrogram of Fig. 2 subtends at O the angle of 120° and thus refers to the time interval lasting from $t=0$ to $t=\frac{1}{3}T$; it can, of course, be extended along the reference circle indefinitely.

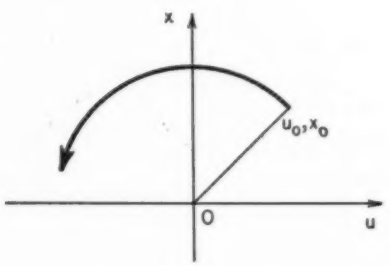

FIG. 2. Gyrogram for a free oscillation starting with the values $x=x_0$ and $v=\omega u_0$, where $u_0=x_0>0$.

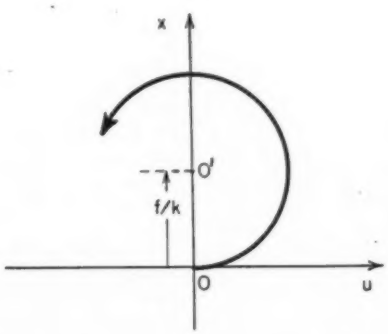

FIG. 3. Gyrogram for a case of a constant force suddenly applied to a system at rest.

CONSTANT EXTERNAL FORCE

If the bob is acted upon by a constant (vertical) external force (for example, the force caused by gravity), so that

$$f(t)=f=\text{constant}, \tag{8}$$

the motion remains simple harmonic and its period is still given by Eqs. (7) and (3). The equilibrium position, however, no longer lies at $x=0$, but at the point $x=f/k$, at which the springs balance the external force. The motion can thus still be described by a reference circle, whose center, however, now lies not at the origin O but at a point O', say, the coordinates of which in the xu plane are

$$x=f/k, \quad u=0. \tag{9}$$

SUDDEN APPLICATION OF A CONSTANT EXTERNAL FORCE TO A SYSTEM AT REST

While the bob is at rest in the absence of external forces, the representative point stays at the origin O of the xu plane. At the instant when the constant force f is applied, the representative point starts moving with the constant angular velocity ω along the appropriate reference circle. The center of this circle lies at the point O', having the coordinates $x=f/k$ and $u=0$; this circle passes through the point O, where the representative point is originally located, and hence the gyrogram has the form shown in Fig. 3, drawn for a case when f is directed upward.

SUDDEN APPLICATION OF A CONSTANT EXTERNAL FORCE TO A SYSTEM IN MOTION

Let the motion begin at the instant $t=0$ with the initial values $x=x_0$ and $v=v_0$, and continue in the absence of external forces for one-third of the period, but at the instant $t=t_1=\frac{1}{3}T$ let a constant force f be suddenly applied to the bob. A gyrogram for such a case is shown in Fig. 4. The arc beginning at the point (u_0, x_0) and ending at the point marked t_1 is taken from Fig. 2; it refers to the first one-third of the period, when the motion is free and when the center of the reference circle lies at O. The rest of the gyrogram has its center of curvature at O', namely,

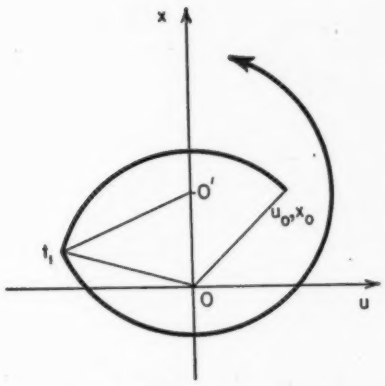

FIG. 4. Gyrogram for a case of a constant force suddenly applied to a system in motion.

at the point whose coordinates are $x=f/k$ and $u=0$, as in Fig. 3.

The fact that the two arcs of the gyrogram in Fig. 4 join at the point marked t_1 represents graphically the fact that x and v vary continuously at the instant t_1, while the kink in the gyrogram at this point corresponds to the fact that the acceleration of the bob, as well as the higher derivatives of x with respect to t, change discontinuously at the instant t_1.

A STEP-LIKE EXTERNAL FORCE

Let the bob be at rest until the instant $t=0$, when the step-like external force shown in Fig. 5 is applied to it. The interval OT in the figure marks the assumed natural period of the system. The symbol f_{01} denotes the constant external force acting from $t=0$ to $t=t_1$, and so on. The round-figure numerical data that we adopt in this example are given in Table I.[5]

We need not know the actual values of t_1, t_2, and so on, but only their ratios to the period T (which corresponds to 360°); accordingly, we give in the second column of Table I the assumed values of ϕ_1, ϕ_2, and so on (that is, ωt_1, ωt_2, and so on), expressed in degrees.

Similarly, we need not know the actual values of f_{01}, f_{12}, and so on, but only their ratios to the restoring constant k; the assumed values of these ratios are given in the last column of Table I.

The graphical procedure is now as follows (Fig. 6):

[5] We use the c.g.s. system of units and express m in grams, k in dynes per centimeter, f in dynes, v in centimeters per second, and x, u, and f/k in centimeters.

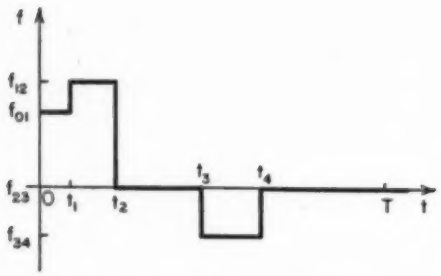

FIG. 5. A step-like external force.

1. On a sheet of rectangular graph paper, draw the vertical x axis and the horizontal u axis, directed as shown, and choose a scale unit (the same unit for x and u) to represent a centimeter.

2. Along the x axis mark the points O_{01}, O_{12}, and so on, whose respective ordinates are equal to the values of f/k listed in Table I (for example, the ordinate of O_{01} equals f_{01}/k, namely, 2.5 cm).

3. Using the values of $\Delta\phi$ listed in Table I, draw counterclockwise the following circular arcs: the arc Ot_1 (center O_{01}, radius $O_{01}O$, angle 30°); the arc t_1t_2 (center O_{12}, radius $O_{12}t_1$, angle 50°); the arc t_2t_3 (center O_{23}, radius $O_{23}t_2$, angle 90°); the arc t_3t_4 (center O_{34}, radius $O_{34}t_3$, angle 60°); and, finally, the thin-line circle (center O, radius Ot_4) which refers to the motion after the instant t_4.

The gyrogram, which enables us to estimate the values of x and v at any instant t, is now complete. We note, for example, that the first maximum of x equals about 4.0 cm. To estimate the time of its occurrence, we add the angle between $O_{23}t_2$ and the x axis (namely, about 52°) to ϕ_2, getting about 132°, or about $0.37\times360°$; hence the first maximum of x occurs at about the instant $t=0.37T$. The first maximum of u occurs at $t=t_2$ and equals about 3.2 cm; hence the first maximum of v occurs at $t=t_2$ and equals about 3.2ω cm/sec. And so on.

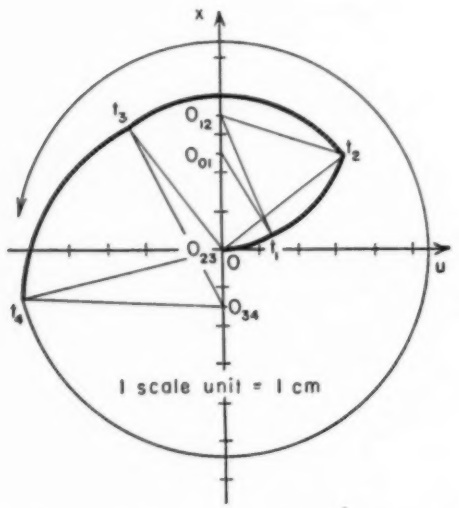

FIG. 6. Gyrogram for the case of the external force described in Fig. 5 and Table I.

SUMMARY OF METHOD

If $f(t)$ has the constant value f_{ab} during an interval extending from $t=t_a$ to $t=t_b$, the segment of the gyrogram for this interval is a counterclockwise circular arc; its center of curvature lies at the point O_{ab}, whose coordinates are $x=f_{ab}/k$ and $u=0$, and the angle ϕ_{ab} that it subtends at O_{ab} equals $\omega(t_b-t_a)$ radians. This arc begins at the terminus of the preceding segment of the gyrogram, or, if t_a is the initial instant of the motion, this arc begins at the point in the xu plane specified by the initial conditions.

In describing the method, we have relied on an intuitive appeal to the familiar "reference circle." To justify it more properly, two steps are necessary: first, to show that, if f is constant, the first integral of Eq. (1) can be written as

$$(x-f/k)^2+u^2=\text{constant}=r^2, \qquad (10)$$

which is the equation of a circle in the xu plane; and, secondly, to show that, if f is constant, the differential of arc of the gyrogram, namely, $[(dx)^2+(du)^2]^{\frac{1}{2}}$, equals $rd\phi$, where r is the constant of integration appearing in (10), and ϕ is expressed in radians. The proofs are left to the reader.

CONCLUDING REMARKS

If $f(t)$ is a step function, the present method is in principle exact and is subject only to the errors of draftsmanship. If $f(t)$ is continuous, as is usually the case in practice, the method can still be used, provided that $f(t)$ can be adequately approximated by a step function having comfortably few steps; but then, of course, analytical errors creep into the work. The decision on the adequacy of the approximation is best left to the computer familiar with the practical aspects of the problem. The effect of the lengths and shapes of the steps of the approximating step function on

the graphical results can of course be studied by trial computations.

If all the $\Delta\phi$'s involved in a computation are equal, the graphical work can be simplified with the help of a wedge of angle $\Delta\phi$, cut out from a sheet of polar graph paper so that its vertex lies at the printed origin of the polar coordinate system. After marking their centers of curvature on the work-sheet, the terminal points of the various circular arcs of the gyrogram can then be located by means of this wedge alone, without using either ruler, compasses, or protractor, and the arcs themselves can be drawn in later, using only compasses. A set of such wedges is convenient to have on hand even if not all the $\Delta\phi$'s are equal, but if some of them recur sufficiently often.

In certain problems the arithmetic can be shortened by replacing x and u by variables proportional to them; for example, if equivalent static loads are being estimated, it is convenient to use kx and ku, rather than x and u, for the vertical and the horizontal coordinate, respectively.

TABLE I. Numerical data on the force of Fig. 5.

t sec.	ϕ	$\Delta\phi$	f dynes	f/k cm
0	0°			
		30°	f_{01}	2.5
t_1	30°			
		50°	f_{12}	3.5
t_2	80°			
		90°	f_{23}	0.0
t_3	170°			
		60°	f_{34}	−1.5
t_4	230°			
		∞	$f_{4\infty}$	0.0
∞	∞			

Analytic expressions for various quantities can be obtained from gyrograms trigonometrically. For example, in Fig. 4 the first and the second extreme values of x are r and $fk^{-1}-(r^2-2fk^{-1}r\sin 15°+f^2k^{-2})^{\frac{1}{2}}$, respectively; here $r=(x_0^2+u_0^2)^{\frac{1}{2}}$.

I am indebted to Professor W. N. Thomas, Dr. F. Garwood, Mr. R. J. Hansen, and Professor H. F. Bohnenblust for helpful discussions.

Large Plastic Flow and the Collapse of Hollow Cylinders

P. W. BRIDGMAN
The Lyman Laboratory of Physics, Harvard University, Cambridge, Massachusetts
(Received November 20, 1947)

The collapse of heavy steel cylinders under external pressures running up to 412,000 p.s.i. was studied during the war under contract with the Watertown Arsenal. The distortions are so large that the conventional small strain analysis is not adequate. The presence of large strains is recognized in the analysis by writing the stress equations of equilibrium in terms of the final displaced positions of the particles instead of in terms of the initial positions. The conventional assumption of negligible volume change is retained. Attention is called to a purely geometrical condition on the strains. In the experiments the cylinders showed no change of length. The generality of the conditions under which this may be expected is examined. A linear relation was found experimentally between collapsing pressure and $\log(r_{ext}/r_{int})$. Furthermore, $P/\log(r_{ext}/r_{int})$ is not constant but rises continually with increasing collapsing pressure. These results indicate that the strain hardening increases continually with increasing distortion, but at a rate two- or threefold less than would be given by experiments in simple tension. The collapse was pushed experimentally to such extremes that the geometrical symmetry was lost because of the grain structure. This limits the region of applicability of any simple theory.

PROFESSOR MacGregor was so kind as to let me see the manuscript of the preceding paper at the same time that he was submitting it for publication in this journal. At that time he made the suggestion that, in view of the close connection between our respective investigations and the comparative inaccessibility of my own publication, it would be of interest if I should outline here the general character of my results. The editor, Dr. Hutchisson, has fallen in with this suggestion, and I am glad to avail myself of the opportunity thus offered. My original work was done during the war under contract with the Watertown Arsenal. It was unclassified and permission has been given for independent and duplicate publication.

With regard to the theoretical discussions, Professor McGregor has already intimated that they are essentially the same. The details, and in particular the order of the analysis, were not always the same however, and it seems to me worth while to restate certain of my theoretical results in view of the contemplated application to experiment, and in order that the degree of generality of the assumptions on which the results depend may be more apparent.

In the first place, there is a purely geometrical condition on the strains (large) independent of any connection between stress and strain. This is, in MacGregor's notation:

$$u=[(r+u)^2(1+e_z')-c^2]^{\frac{1}{2}}-(r+u).$$

Here c is a constant of integration determined by the boundary conditions. In the deduction of this equation the only assumptions are that the strains satisfy the condition of constancy of volume

$$\epsilon_r+\epsilon_t+\epsilon_z=0$$

and that the *ordinary* (not natural or logarithmic) axial strain e_z' is constant across the section and along the length, a constancy demanded by considerations of symmetry. Incidentally, the formulas become somewhat simpler if expressed in terms of the coordinates of the finally displaced particles instead of in terms of the initial positions, as above.

It is an experimental result, both in Professor MacGregor's and my own work, that there is no change of length, or $e_z'=0=\epsilon_z$. In Professor MacGregor's analysis this result was deduced under the assumption of the distortion energy law of yielding. The same result holds, however, under somewhat less restrictive conditions, namely, if the relation between stress and strain is:

$$\epsilon_r=\alpha[\sigma_r-\tfrac{1}{2}(\sigma_t+\sigma_z)],$$
$$\epsilon_t=\alpha[\sigma_t-\tfrac{1}{2}(\sigma_z+\sigma_r)],$$
$$\epsilon_z=\alpha[\sigma_z-\tfrac{1}{2}(\sigma_r+\sigma_t)].$$

This is the integrated form of the relation which holds in the case of isotropy. These equations and the corresponding assumptions embrace both the strain hardening case, in which α is a function of stress or strain or both, as in MacGregor's

analysis, and the non-strain hardening case, which is a degenerate case in which α may be a function of geometry and not of physical properties.

My experiments were experiments on the collapse by inward radial flow of hollow steel cylinders closed at both ends and exposed to hydrostatic pressure over the entire external surface. In all, 27 experiments were made on 27 specimens of five different grades of steel. Each experiment consisted of exposing a virgin specimen to a monotonically increasing pressure to a predetermined maximum, maintenance at the maximum for an interval, and monotonic release of pressure to zero. The cylinders were initially all of the same dimensions: 1.813″ long, 0.3125″ o.d., and 0.0998″ i.d. They were exposed to different maximum pressures varying from 71,000 to 412,000 p.s.i. After exposure to pressure the permanent change of dimensions was determined. In general, pressure was increased to the maximum in about 10 minutes, maintained for 10 minutes, and released to zero in 2 or 3 minutes. In these limits there were no measureable time effects, as proved by control experiments in which pressure was immediately released after reaching the maximum, or maintained at the maximum for 2 hours. Of the 27 specimens, 5 were of a 1020 steel left dead soft (designated as *B* in Figs. 3 and 4). The other 22 were all of the same 1045 steel in four different heat treatments. These were all heated to 1575°F. From this temperature a first set was quenched into salt at 1100°F (designated as *A*5), a second set quenched into salt at 800°F (*A*6), a third set quenched into water and drawn at 800°F (*A*7), and a fourth set quenched into water and drawn at 1100°F (*A*8). The heat treatments were made at the Arsenal.

The assumption of no permanent change of volume was checked from the measured change of dimensions. Actually a permanent decrease of density averaging around 0.2 percent was found. This is too small to invalidate the theoretical analysis; it is in agreement with other well-known results on the effect of cold work. The analysis neglects the elastic component of volume change. In the extreme case of any of the experiments the maximum component of radial displacement due to elastic distortion occurs at the external surface and is 7 percent of the displacement due to plastic flow. In all cases the elastic part vanishes in comparison with the plastic part at the inner surface.

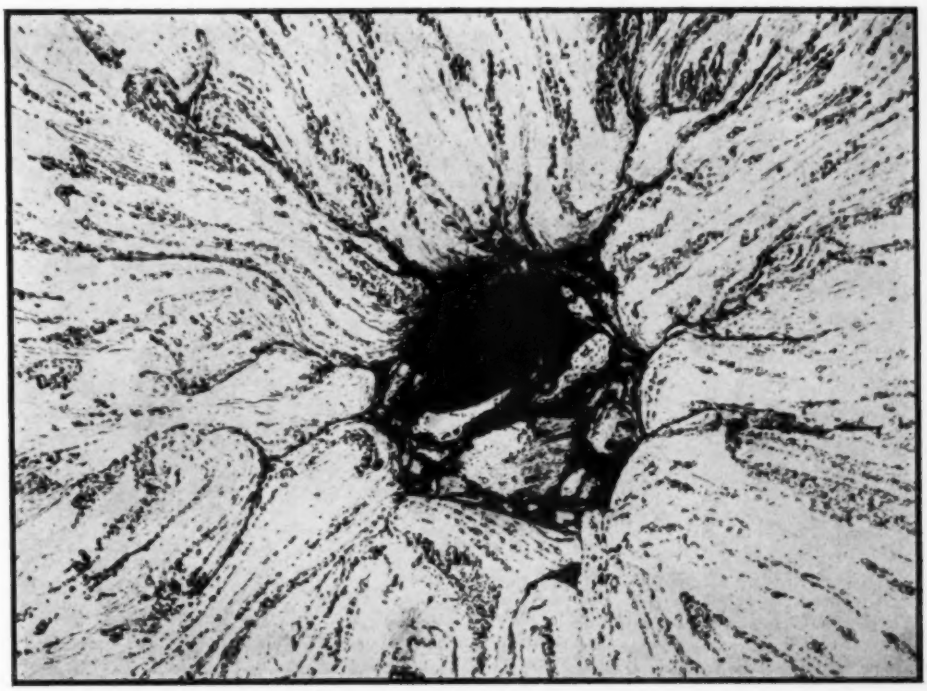

FIG. 1. The immediate neighborhood of the internal cavity, under an original magnification of of 200, of the cylinder of 1020 steel after exposure to a maximum collapsing pressure of 355,000 p.s.i.

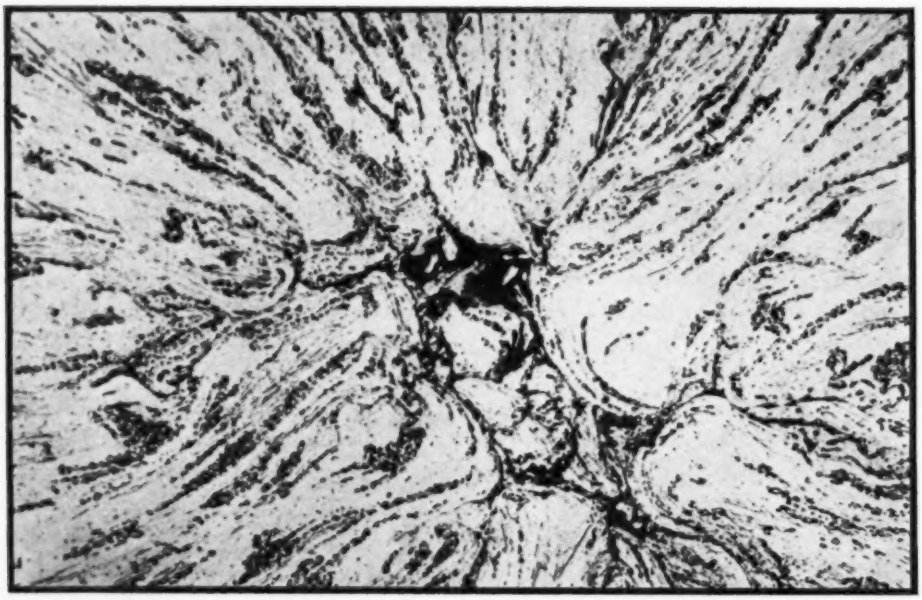

FIG. 2. The immediate neighborhood of the internal cavity, under an original magnification of 200, of the cylinder of 1020 steel after exposure to a maximum collapsing pressure of 412,000 p.s.i.

The permanent changes of length varied between extremes of +0.11 and −0.19 percent. This change of length is probably due to effects at the ends, where friction of the closing caps introduces some unavoidable local warping. In any event it would seem to be sufficiently close to the theoretical value zero to justify the analysis.

The radial flow in the case of the softer samples was extreme, resulting in what to superficial examination appeared as complete closing of the internal bore. The extremes to which plastic flow may be forced are shown in Figs. 1 and 2. These are microphotographs, made at the Arsenal, which show under a magnification of 200-fold the general region of the internal hole of the two specimens of 1020 steel exposed to maximum pressures of 355,000 and 412,000 p.s.i., respectively. These photographs show the enormous distortion in the original grains and make

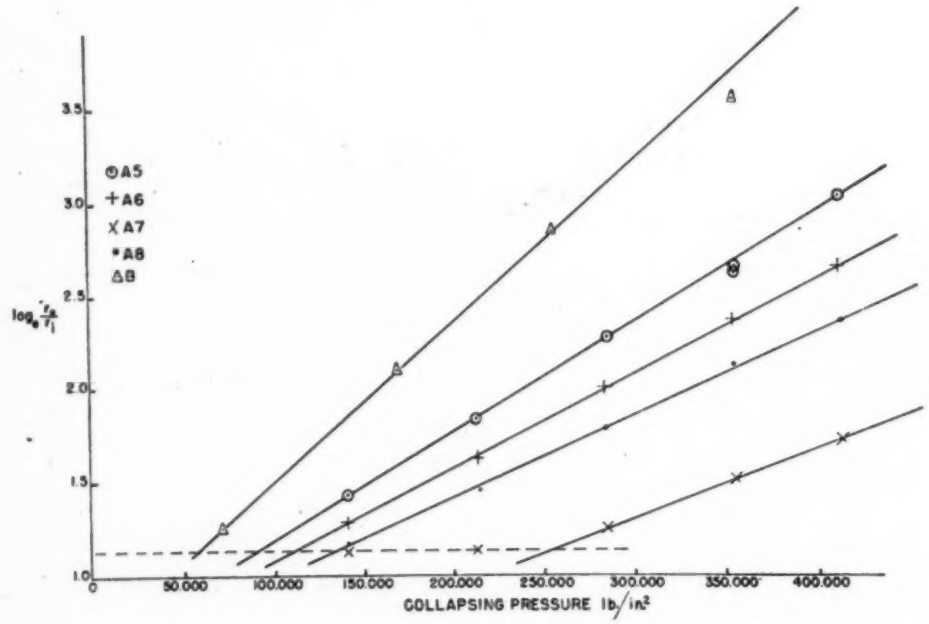

FIG. 3. The natural logarithm of the ratio of final external to final internal radius for the various steels described in the text as a function of maximum collapsing pressure.

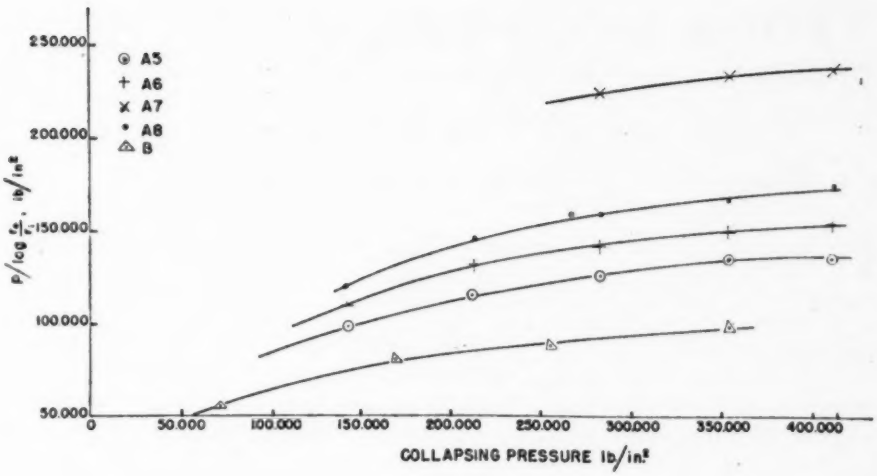

FIG. 4. The ratio of pressure to the ordinate of Fig. 3 as a function of pressure. This function would be a constant if the maximum shearing stress criterion of plastic yield were valid.

clear that even in the absence of other limiting factors the mathematical analysis cannot be pushed to extreme distortions because of failure of physical and geometrical isotropy and homogeneity due to the grain structure of the material.

In Fig. 3 are plotted the various values of the natural logarithm of the ratio of the final external to internal radius as a function of collapsing pressure. The initial value for the uncollapsed virgin specimen is 1.139, indicated in Fig. 3 by a dotted line. It is seen that within experimental error, after plastic flow has once started, there is a linear relation between pressure and $\log(r_{ext}/r_{int})$. This holds into regions of deformation so large that geometrical uniformity is lost and the granular structure begins to dominate. If the linear relation held indefinitely, the hole would become vanishingly small only for infinite pressure. This is contrary to some early experiments of mine[1] in which copper tubes were pushed to apparent complete collapse, and extrapolation indicated complete collapse of mild steel in the neighborhood of 320,000 p.s.i. It is now apparent that these results, which were unexpected because they indicated a strain softening instead of a strain hardening for extreme distortions, are to be explained in terms of a failure of geometrical regularity due to increasing dominance by the individual grains.

The theoretical equations give the means for deducing the form of the curves of Fig. 3 in either of two cases: (a) There is strain hardening and the general relation between stress and strain is determined by some such criterion as a universal functional relation between "significant" stress and "significant" strain; (b) there is no strain hardening and flow is determined either by the maximum shearing stress criterion or the maximum shearing energy criterion, which under these particular conditions become identical. In the latter case the result is particularly simple, and is $P/\log(r_{ext}/r_{int}) = \text{const.}$, where the constant is the critical shearing stress. In Fig. 4 $P/\log(r_{ext}/r_{int})$ is plotted as a function of P; it is not constant, but in all cases rises continuously with increasing pressure. Hence, under these conditions the maximum shearing stress criterion is not valid, but there is strain hardening, which continues increasingly over the entire range, with no lapse into a strain softening. Theoretically, it should be possible to work backwards from the curves of Fig. 4 and deduce the strain hardening curve, in conjunction with some such assumption as a functional relation between significant stress and strain. However, such a procedure turns out not to be sensitive, and only rough conclusions can be drawn about the strain hardening curve. It is definitely indicated that the hardening which would account for the curves of Figs. 3 and 4 increases with strain at a rate considerably less than the rate given by ordinary tension tests, probably less by a factor of 2 or 3. This is in line with other evidence which indicates that under large plastic deformations strain hardening in compression is less rapid than in tension.

[1] P. W. Bridgman, Phys. Rev. **34**, 1 (1912).

Letters to the Editor

"Physical Basis of Bird Navigation"

JOSEPH SLEPIAN
Westinghouse Research Laboratories, Pittsburgh 30, Pennsylvania
January 6, 1948

IN his remarkable paper on the above subject in the Journal of Applied Physics,* Dr. Yeagley describes the astonishing experimental support to his hypothesis that navigating birds are "sensitive" to the magnetic field and Coriolis forces associated with the earth. Astonishing as this hypothesis may seem, I do not know of any fundamental law of physics which is contradicted by it, or which would rule it out, as thus stated.

However, Dr. Yeagley, in his paper, states his hypothesis in a more limited manner, and to this more limited hypothesis, it seems to me, serious objection can be made. Dr. Yeagley states that the birds are "sensitive" to the effect of motion through the earth's magnetic field (p. 1036, second column), or to the effect of flying through a magnetic field (p. 1037, second column). In both cases, I presume Dr. Yeagley means a uniform motion through the magnetic field.

The restricted principle of relativity applied to this case tells us that in a system, such as the flying bird, in uniform motion relative to the earth, electrical and magnetic phenomena will proceed in exactly the same way as if the system were at rest, that is, the bird on the ground, and the electric and magnetic field in the system changed by the following scheme:

$$E_x' = E_x, \qquad H_x' = H_x,$$

$$E_y' = \frac{E_y - \frac{v_x}{c}H_z}{\left(1-\frac{v_x^2}{c^2}\right)^{\frac{1}{2}}}, \quad H_y' = \frac{H_y + \frac{v_x}{c}E_z}{\left(1-\frac{v_x^2}{c^2}\right)^{\frac{1}{2}}}, \tag{1}$$

$$E_z' = \frac{E_z + \frac{v_x}{c}H_y}{\left(1-\frac{v_x^2}{c^2}\right)^{\frac{1}{2}}}, \quad H_z' = \frac{H_z - \frac{v_x}{c}E_y}{\left(1-\frac{v_x^2}{c^2}\right)^{\frac{1}{2}}}.$$

Here E_x, E_y, E_z, and H_x, H_y, H_z, are the components, respectively, of the earth's electric and magnetic fields, v_x, the velocity of the bird moving in the x direction, and c, the velocity of light. E_x', E_y', E_z', H_x', H_y', H_z' are the components of the electric and magnetic fields to which the bird at rest on the earth must be subjected if it is to be "sensitive" to exactly the same effects as the bird moving with velocity v_x through the fields E_x, E_y, E_z, H_x, H_y, H_z.

If we neglect v_x^2/c^2 relative to (1), and also neglect the effect of motion through the earth's electric field, that one of the above equations which is relevant to my argument becomes

$$E_y' - E_y = -\frac{v_x}{c}H_z. \tag{2}$$

Hence any "sensitivity" which the bird may have to its uniform motion, v_x, through the vertical component of the earth's magnetic field, H_z, will be indistinguishable from its "sensitivity" to a change in the horizontal component of the earth's electric field given by (2).

Unfortunately, the intensity of the earth's electric field is normally thousands of times larger than the quantity v_x/cH_z in Eq. (2). If the earth's surface were perfectly smooth and horizontal, and if there were no clouds or other disturbing charge distributions in the air, we might argue that the horizontal component of the earth's electric field, E_y, remains always zero. But with actual terrain, local winds, and clouds, E_y will always be large, and variable. Hence, we may conclude that whatever "sensitivity" the bird may have to its motion, v_x, in the field, H_z, it will be quite completely overshadowed and obliterated by the indistinguishable "sensitivity" to changes in the earth's horizontal electric field, E_y.

I have frequently had occasion in the past to use the above argument to convince inventors who aspire to measure the velocity of an airplane by observing the effects of its motion through the earth's magnetic field upon suitable electrical apparatus on the plane. No matter how ingeniously they devise their apparatus, the effect of changes in the earth's horizontal field is indistinguishable from, and overshadows, the effect they are trying to observe.

It seems to me, then, that Dr. Yeagley will need to postulate a "sensitivity" of the navigating bird to the magnetic field directly, rather than a "sensitivity" to the effect of the uniform motion of the bird through the field. He will also need to assign to the necessary observation, which the bird must have of the ground over which the bird is flying, a role more primary than that of merely cooperating with the "sensitivity" to its motion through the magnetic field (p. 1037, second column).

* Henry L. Yeagley, J. App. Phys. **18**, 1035 (1947).

Remarks on: "A Preliminary Study of a Physical Basis of Bird Navigation"*

RUSSELL H. VARIAN
Microwave Laboratory, Department of Physics, Stanford University, Stanford, California
January 22, 1948

TO support his very interesting theory of the mechanism of bird navigation, the author presents very strong experimental evidence for the conclusion that pigeons, and presumably other birds, find their way home over territory which is unfamiliar, by the aid of two senses. One is a sense of latitude, the other a sense of the strength of the vertical component of the earth's magnetic field. Since the magnetic poles of the earth are displaced from the axis of rotation, the lines of equal vertical component intersect the latitude lines, forming a grid which may be used to define a location.

The author appears to jump to unwarranted conclusions concerning the operation of these senses.

First, he postulates that the indication of the vertical component of the earth's magnetic field is provided by some organ which can measure the e.m.f. produced in a conductor cutting the lines of force of the earth's magnetic field.

The primary reason for writing this letter is that the present writer, in his student days, conceived the idea of utilizing this effect to construct a ground speed meter for airplanes, and stirred up quite a bit of interest before he discovered that the method was fundamentally fallacious. Later, Dr. D. L. Webster produced a more general refutation than that of the writer. This argument, which is based on relativity, is here outlined.

In relativity, an identity exists between an electrostatic field and a magnetic field moving relative to a frame of reference. It then follows that any attempt to shield a pick-up system from spurious electrostatic forces must shield the pick-up from the influence of the moving magnetic field. This is briefly treated by W. R. Smythe, *Static and Dynamic Electricity* (McGraw-Hill Book Company, Inc., New York, 1939), pp. 499–501. If we dispense with shielding, we are then confronted with the conductor. This reduces itself to measuring a potential difference between the conductor ends and the atmosphere, but the atmosphere is moving with respect to the magnetic field and therefore has an electrostatic field caused by its motion. Thus, if the formidable obstacle of extraneous electrostatic forces is successfully overcome, the end result is a measurement of air speed. Since pigeons cannot measure the vertical component of the earth's field by measuring the rate of cutting magnetic lines of force, the alternative appears to be that they possess an organ capable of acting as a magnetometer.

The author's second postulate is that the detection of latitude is made by measurement of the Coriolis force. This he computes for his case to be 0.0061 ft. per sec. per sec., or about 1/6000 g. In order for pigeons to locate themselves within 25 miles or so, a measurement of less than 1 percent of this would have to be made, or very roughly a measurement of 10^{-6} g. The only way the acceleration of gravity may be removed from the measurement is by a knowledge of its direction of action to about 10^{-6} radian without reference to the force of g for determining that direction. This appears to be practically impossible, even though it may be theoretically possible. It would therefore appear that as far as the evidence presented in the article is concerned, the determination of latitude by the sun is more likely than determination by Coriolis force.

The hypothesis that a bird measures latitude by the elevation of the sun should receive attention. The sun appears as a fairly large object, yet determination of its elevation to one solar diameter would give latitude within 30 miles; thus, it appears that if solar elevation is used, no great precision is required to determine latitude within the pigeon's apparent accuracy. The cited fact that pigeons are unable to navigate in thick haze or fog or complete darkness is concordant with this view.

It should be further pointed out that either mutation or chance development of an organ for another function must produce an organ capable of measuring Coriolis force sufficiently well to be of survival value before evolution can take hold to produce further refinement. This seems to be almost an impossible occurrence.

The following experiments to throw further light on the nature of the organs involved suggest themselves:

1. Attach magnets to the birds where they will be stationary with respect to the body of the bird, but will produce a change in vertical component of magnetic field.
2. Determine definitely whether pigeons can navigate under conditions of good visibility but heavy overcast. This last experiment would be conclusive if it showed pigeons could not navigate under heavy overcast, but if the result were the reverse it would not rule out an organ sensitive to extreme infra-red which could operate through considerable overcast.

* Henry L. Yeagley, J. App. Phys. **18**, 1035 (1947).

Remarks on: "The Physical Basis of Bird Navigation"

LEVERETT DAVIS, JR.
California Institute of Technology, Pasadena, California
January 19, 1948

IN a recent article[1] H. L. Yeagley describes experiments with homing pigeons which he interprets as indicating that homing ability is based on the detection of induced electromotive forces due to motion with respect to the earth's magnetic field and on the detection of the Coriolis force due to motion with respect to the rotating earth. However, even if it is assumed that a pigeon can make any required measurements with infinite accuracy, it seems conceptually impossible for it to detect either the electromotive force or the Coriolis force. A discussion of the impossibility of determining the electromotive force is given by Smythe,[2] who bases his discussion on the well established principal that the electric fields observed by virtue of motion through a uniform magnetic field are indistinguishable from uniform static fields. Since the static fields due to atmospheric electricity[3] are of the order of one volt/cm and are quite variable, it would appear impossible to detect a superposed field of 10^{-5} volt/cm due to motion. It is also impossible that these fields should produce physiological effects, as suggested by Yeagley. The situation with respect to Coriolis force is even worse. It is difficult to conceive of a device that responds to Coriolis force that does not respond equally to gravitational force, certainly no mechanical device will. Hence it is impossible to separate the Coriolis force from the force of gravity except by comparison of measurements of two observers having different velocities, and hence different Coriolis forces. It does not help the pigeon to change its speed unless it can, in effect, determine the position of the vertical when stationary on the ground and then recognize the position of this line by visual observations (or by the use of a gyroscope), to about 0.1 second of arc for comparison with the apparent vertical when flying. When flying over water or fog where the solid earth is not visible, it would seem to be impossible for the pigeon to determine either its speed or acceleration with respect to the earth, both being needed

for a determination of latitude by means of the Coriolis force, and the speed being needed for a determination of the vertical component of the magnetic field from the induced electromotive force.

Even though it is impossible for the pigeon to detect the induced electromotive force produced by flying through the earth's field, and thereby determine the vertical component of the field, there is no such reason to suppose that the bird cannot measure the field directly, perhaps by means of the e.m.f.'s induced in moving blood. And there are many ways whereby latitude can be measured without measuring Coriolis force. Offhand, it would seem easier for the pigeon to observe the sun or the stars or to measure the acceleration of gravity, which depends on latitude, than to measure a force of the order of the Coriolis force. It is evident, therefore, that Yeagley can meet the above objections without an essential change in his theory merely by adopting some other mechanisms by which a pigeon measures the vertical component of the magnetic field and the latitude. It is obvious that this would not affect any of the experiments he describes.

Because it seems desirable to test such a remarkable theory in as many ways as possible in spite of the amazing experiments already reported, those of the following experiments that have not yet been tried might well be considered. To distinguish between Yeagley's assumption that pigeons are sensitive to electric fields, the assumption that they are sensitive to magnetic fields, and the assumption that they are sensitive to neither, the most direct experiment would be a maze experiment or a feeding apparatus experiment in which the essential clues that the bird would have would be appropriate fields. Similar experiments in slowly accelerating elevators or rotating houses might show whether pigeons were sensitive to small accelerations and hence that such a sensitivity could be used for the determination of latitude. It would be interesting to know the effect on homing ability of a magnet fastened to the bird's body rather than to its wings and of the effect of magnetic storms. Experiments, such as the Special Release No. 1 of Yeagley's First Nebraska Experiment, in which birds flew toward a conjugate point to which they had never been would seem to be somewhat freer of unexpected alternative explanations than experiments in which the pigeons knew their loft was at the conjugate point because they had seen it there.

[1] H. L. Yeagley, J. App. Phys. **18**, 1035 (1947).
[2] W. R. Smythe *Static and Dynamic Electricity* (McGraw-Hill Book Company, Inc., New York, 1939), §14.14.
[3] W. F. G. Swann, Int. Crit. Tab. **6**, 442.

A New Method of Measuring Diffusion Coefficient in Solids with Radioactive Tracers

G. C. Kuczynski
Metallurgical Research, Sylvania Center, Bayside, New York
January 16, 1948

TWO experimental methods have been used up to the present time in the determination of the diffusion coefficient with the help of radioactive tracers. The older one, as described by W. A. Johnson,[1] requires the slicing of a specimen previously heated to a certain temperature for a long period of time. From the dissolved slices the average concentration of the radioactive material is determined and the concentration *versus* depth curve is constructed. From this curve, coefficient of diffusion D can readily be determined. The other method (2) dispenses of cutting, and from one reading of radioactive intensity and knowledge of the absorption coefficient for a given material the diffusion coefficient can be determined. In both methods the appropriate correction has to be made for radioactive decomposition during heating time.

The present method does not require cutting of the specimens, nor the knowledge of the absorption coefficient.

One face of a rectangular specimen a few centimeters in length is covered with a thin layer of radioactive material whose diffusion is to be measured and is then heated for a long period of time. Afterwards, the flat surface perpendicular to the activated face is etched electrolytically. The specimen is then transferred to a lead box (Fig. 1) with its etched surface up. The sliding cover is moved so that edge A is at an arbitrary distance x_1 from the radioactive layer and a reading of the radioactivity I_1 is taken. Then the sliding cover is moved to the left so that edge B will take the position x_2 such that the radioactivity reading I_2 from this portion of the specimen is equal I_1. From these two readings only, the diffusion coefficient can be calculated as follows:

$$I_1 = bL_0\alpha\pi^{-\frac{1}{2}}\int_0^{x_1/2(Dt)^{\frac{1}{2}}} e^{-z^2}dz,$$

where α is a factor expressing absorption, b the width of the specimen, and i_0 the original concentration of the radioactive material on the activated face.

$$I_2 = \frac{bL_0\alpha}{2}\left\{1-\tfrac{1}{2}\pi^{-\frac{1}{2}}\int_0^{x_2/2(Dt)^{\frac{1}{2}}} e^{-z^2}dz\right\}.$$

From $I_1 = I_2$ denoting

$$\pi^{-\frac{1}{2}}\int_0^{x/2(Dt)} e^{-z^2}dz = \phi(y)$$

one obtains

$$\phi(y_1)+\phi(y_2)=\tfrac{1}{2},$$

where

$$y_1 = x_1/2(Dt)^{\frac{1}{2}} \quad \text{and} \quad y_2 = x_2/2(Dt)^{\frac{1}{2}}.$$

Since

$$\frac{y_2}{y_1}=\frac{x_2}{x_1}, \quad \phi(y_1)+\phi\left(\frac{x_2}{x_1}y_1\right)=\tfrac{1}{2}.$$

This equation can easily be solved by graphical methods. When y_1 is known, D is calculated from

$$D = (1/t)(x_1/2y_1)^2.$$

It can be seen that the determination of D does not depend upon knowledge of the absorption coefficient and original concentration of the radioactive material on the activated face.

This method is expected to produce results under the following conditions: 1. The radioactive layer should be thin. 2. The surface from which the readings are taken should be deeply and uniformly etched to remove all

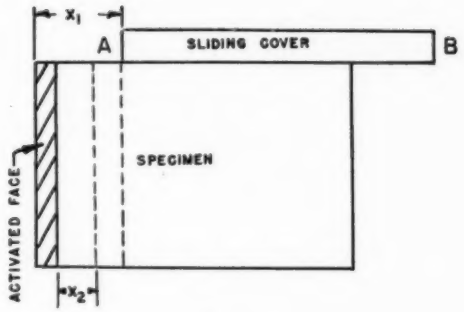

FIG. 1.

radioactive material which has spread too far because of the possibly accelerated surface diffusion. 3. The time of heating should be long in order to obtain a deep penetration measurable in terms of x_1 and x_2. 4. x_1 and x_2 should be measured with great accuracy (0.001 cm or better). 5. The length of the specimen should be great in comparison with x_1 and x_2.

Arrangements are being made to test this material experimentally in Sylvania Bayside laboratories.

W. A. Johnson, Trans. A.I.M.M.E. **143**, 107 (1941).
J. Steigman, W. Shockley, and F. C. Nix, Phys. Rev. **56**, 13 (1939)

New Booklets

The Esterline-Angus Company, Inc., P. O. Box 596, Indianapolis 6, Indiana, recently published technical bulletin No. 247, entitled *Operation Recorders—Their Selection and Use*. A lengthy list of applications is included. 16 pages, free on request.

Burrell Technical Supply Company, 1942 Fifth Avenue, Pittsburgh 19, Pennsylvania, has issued its bulletin No. 207, describing the Burrell "Wrist-Action" Shaker, for use in all types of laboratories. This device simulates hand shaking. 4 pages, free on request.

The Apparatus Department of General Electric Company, Schenectady 5, New York, has published a 48-page brochure entitled *Specialized Testing and Measuring Equipment Catalog*.

Tube Department of Radio Corporation of America, Harrison, New Jersey, has issued the following Application Notes: *Suppression of Arc-Over, Corona, and High-Voltage Leakage in the 5TP4 Kinescope* (4 pages) and *Blower Requirements for RCA Forced Air-Cooled Tubes* (12 pages).

Brooks and Perkins, Inc., magnesium fabricators of Detroit 1, Michigan, issued in December the first issue of their selling magazine, *Magnesium*. The issue contained 12 pages and included several articles on magnesium and its place in the manufacturing picture. Illustrated with photographs.

Armour Research Foundation of Illinois Institute of Technology, Chicago 16, Illinois, has published a 16-page booklet entitled *Precision Gage Laboratory—Another A.R.F. Service to Industry*. Free on request.

Fischer and Porter Company, Department 6F-H, Hatboro, Pennsylvania, announces its new bulletin, No. 88, containing more detailed information on the company's Viscorator for viscosity measurement. 4 pages, free on request.

North American Philips Company, Inc., 100 East 42nd Street, New York 17, New York, is distributing Volume 9, Number 6 of *Philips Technical Review*, published in Holland. Following are the titles of articles contained in the issue: "A 48-channel carrier telephone system," "An improved method for the air-cooling of transmitting valves," "Improvements in the construction of cathode-ray tubes," and "On the crystalline structure of ferrites and analogous metal oxides."

Here and There

Personnel

Two appointments were recently announced by the National Bureau of Standards. Dr. Wallace R. Brode, chemist, has been named Associate Director of the Bureau, succeeding Dr. Hugh L. Dryden, who was recently appointed Director of Aeronautical Research of the National Advisory Committee for Aeronautics. Dr. Brode was formerly at Ohio State University. John Todd, British mathematician, has also been appointed to the staff. On leave of absence from Kings College, University of London, he will aid in the development and application of high speed automatic digital computing machines.

Dr. Samuel E. Sheppard, widely known for his research on the sensitivity of photographic materials, retired January 1 after 35 years with Kodak Research Laboratories.

Conference on Surface Reactions

The Pittsburgh International Conference on Surface Reactions will be held at the Mellon Institute for Industrial Research in Pittsburgh, June 7–11, 1948. The Conference Committee is led by Dr. Earl Gulbransen of Westinghouse Research Laboratories. Preliminary plans call for technical sessions mornings and evenings and, in the afternoons, visits to Pittsburgh research laboratories which are working on surface reactions. Scientists, engineers, and educators from many parts of the world have been invited to participate, and several will present papers.

General Electric Fellowships

The General Electric Company is again offering (for the summer of 1948) fellowships for a six-weeks course at Union College and at Case Institute of Technology to high